Characteristics of storm surges along the east coast of India and the head of Bay of Bengal

A thesis submitted to Goa University for the award of the Degree of

Doctor of Philosophy

in

Marine Sciences

By

Charls Antony

Research Guide

A. S. Unnikrishnan

Goa University

Taleigao, Goa

February 2018

Statement

As required under the University Ordinance OB-9.9, I state that the present thesis entitled "Characteristics of storm surges along the east coast of India and the head of Bay of Bengal" is my original contribution and the same has not been submitted on any previous occasion.

The literature related to the problem investigated has been appropriately cited. Due acknowledgements have been made wherever facilities and suggestions have been availed of.

Charls Antony

CSIR-National Institute of Oceanography, Goa
16 February 2018

Certificate

This is to certify that the thesis entitled “Characteristics of storm surges along the east coast of India and the head of Bay of Bengal” submitted by Charls Antony, to the Goa University for the degree of Doctor of Philosophy, is based on his original studies carried out under my supervision.

The thesis or any part therefore has not been previously submitted for any degree or diploma in any university or institution.

A. S. Unnikrishnan

CSIR-National Institute of Oceanography, Goa
16 February 2018

Acknowledgements

Doctoral research life has been an interesting period for me. I have been benefitted from various persons and institutions from the beginning since I joined CSIR-National Institute of Oceanography (NIO), Goa, till the completion of this thesis. I convey my gratitude to all of them.

I am very much thankful to Dr. A. S. Unnikrishnan for his supervision. A lot has been learned from him as a research supervisor which needs to be carried forward. He is simply the best. Thanks to the constant support from Dr. P. Vethamony (Vice Chancellor's nominee), who took the efforts to monitor the progress of my thesis and Dr. M. R. RameshKumar (Co-guide).

Thanks to CSIR-NIO and the Director for providing me the opportunity to work in the institute. I acknowledge the High Performance Computing (HPC) facility, Pravah, in the institute, which I used for numerical investigations. Thanks to the Physical Oceanography Division members, particularly, Dr. D. Shankar, Dr. S. G. Aparna, Mr. D. Sundar, Mr. G. S. Michael and Mr. A. Kankonkar for their support from time to time. I acknowledge the interactions with Dr. S. V. Samiksha.

I am thankful to the Vice Chancellor, Goa University, faculty members of the Department of Marine Sciences, Prof. G. N. Nayak, Prof. H. B. Menon, Prof. C. U. Rivonker and the office staff, Mr. Yeshwant. Their support has made the academic interactions with the university easy.

I am thankful to Dr. Laurent Testut and Dr. P. L. Woodworth who have co-authored in my publications. It was a great honour to collaborate with a top sea level scientist, Dr. P. L. Woodworth. Thanks to Mr. P. L. N. Murty for his help in implementing the storm surge model. Thanks to Dr. Yann Krien for his suggestions for the numerical modeling. He made available the bathymetry data used in the thesis. Thanks to the visiting French scientists in NIO, Dr. Matthieu Lengaigne, Dr. Takeshi Izumo and Dr. Fabien Durand.

My friends made my reseach lively and enjoyable. The time spent with them was precious. I extend my sincere gratitude to all of them.

I am very much thankful to various organisations that made available the data and software used in the thesis. The tide-gauge data along the Indian coast were provided by the Survey of India and the Indian National Centre for Ocean Information Services (INCOIS). Rest of the tide-gauge data were obtained from the University of Hawaii Sea Level Centre (UHSLC). Altimetry data used in this study were developed, validated and distributed by the CTOH/LEGOS, France. The cyclone data used in the present study were obtained from India Meteorological Department (IMD) and Joint Typhoon Warning Centre (JTWC). Thanks to the Generic Mapping Tools (GMT) team. GMT was used to draw the maps and graphs.

I am thankful to the University Grants Commission (UGC), Govt. India for providing a research fellowship, which enabled me to carry out this research.

I recollect the support from my parents, sister and brothers. I dedicate this thesis to them.

Abstract

The present thesis investigates characteristics of storm surges and extreme sea levels in the Bay of Bengal using hourly sea-level observations spanning 34 years from tide gauges along the east coast of India and at the head of the Bay of Bengal. An attempt was made to explore the usefulness of satellite altimeter data for storm surge studies. Finally, numerical modelling was also undertaken for studying tide-surge interaction during extreme events.

In the present thesis, data from four tide gauges, three along the east coast of India (Chennai, Visakhapatnam and Paradip) and one at the head of the Bay of Bengal (Hiron Point) were used. Characteristics of storm surges, as observed in tide-gauge records, can be briefly described as follows. Frequency histogram of surge series at different locations shows that surge heights are small at Chennai and are large at Hiron Point. The surge distributions are positively skewed, showing, the presence of large positive surges than negative surges. Many of the low-pressure systems cross the northern coast of the Bay. Also, the northern part of the Bay has wide continental shelf, shallow depths and converging coast, which result in large surge heights.

The present thesis demonstrates that satellite altimetry can be a useful complementary dataset for the study of storm surges in the Bay of Bengal. The magnitudes of surges observed by altimeters are consistent with those recorded in the nearest tide gauges. Though observing storm surges by altimeters rely purely on a chance, the presence of multiple satellite tracks in a region can considerably enhance the chances of capturing the signals of extreme events. Altimeters provide information on cross-shelf variations of storm surges, which is useful for model validation and data assimilation.

The highest water levels above mean sea level have the greatest magnitude towards the northern part of the Bay, which decrease towards the southwest. Extreme high waters are a combination of moderate, or even small, surges with large tides at these stations in most of the cases. At interannual time scales, changes in extreme high waters are found to be influenced by the El Niño-Southern Oscillation and Indian

Ocean Dipole. Long-term increasing trends, which are significant, have been observed in the extreme high waters at Hiron Point, at the head of the Bay of Bengal. For the other stations, no significant trends have been observed.

The distribution of surge heights above 99th percentile threshold with respect to tidal heights and phases has been used to explore the observed tide-surge interaction patterns. The distribution patterns reveal that the surge heights have a greater dependency on tides at Hiron Point than other stations. At Hiron Point, surges peak more frequently about 4 hours before the high tide. A detailed examination of surges above 99.9th percentile at Hiron Point shows that many of the events have a phase alteration between tide and sea level and also in some cases, the surges are noticed to be modulated by tides.

Tide-surge interaction during the Cyclone Aila, which crossed the West Bengal coast in May, 2009, has been investigated using a numerical model. The results show that interaction is significant, with interaction heights attaining 40 cm and above at many locations. When the experiments have repeated for the hypothetical occurrence of the Cyclone Aila at different tidal phases, it is found that surge heights are lower during high tide compared to those during other tidal phases. Further investigation suggests that interaction heights change in proportion to surge height. Increasing surge height is found to result in increased interaction height. Strong dependency of interaction on spring-neap cycle of tide is also noticed with higher interaction heights during spring tide than those during neap tide.

Contents

List of Figures

List of Tables

Chapter 1

Introduction

1.1 General

Historically, human settlements have shown an affinity towards water resources. Ancient civilisations flourished on the banks of rivers, as they provided a continuous supply of fresh water for daily needs as well as for irrigation of land for cultivation, besides serving as a means of transportation. Many ancient civilisations including the Indus Valley, Egyptian and Mesopotamian civilisations relied on rivers, this close interaction and curiosity to explore beyond rivers led to the development of maritime activities. History shows that civilisations had greater interactions through seas than land for their trade and commerce, as seas provided an efficient mobility of bulk quantities of goods. With the evolvement and expansion of civilisations and empires and the trading between them, coastal regions became preferred areas of interest, since oceans provided the cheapest mode of transportation along with other resources. This eventually led to the establishment of ports around the world, as ports were a key element of maritime transport, and they became the base for human activities. Throughout the history, many factors including colonialism and associated trade also contributed to the emergence and development of coastal cities and related populations (McGranahan et al., 2007).

Small and Nicholls (2003), in a study on the global coastal population, estimated the near-coastal population (population within 100 km of the coastline and below 100 m land elevation) of the world in 1990 as about 23% of the total global population. The average density of population (112 people/km^2) in the coastal regions was several times higher than that of the global average (44 people/km^2). The authors also noted

that the preferred settlement locations had been regions close to coastlines. More specifically, the Low Elevation Coastal Zone (LECZ; land below 10 m height above sea level and contiguous along the coast), accounts for nearly 2% of the total land area and about 10% of the total human population, as per the estimates made for the year 2000 (McGranahan et al., 2007). Population density in the LECZ (241 people/km^2) was about five times the global average (47 people/km^2), and nearly 83% of the LECZ population was in the less developed nations as per the estimates for the year 2000 (Neumann et al., 2015). The countries which share significant portion (more than 50%) of the LECZ population were from the eastern, southcentral and southeastern Asia including China, India, Bangladesh, Indonesia and Vietnam (Neumann et al., 2015). Many of the megacities, which are large agglomerations of the human population exceeding 10 million, and other large cities of the world, are located in the low-lying coastal zones (UN-Habitat, 2016).

Today, human population in the coastal regions is increasing much faster than ever before. Various factors account for this increased rate include critical regions for industries, ports, recreations, tourism, fishing, farming and increased migration (Agardy et al., 2005; McGranahan et al., 2007). Population projection by Neumann et al. (2015) shows a significant increase in the population (625 million to 879 million) in the LECZ by 2030 (from the year 2000) for a low-end scenario. Coastal regions are home to a large percentage of the human population and for infrastructure; at the same time, they also pose serious threats from storm surges, tsunamis, flooding associated with sea-level rise, etc. Increasing coastal population results in more people at the risk of extreme events. Events like the Hurricane Katrina, Sandy (east coast of the USA), Cyclone Nargis (Myanmar) and the 2004 Indian Ocean tsunami remind the vulnerability of the coastal population to extreme events. Future flood damage loss is also expected to increase while accounting for various factors such as climate change, local subsidence in some regions and socio-economic growth (Hallegatte et al., 2013). These facts put forward a great challenge in protecting a rising population and their assets from various coastal hazards. On the other hand, the population pressure on the coastal environment such as increased exploitation of natural resources and pollution,

which eventually transforms the environment resulting in the degradation of coastal ecosystems (Creel, 2003). Coastal wetland reduction, contamination of coastal waters and decline in fisheries population are some of the visible changes in the coastal zones due to human pressure. These issues indicate the need for an integrated coastal zone management for sustainability.

1.2 Coastal processes and hazards

A coast is the narrow portion of the land that lies close to the ocean. It extends landward from the ocean to the first major change in terrain features that are not influenced by the coastal processes (Mangor, 2008). A coastline, the frontier between the marine and the terrestrial regime, is dynamic in nature. Coastline changes from time to time as the sea level changes. Coastal zone is the transition area which includes the land and oceanic regions. In literature, it is difficult to find a consistent definition of the coastal zone regarding its land and ocean boundaries. The definition varies depending on the specific interest of the study. The Land-Ocean Interaction in the Coastal Zone (LOICZ) science plan (Holligan and Boois, 1993) defines coastal zone as the region 'extending from the coastal plains to the outer edge of the continental shelves, approximately matching the region that has been alternately flooded and exposed during the sea-level fluctuations of the late Quaternary period'. As discussed in the previous section, coastal zones are critical regions of interest, as they are used for various human activities. These areas are also known for their richness and diversity of various natural resources and ecosystems. Human beings have been utilising these areas since thousands of years. Coastal zones are the regions where land, ocean and atmosphere interact. Various physical processes deform the coast into diverse coastal landforms. These processes include erosion, transportation and accretion of sediments, which are caused by waves, tides and currents.

A hazard can be considered as a process, which poses a threat to human life, property or environment. These hazards can be natural or human induced. Coastal hazards can be unique to this area (for example, hazards associated with storm surges

and tsunamis), or common to any region, account for a broad topic including coastal flooding, erosion, pollution, groundwater reduction, harmful algal bloom, oil spills, etc. I limit the present discussions on coastal hazards to the geophysical factors, which cause changes in sea level resulting in flooding and erosion. Focus is given more on storm surges, which is pertinent to the interest of the present thesis and other factors are discussed briefly. An elaborate description of coastal hazards can be found in Finkl (2013) and Ellis and Sherman (2014).

The changes in coastlines are considered as a coastal hazard when they become a threat to human life, property or environment. The hazards at the coast due to the interaction between land and ocean include coastal flooding and erosion. The principal drivers of these hazards include waves, tides and currents. Disastrous and catastrophic coastal hazards, which cause rapid and severe damage to the coast, are caused by tsunamis and storm surges. In a long time scale, sea-level rise has the potential to dislocate the coastal habitats. Increasing of mean sea level (MSL) potentially exacerbates the impacts due to storms, tides and waves.

The causes or the drivers of coastal hazards vary from place to place, in time scales, frequency and intensity. In small scales of time and space, waves and currents induce flooding and erosion. These short-term risks are observed in most of the coastal regions. Ocean surface gravity waves are generated by winds. The energy transferred from the wind is finally dissipated by wave breaking at the coast. This process can gradually deform the coastal landforms including, erosion and deposition along the beach, eroding cliff, etc. and creates irregular coastlines. These waves do not produce any hazardous effects, except during extreme conditions when their effects become considerable (for example, during storm events).

Unusually high waves can happen at the coast or in the open ocean, which are typically double that of the significant wave height (average of one-third of the highest waves in a wave record), a common criterion used to identify them (Mori, 2009), and not associated with local weather conditions, potentially hazardous to wipe coastal areas. These waves are known as freak or rogue waves. Globally, several regions have relatively high occurrences of freak waves, for example, seas around the

Great Britain, the southeast coast of Australia and Tasmania, the south coast of Africa and Northern California, U.S.A. (Nikolkina and Didenkulova, 2011). In shallow waters, these waves are formed by wave-wave, wave-current interactions, basin geometry and bathymetry effects and various other mechanisms which amplify the wave heights. These waves cause a threat to ships (Monbaliu and Toffoli, 2003), coastal infrastructures and result in human fatalities and injuries (Nikolkina and Didenkulova, 2011). Freak waves reaching up to 7 m have been observed along the west coast of India (Glejin et al., 2014). High wave occurrences have been reported along the southern coast of India during pre-monsoon season (April–May), which is locally known as 'Kallakkadal' (Kurian et al., 2009). These events are caused by swells propagating from the southern Indian Ocean (south of 30°S) (Remya et al., 2016).

Tides are periodic fluctuations of sea level, which are astronomically forced. Tidal ranges vary from a few tens of centimetres to a few metres at various locations around the world (Figure 1.1). At most of the locations, the tides are either semidiurnal (two highs and lows in a day, which are of about the same height) or mixed (heights of successive highs and lows are different) in nature, whereas it is diurnal (single high and low) at very few locations (Figure 1.2). During spring tides (forcing of sun and moon is aligned in the same direction), tidal ranges are larger than average tides. Spring tides repeat every 14.8 days during full and new moons. Extreme tides are of interest for its potential impact for coastal flooding, combined with waves, especially in the low-lying areas. Very large spring tides can occur depending on the specific position of moon and sun. It has been shown that long period tidal modulation (18.61-year lunar nodal modulation) contributes significantly to changes in coastlines and influence coastal flooding in specific regions like French Guiana (Gratiot et al., 2008) and western Australia (Eliot, 2010). Nodal modulations are predominant for regions of large diurnal tides (> 4 m) (for example, South China Sea) and 4.4-year perigean cycle (8.85-year cycle of Lunar perigee affects high tide as a quasi 4.4-year cycle) is largest for semidiurnal tides (> 6m) (for example, English Channel) (Haigh et al., 2011). It is to be noted that, in a scenario of rising MSL, the potential impact of high

tide is to cause frequent minor flooding instances, as noted by some authors like Ray and Foster (2016).

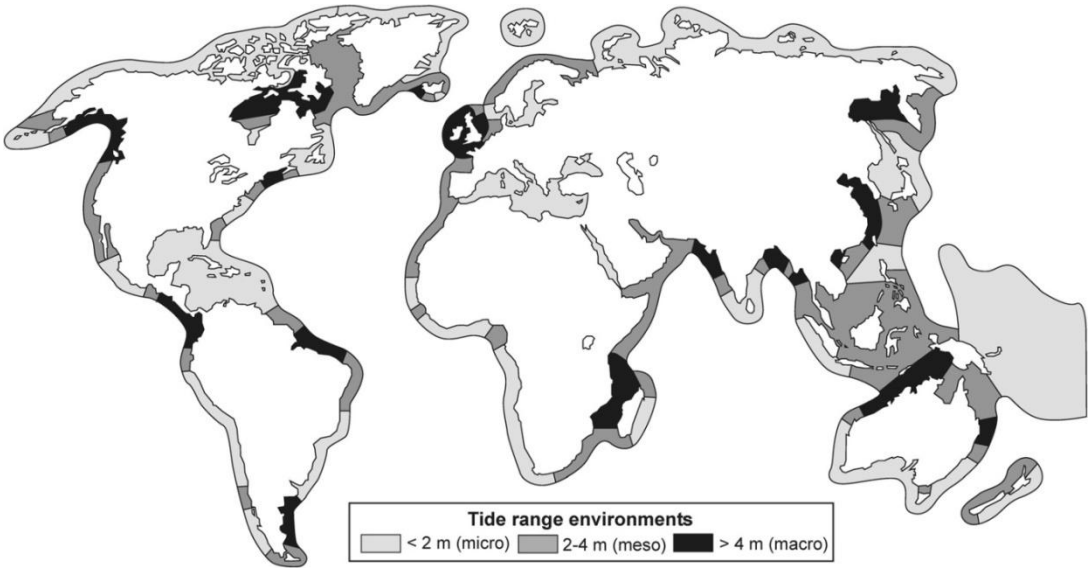

Figure 1.1 Global distribution of tidal range (Source: Appelquist and Halsnæs, 2015).

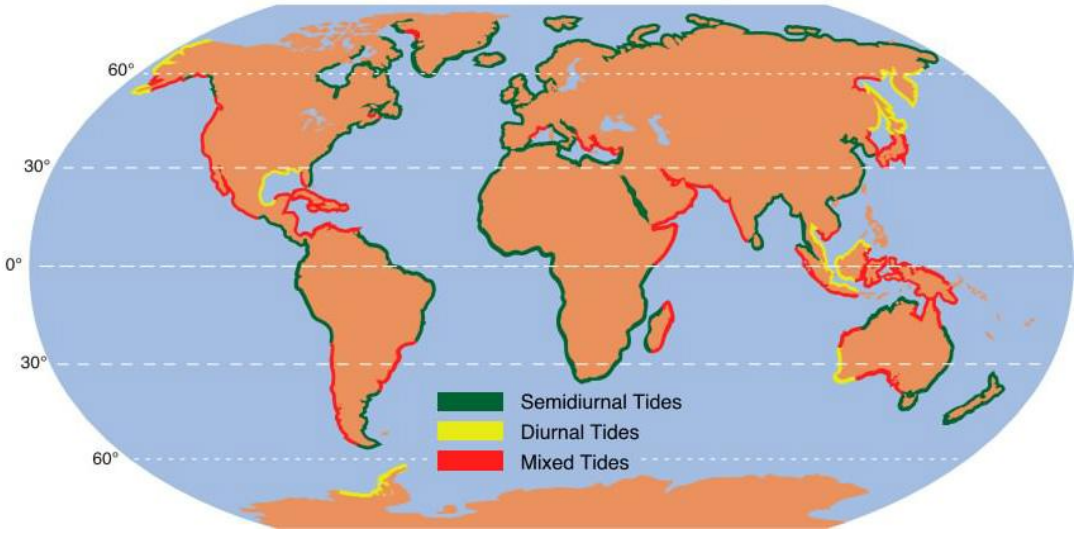

Figure 1.2 Global distribution of three types of tides (Source: Pidwirny, 2006).

Tsunamis (meaning 'harbour waves' in Japanese) are considered as severe natural calamities, as they can affect a vast stretch of coastal regions. Tsunamis are ocean

waves generated due to displacement of large volume of water. The most common cause for this water displacement is underwater earthquakes (Joseph, 2011). Other less common events that cause such a bulk water displacement include submarine volcanic actions, landslides, and asteroid impacts. Tsunamis travel several thousand kilometres across the oceans from where they originate, impacting distant coasts. The wave amplitude in deep water is less than 1 metre, which amplifies to several metres in shallow coastal regions. Tsunami travels with a speed of about 700 km/h in deep water (4000 m). In the shallow water (10 m), tsunami wave speeds are about 36 km/h (Joseph, 2011), which makes it hard for the beach users to escape from these waves. The devastating Indian Ocean tsunami of December 2004 was a notable event in the modern times. This tsunami has caused nearly 300,000 deaths (Lay et al., 2005). Though tsunamis have been noted in the past, major tsunamis are found to be less frequent in comparison to other coastal flooding events, but their damaging potential is high. Countries around the rim of the Pacific Ocean are at a high risk from tsunamis (Levin and Nosov, 2009). Tsunamis risk is relatively moderate in the Indian Ocean and low in the Atlantic Ocean compared to that in the Pacific Ocean (Figure 1.3).

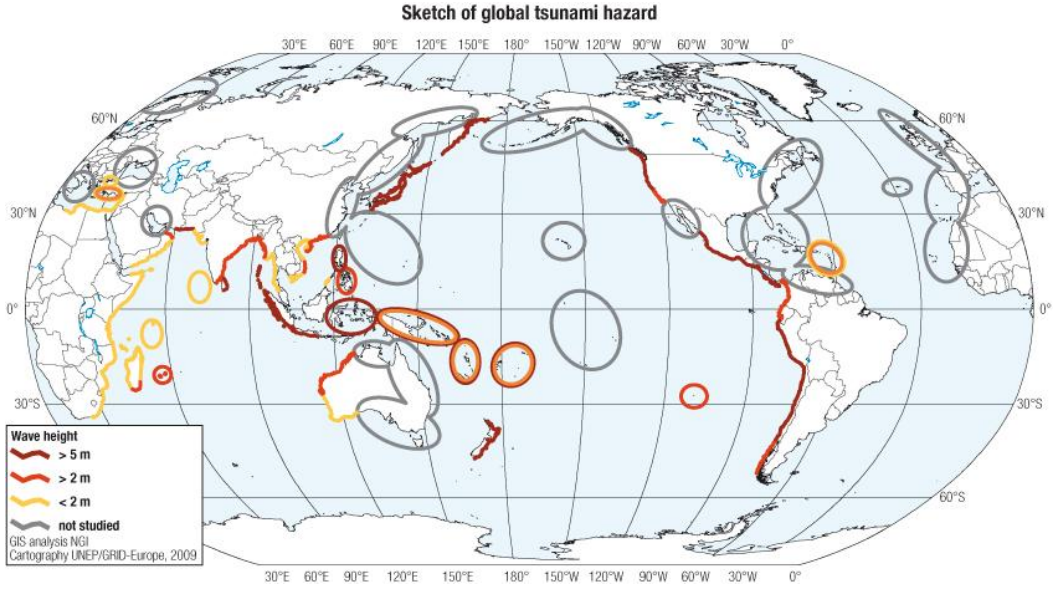

Figure 1.3 A sketch of global tsunami hazard(Source: http://preventionweb.net/go/10602).

Meteotsunamis are sea-level fluctuations of meteorological origin with same frequencies and spatial scales as tsunami waves and capable of massive destructions. Severe meteotsunamis are limited to specific bays and inlets owing to the local topographic resonance (Monserrat et al., 2006; Bechle et al., 2016). The strongest known meteotsunami occurred in Vela Luka (Croatia), had a wave height about 6 m (Vilibić et al., 2014). Meteotsumanis are observed in many parts of the world (Figure 1.4) and are known by different local names: "*šćiga*" in the Adriatic Sea, "*rissaga*" in the Balearic Islands, "Seebär" in the Baltic Sea "*abiki*" in Japan, "*milghuba*" in Malta and "*marubbio*" in Sicily (Monserrat et al., 2006; Rabinovich, 2009).

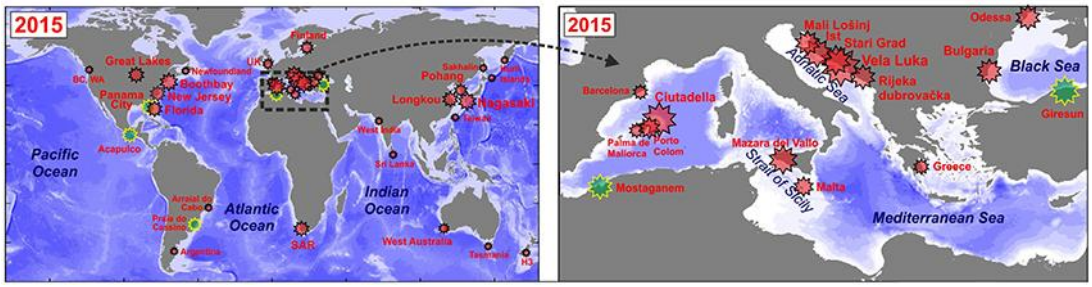

Figure 1.4 Global map of meteotsunami locations (based on data up to the year 2015). Red stars indicate documented events. Green stars indicate locations where meteotsunami-like events occurred but not confirmed by scientific research. The size of the stars is proportional to the intensity of the incident (Source: Vibilić et al., 2016).

Storm surges are increase or decrease in sea level associated with a storm. Strong winds and low air pressures associated with a storm cause sea level to rise, which results in coastal flooding. In extreme cases, surge heights can reach many metres (Pugh and Woodworth, 2014; Needham et al., 2015). Many regions of the world's coastline are affected by storm surges, which are caused by tropical and extratropical storms. Major cyclone affected coasts in terms of economic and human loss include the Gulf Coast of USA, the coasts of western and northern Bay of Bengal, the coast of Australia, coasts of the North Sea, etc. Storm surges are described in detail in Section 1.3.

Seiches are standing waves of periodicities varying from tens of seconds to a few hours observed in the enclosed water bodies (Rabinovich, 2009). They are specifically

called harbour oscillations when occurring in semi-enclosed water bodies and harbours, which are connected to the sea. Seiches are forced by winds, atmospheric pressure variations and seismic activity. Harbour oscillations are mostly generated by long waves entering the water body (Rabinovich, 2009). Seiches are known to cause severe flooding, damages and even casualties (Ichinose et al., 2000; Rabinovich, 2009).

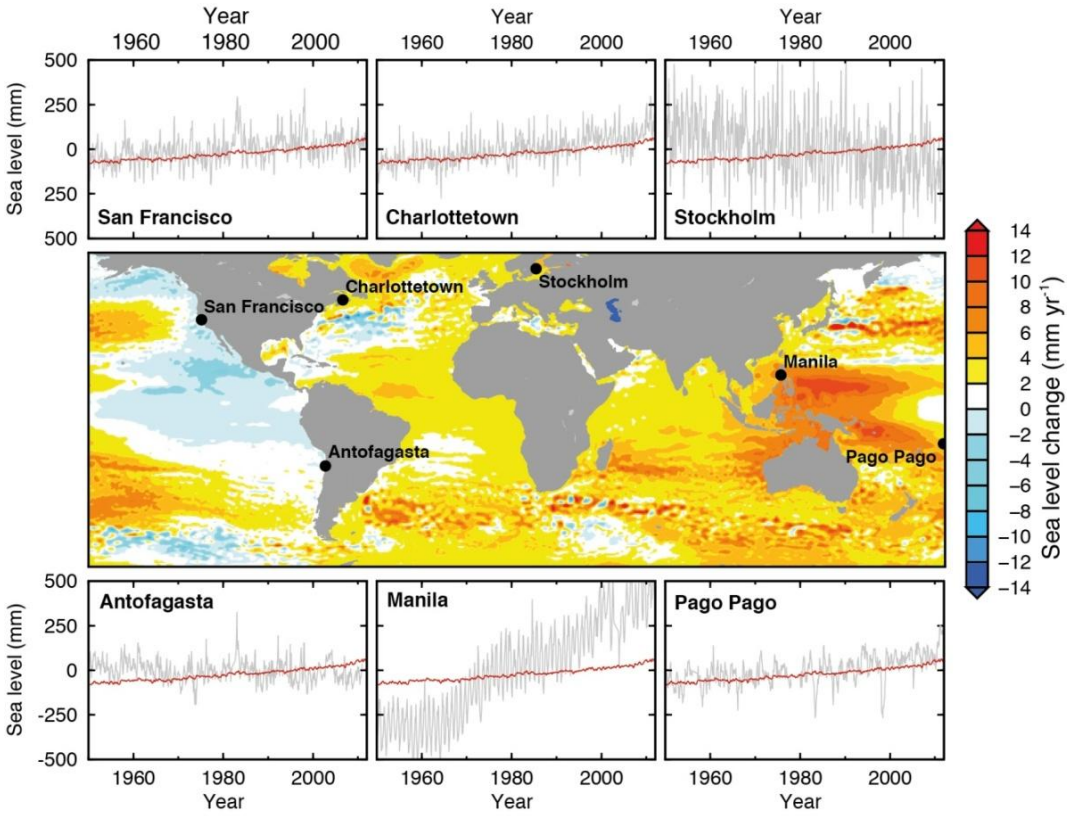

Figure 1.5 Sea level changes during 1993–2012 from satellite altimetry. Relative sea level change from selected tide gauges (Gray) and global MSL change (red) are shown (Source: Church et al., 2013).

It is a fact that sea level has been rising in the past due to global warming and will continue to rise in future. Rising mean sea level is a serious issue. Slowly rising sea level can permanently submerge low-lying coastal areas in future. One immediate effect of rising sea level is the occurrence of frequent flooding. Global MSL has been

rising at a rate of about 1.7 mm/yr since 1900; since 1990, the rates are much higher, about 3.2 mm/yr, and the sea level rise is expected to continue beyond the 21st century (Church et al., 2013). Main factors which contribute to the rising of sea level are thermal expansion of oceans and melting of ice (Green Land, Antarctica and other sources of land ice). Specifically for some regions, subsidence due to either being a delta or extensive groundwater pumping (Manila) (Figure 1.5) adds to the above factors. Notably, in some regions, for example, the Indo-Gangetic delta undergoes subsidence at about 4 mm/yr (Goodbred and Kuehl, 2000). In some regions, for instance, at Stockholm (Figure 1.5), sea level is falling due to vertical land movement caused by glacial isostatic adjustment.

Most of the above discussed causes of coastal hazards are natural phenomena; human interaction with these natural processes makes them hazardous. Increasing population in the coastal regions causes the impacts of natural hazards to increase. Coastal zone hazard risk management and adaptation including identification and evaluation of risk, implementation of protection measures, proper early warning systems and measures for the necessary evacuation during extreme events can reduce the destruction.

1.3 Storm surge

Storm surge is an abnormal rise or fall in sea level associated with a storm (Figure 1.6). These changes are noticed to be sudden and lasting for a few hours to a few days. To understand this more clearly, hourly tide-gauge observations of sea level at Akyab (Myanmar), during Cyclone Akash, 13–15 May, 2007, is shown in Figure 1.7. A tide gauge records the sea level at a location as a function of time with respect to a reference level. This sea level is the sum of MSL, tides and residual sea level. The time series of residual sea level reveals the nature of surge caused by the storm. The storm surge caused an additional increase in sea level by about 1 m than the predicted tide. The maximum sea level was higher than the highest astronomical tide by about 50 cm for the same year.

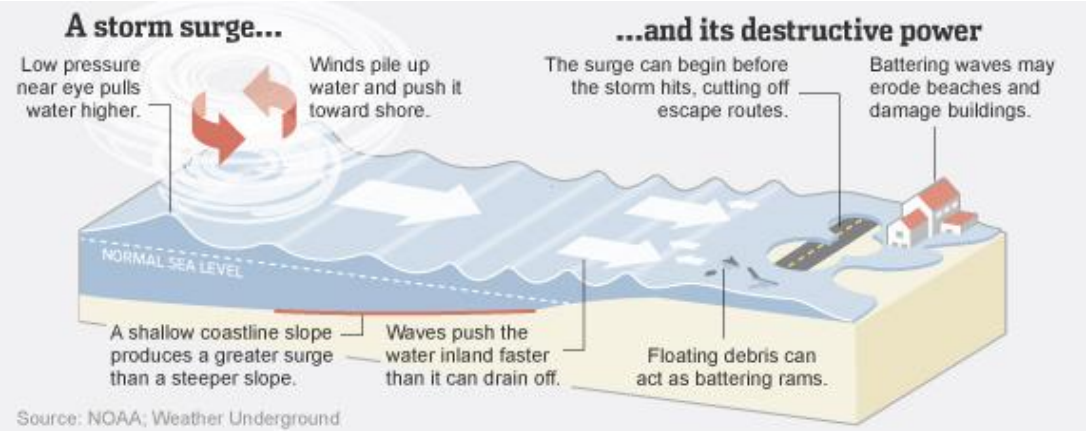

Figure 1.6 A schematic diagram showing storm surge and its impact (Source; National Oceanic and Atmospheric Administration, U.S.A.).

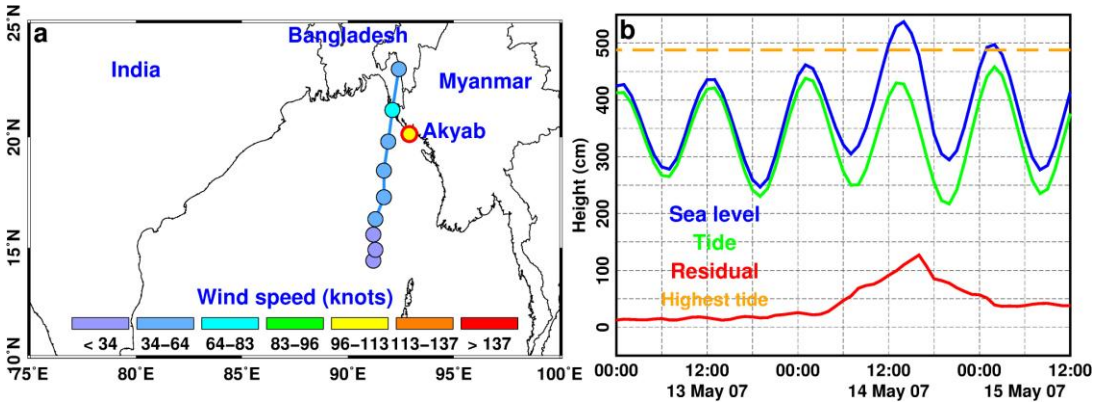

Figure 1.7 a) Tropical Cyclone Akash (13–15 May, 2007) with wind intensities shown. b) Time series of sea level, predicted tide and residual sea level during the Cyclone Akash at Akyab in the northeastern Bay of Bengal (northwestern Myanmar). The highest tide (dash line in orange colour) is the largest among the predicted tides for the year 2007.

A storm surge can be positive or negative, depending on whether storm winds are onshore or offshore direction (Figure 1.8a and b). A negative surge decreases the sea level, whereas a positive surge increases the sea level than the expected. The magnitude of the surge can be obtained as the algebraic difference between observed sea level and predicted tide (Blier et al., 1997). Hence, a positive (negative) surge has positive (negative) magnitude. The damage caused by a positive surge and the safety measures required for it are of much concern than that of a negative surge in a practical sense (Lopeman et al., 2015). This may be the reason why research interests

and discussions are most often limited to positive surges and a storm surge usually refers to a positive surge, and in most of the definitions, it is a rise in water level. A large positive surge poses a threat to life and property, whereas a negative surge often affects the investments and infrastructures in the coastal seas related to aquaculture and navigation (grounding of ships), and less destructive. However, a number of studies point out the importance of negative surges (El-Sabh et al., 1988; As-Salek, 1997; D'Onofrio et al., 2008).

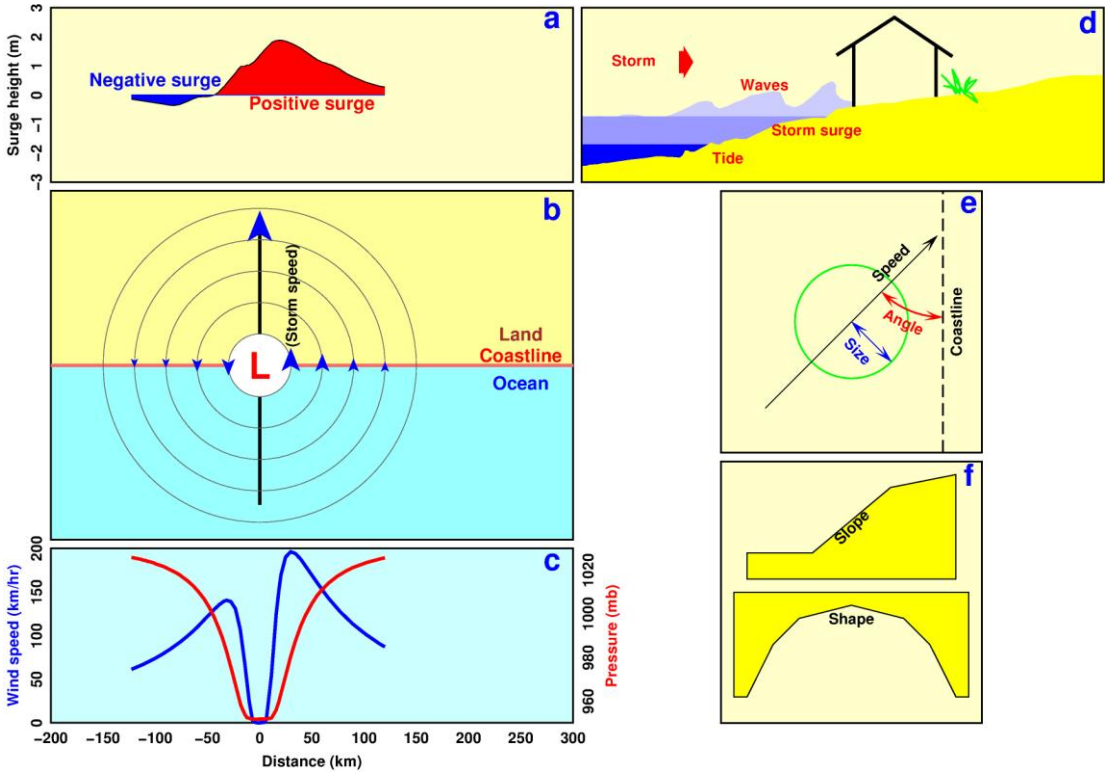

Figure 1.8 A Schematic diagram of a storm surge. a) and b) Surge produced at the coast and the cyclone hitting normal to the coast respectively. In panel b, cyclonic wind fields are shown. c) The wind and pressure profile of the cyclone. d) A side view of cross section of storm surge. Various factors controlling storm surge, e) the storm speed, angle of approach, size of the storm in terms of radius and f) geometry of the coast (slope and shape).

As mentioned earlier, storm surges are generated by storms; these storms include tropical and extratropical cyclones. Tropical cyclones are characterised by persistent winds and low pressure at the centre of the cyclone. The cyclone winds are directed

towards the centre and rotate around the low. The rotation is counter-clockwise in the northern hemisphere and clockwise in the southern hemisphere. A drop in atmospheric pressure causes the generation of a surge by a process known as the inverse barometric effect. A reduction of atmospheric pressure by 1 mb causes sea level to rise by 1 cm approximately. A simple equation which estimates the contribution to sea-level change by pressure drop during a storm is, $\eta = (P_{env} - P_c)\ 0.01$ (Pugh and Woodworth, 2014), where, η is the sea level change in metres, P_{env}, and P_c are environmental pressure and pressure at the centre of the storm. Strong onshore (offshore) winds raise (drop) the sea level at the coast. Additionally, wave-induced set-up (set-down) adds to above effects, resulting in changing the total sea level. The other factors which determine the features of the storm surge are size, forward speed, and angle of approach of the cyclone to the coast, the geometry of the coastline (Needham and Keim, 2011), which are shown schematically in Figure 1.8. Storm surges are also affected by the Coriolis force (Le Cozannet et al., 2013). This in turn increases the surge height on the eastern side for a storm moving northward in the northern hemisphere.

Several coastal regions of the globe are prone to the occurrence of severe storms and associated surges (Figure 1.9). These regions include the coasts of north Atlantic, northwest Pacific, northeast Pacific, southwest Pacific, north Indian, southwest Indian, and southeast Indian Oceans. Tropical cyclones are known by different names in different regions. In the Atlantic and the eastern Pacific, they are called Hurricanes, in the Indian Ocean as Cyclones, and in the northwest Pacific as Typhoons.

Tropical cyclones form over the tropical oceans with relatively warm water (sea surface temperature above 26° C to a depth of 60 m) (Gray, 1975). Other prerequisites for cyclone formation include low vertical wind shear, pre-existing disturbances, high relative humidity in the lower and mid troposphere, potentially unstable atmosphere and enough Coriolis force to sustain the low pressure (Gray, 1975). Latent heat of condensation derived from the expansion of moist surface air associated with warm waters remains the source of energy for tropical cyclones. They form as low-pressure systems and intensify into tropical cyclones. Usually, tropical cyclones travel from

east to west, as they are embedded within the surrounding tropical easterly winds. This steering flow accounts for about 70-90% of the cyclone motion (Neumann, 1992). Divergent motions exhibited by cyclones result from various other mechanisms including the Coriolis Effect. When these systems reach to extratropics, they turn into extratropical cyclones and move in westward directions following the background westerly winds.

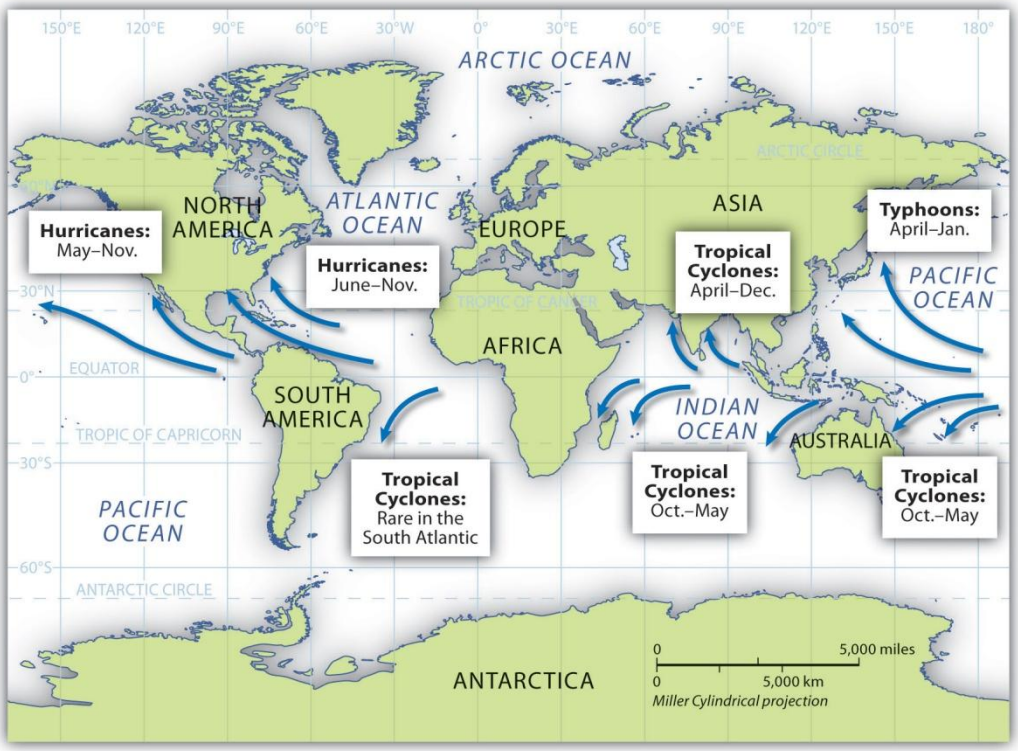

Figure 1.9 A map of tropical cyclone distribution
(Source: https://saylordotorg.github.io/text_world-regional-geography-people-places-and-globalization/s08-05-tropical-cyclones-hurricanes.html).

Generally, tropical cyclones neither form close to (5°S–5°N) latitudes nor they cross the equator. Preferred genesis locations of tropical cyclones are 5°–15° latitudes in northern and southern hemispheres. Most of the tropical cyclones form during the summer season. However, in the western Pacific, cyclones develop throughout the year. In the north Indian Ocean, cyclone seasonality is bimodal with most of them occurring in the months November and May. The north Indian Ocean basin is the

least active among the various cyclone basins. No cyclones are observed in the southeastern Pacific and the southern Atlantic Ocean. A well-known cyclone intensity classification scale is the Saffir–Simpson hurricane scale (Table 1.1), which is used to give cyclone warnings. The scale also provides expected surge heights at cyclone landfall.

Table 1.1 Saffir–Simpson hurricane scale (Source: Kantha, 2006).

Category	Pressure (mb)	Wind speed (m/s)	Surge (m)
Tropical depression	1007	<17	-
Tropical storm	< 1000	17-33	-
Category 1	980	33-42	1.2-1.5
Category 2	979-965	43-49	1.8-2.4
Category 3	964-945	50-58	2.7-3.7
Category 4	944-920	59-69	4.0-5.5
Category 5	<920	>70	>5.5

Tropical and extratropical cyclones have different characteristics, and surges generated by them also show variations (von Storch and Woth, 2008) (Table 1.2). Extratropical storms are much larger systems compared to tropical storms, but tropical storms remain most intense, and hence, the surges associated with it. The spatial extent of extratropical cyclones reaches to more than 1000 km, whereas it is only a few hundred kilometres for tropical cyclones. Extratropical cyclones occur in the 30°–60° band latitude, and these systems move from west to east. In the north Indian Ocean, storm surges are caused by the tropical cyclones, and in the North Sea, they are caused by extratropical cyclones.

Table 1.2 Characteristics of tropical and extratropical cyclones (Source; von Storch and Woth, 2008).

Parameter	Tropical cyclone	Extratropical cyclone
Size	500±200 km	1000±500 km
Surge height	Larger	Smaller
Surge duration	Several hours, up to half a day	2–5 days
Length of coastline affected by the surge	Less: usually < 200 km	Several hundred kilometres

1.4 Bay of Bengal

The Bay of Bengal, a marginal sea of the Indian Ocean (Figure 1.10), is also a tropical cyclone risk water body. The approximate geographical extent of the Bay is between 80˚–95°E and 5°–22°N (top panel Figure 1.10). The Bay is bordered by Sri Lanka and India to the west, Bangladesh to the north and Myanmar and Andaman and Nicobar Islands to the east. Continental shelf is narrow along the east coast of India. The head of the Bay (northern region) is characterised by a wide continental shelf with shallow waters, low-lying coast and the presence of numerous rivers opening into the Bay (bottom left panel Figure 1.10). Tides in the Bay are semidiurnal in nature. The head of the Bay is characterised by large semidiurnal tides with tidal ranges exceeding 4 m in some regions (Figure 1.1). The coastal regions of the Bay are densely populated.

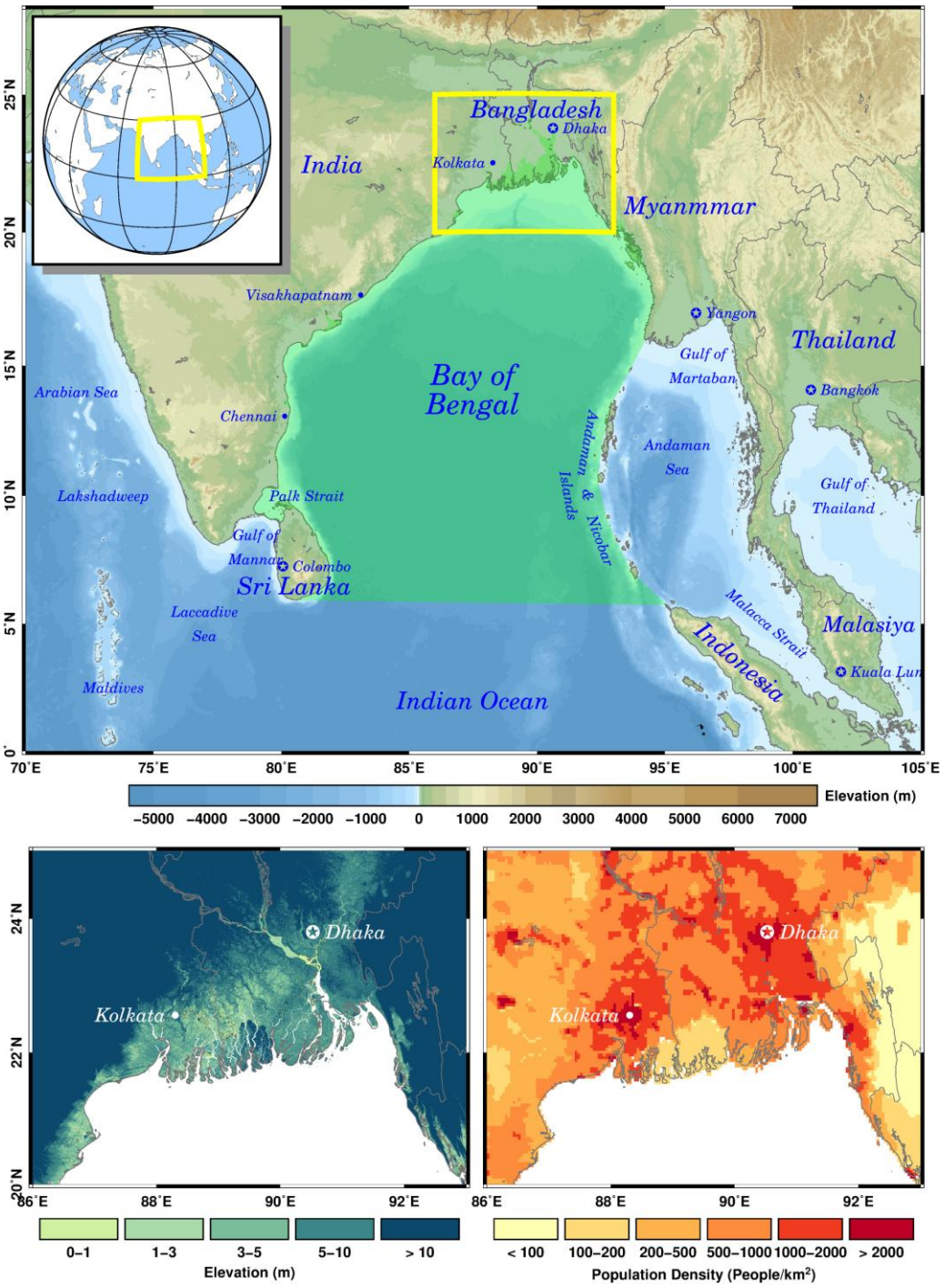

Figure 1.10 Map of the Bay of Bengal and adjacent regions (top panel). Shaded portion is the boundary of the Bay of Bengal as defined by International Hydrographic Organisation. Topography (Shuttle Radar Topographic Mission Digital Elevation Data) and population density (Socioeconomic Data and Applications Center, NASA) of the northern Bay of Bengal coast (bottom left and right panels respectively).

1.5 Storm surges in the Bay of Bengal

The Bay of Bengal accounts for about 4 tropical cyclones in a year (Niyas et al., 2009). This comes to only 5–6% of the cyclones formed over the tropical waters in global oceans. Hence, the number of occurrence of tropical cyclones in the Bay is relatively low. However, the impacts associated with cyclones and storm surges in the Bay of Bengal are very high. The primary reason for this is the large human population residing along the coastal regions of the Bay (bottom right panel Figure 1.10). Geographically, the head of the Bay is more vulnerable to storm surges. The head of the Bay has a frequent occurrence of cyclones compared to other parts of the Bay. Wide and shallow shelf and triangular shaped coast tend to amplify the effects of storm surges with rivers carry the surges further inland. The Bay of Bengal has the highest occurrence of largest surges (≥ 5 m) compared to any other storm surge prone regions (Needham et al., 2015). Moreover, the large tidal amplitudes at the head of the Bay can cause a significant impact when storm surges occur combined with high tides. Moderate surges occurring at high tide could be more disastrous than large surges occurring at low tide.

In the Bay of Bengal, cyclones occur mainly during post-monsoon (October–December) and pre-monsoon (April–May) seasons. The southwest Monsoon season (June–September) is characterised by strong wind shear, which hinders the formation of cyclones, even though sea surface temperatures remain high. Cyclone frequency is high in November (primary peak) and in May (secondary peak). The post-monsoon season is more active than pre-monsoon season in terms of cyclone frequency and notable for the occurrence of intense cyclones. A classification of low-pressure systems formed over the Bay of Bengal has been given by the India Meteorological Department, which is shown in Table 1.3.

In the past, storm surge disasters were noted to cause highest losses in terms of both life and property, as they were frequent than other disasters in the Bay. One of the biggest disasters was that associated the Bhola cyclone, which hit the coast of Bangladesh in 1970. About 300000 people lost their lives during this event (Frank and

Husain, 1971). A very severe cyclone event (Bangladesh) in 1991 and the Odisha super cyclone (India) in 1999 were other notable events. There were instances of large events during the last decade such as cyclones Sidr (2007), Nargis (2008) and Aila (2009) with considerable loss of human lives. More recently, during events like cyclones Phailin (2013) and Hudhud (2014), human fatalities are well reduced, mainly due to the success of early warning and evacuation.

Table 1.3 Classification of low-pressure systems in the Bay of Bengal (India Meteorological Department).

Category	Wind speed (m/s)
Low-pressure area	< 9
Depression	9-14
Deep depression	15-17
Cyclonic storm	18-24
Severe cyclonic storm	25-32
Very severe cyclonic storm	33-61
Super cyclonic storm	> 62

Accurate forecasting of storm surges is one of the requirements for storm preparedness because the greatest loss of life and property damage from a storm is due to surge. Numerical models have been used for this purpose in various parts of the world. In the Bay of Bengal, numerical modelling studies of Das (1972) and Flierl and Robinson (1972) were the earliest efforts. These studies came after the most disastrous cyclone in the history, the Bhola cyclone, which hit Bangladesh coast in 1970. Subsequent studies include Das et al. (1974), Johns and Ali (1980), Johns et al. (1981) and Dube et al. (1985). A detailed description of storm surge problem and numerical modelling studies on storm surges in the Bay of Bengal can be found in Murty et al. (1986), Murty and Flather (1994) and Dube et al. (1997). Later modelling works include Jain et al. (2006), Dube et al. (2009), and Dube et al. (2013). Various storm surge and extreme sea level characteristics and processes have been addressed

through numerical modelling in the Bay of Bengal. Coupled models have been used to study the storm surges including the effect of river systems (Johns and Ali, 1980; Dube et al., 1986; Agnihotri et al., 2006). The tide-surge interaction was studied by Johns et al. (1985) and Sinha et al. (2008). Extreme sea level return periods have been estimated by Jain et al. (2010), Sindhu and Unnikrishnan, (2012). A number of location specific studies include those of Dube et al. (2004) and Jain et al. (2006). Very early models have not included the coastal inundation; this has been accounted in later models (Flather, 1994; Madsen and Jakobsen, 2004). Coastal inundation studies were further extended to specific regions, for instance, Rao et al. (2013), Bhaskaran et al. (2014) and Lewis et al. (2013). Studies by Kim et al. (2008), Murty et al. (2014) and Krien et al. (2017) highlight the importance of wave set-up on surge heights.

The operational storm surge forecasting model for the North Indian Ocean is developed by IIT-Delhi. Presently, along with IIT-Delhi storm surge model, ADCIRC model has been used for storm surge forecast purposes in the North Indian Ocean by various organisations like IMD and INCOIS.

Only a limited number of studies have described the characteristics the storm surges and extreme sea levels in the Bay of Bengal using long-term tide-gauge observations (for example, Sundar et al., 1999; Unnikrishnan et al., 2004). Event-specific studies, which discusses the frequency characteristics of storm surges based on tide-gauge observations include Mehra et al. (2015).

1.6 Objectives

There exist a large number of numerical modelling studies on storm surges in the Bay of Bengal since the 1970s. However, only a very few studies have looked at the historical sea-level observations to characterise storm surges and extreme sea levels in the region. In the present thesis, an attempt has been made to understand characteristics of storm surges and associated sea levels in the Bay of Bengal through

observations. Also, numerical modelling results have been used to study tide-surge interaction. The research objectives of the present work are

- Description of past storm surge events based on tide-gauge data.
- Storm surge identification using satellite altimetry.
- Understanding and quantifying tide-surge interaction.
- Modelling the past storm surges to understand the characteristics of surges.

1.7 Structure of the thesis

The present thesis consists of five chapters. The first chapter is the introduction. The chapter describes briefly on various coastal hazards with detailed emphasis to cyclones and storm surges and an introduction to the study region, the Bay of Bengal.

Chapter 2 - Data and Methods

Chapter 2 starts with a brief overview of sea-level measurement techniques, tide poles to satellite altimetry. Further, analysis of sea-level data using harmonic analysis is discussed. The sea-level data used in the thesis, quality checks and reduction of sea level into various components (tide, MSL and residual sea level) are described in detail. The chapter also presents the implementation of the numerical model used in the present study—ADCIRC (ADvanced CIRculation model).

Chapter 3 - Description of storm surges and extreme high waters

A general description storm surge events observed in the tide gauges are presented in Chapter 3 along with tropical cyclones during the same period. The chapter also describes the storm surges observed in the Bay of Bengal from satellite altimeters. The last section of Chapter 3 discusses the characteristics of extreme high waters in the Bay of Bengal, including seasonality, interannual variability and long-term trends.

Chapter 4 - Tide-surge interaction

Tide-surge interaction is a significant phenomenon observed in shallow coastal waters. Interaction contributes significantly to total water level during a storm surge, suggesting that total water level is not a linear combination of tide and pure surge alone. In Chapter 4, tide-gauge observations were used to describe observed

interaction patterns at different locations. Further, a numerical model has been used to study tide-surge interaction during the Cyclone Aila in the shallow coastal regions of the head of Bay of Bengal.

Chapter 5 - Conclusions and future perspectives

Important findings of the present thesis are summarised in Chapter 5. The scope of further research on storm surges and extreme sea levels in the Bay of Bengal is also briefly discussed in this chapter.

Chapter 2

Data and methods

2.1 Introduction

Sea-level measurements are among the oldest ocean measurements for more than 100 years. The oldest sea-level record is from Amsterdam, starting in 1700 (Van Veen, 1954) and the longest record is from Stockholm, since 1774 (Ekman, 1988). In earlier days, sea-level information was used for navigation to facilitate maritime commerce and geodetic purposes. In modern times, sea-level measurements have a wide range of applications like coastal engineering, early warnings for tsunamis, studying storm surges, sea-level variability, sea-level rise, etc.

Tide gauges are maintained by local authorities in each country. For the scientific community, there is a need for a common platform to access the data, which provide data processed through common standards. When data are brought together from various local bodies, sea-level research can be undertaken on regional and global scale. Initiatives by the Permanent Service for Mean Sea Level (PSMSL), Global Sea Level Observing System (GLOSS) and University of Hawaii Sea Level Centre (UHSLC) serve towards data management globally including, coordination of various local bodies, data processing and distributing data routinely to all users. The PSMSL was established to serve as the global data bank for long-term sea-level information from tide gauges. The PSMSL is based at the National Oceanography Centre in Liverpool, U. K. The PSMSL data service has a history back to 1933 and it is one of the oldest geophysical data services (Holgate et al., 2013). At present, the PSMSL has data from more than 2100 tide gauges around the world (Rickards et al., 2015), which are provided by various national authorities. A quality control is done with sophisticated tools, and the data are made available freely for the scientific

community in the form of monthly and annual means through PSMSL website (http://www.psmsl.org/). The aim of GLOSS program is the establishment of high quality global and regional sea level networks for application to climate, oceanographic and coastal sea-level research. The GLOSS was established by the Intergovernmental Oceanographic Commission (IOC) of the United Nations Educational, Scientific and Cultural Organization (UNESCO) in 1985. Since 1990, the GLOSS maintains a network of tide-gauge stations, distributed globally, known as the GLOSS Core Network (GCN). As of 2010, the GCN has 290 tide-gauge stations (Figure 2.1). The UHSLC maintains research quality data in hourly and daily intervals. These data come through a thorough quality control and hence released within 1–2 years after the data collection. Another set of data, which are basic quality controlled, the fast delivery data, are released within 1–2 months of data collection. Although the UHSLC has many tide-gauge stations, the GCN is the main component. Real-time sea-level data are available at the Intergovernmental Oceanographic Commission's Sea Level Station Monitoring Facility (http://www.ioc-sealevelmonitoring.org), operated by the Flanders Marine Institute (VLIZ, Belgium).

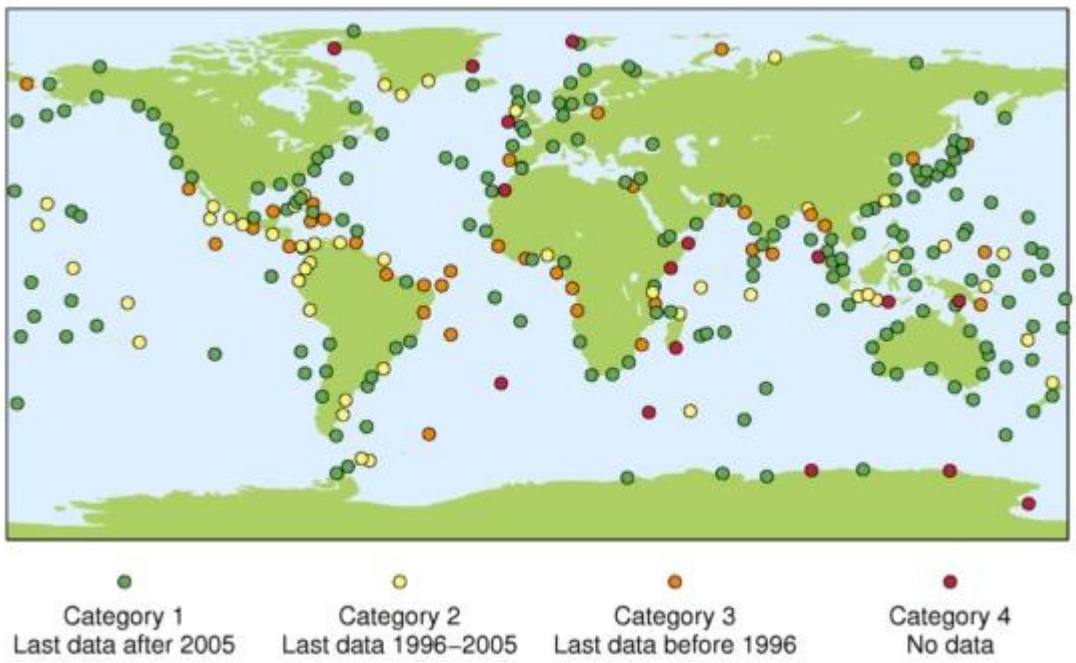

Figure 2.1 The GLOSS Core Network (GCN) of tide-gauge stations (290 stations as of 2010) (Source: http://www.gloss-sealevel.org/network_status/#.WV_znvmGPIU).

Until the emergence of satellite altimetry, sea level observations were limited to coasts and islands. Altimetry has given an opportunity to sample the sea level at a global scale, except in the latitudes poleward of 66°, which in turn resulted a lot of research in oceanography on meso-scale eddies, large-scale currents, global MSL variability and long-term trend, etc. Archiving, Validation and Interpretation of Satellite Oceanographic data (AVISO) website maintains the satellite-derived sea surface height data. Another organisation, the CTOH (Center for Topographic studies of the Ocean and Hydrosphere) contributes to the processing and management of the altimetric data for new scientific applications such as monitoring lake and river levels, the study of the continental snow and the cryosphere, flooded zones and coastal applications.

2.2 Measuring sea level

Sea-level measurements take different forms. The coastal sea-level measurement techniques have advanced much from a simple and easily-usable tide staffs (tide poles) to sophisticated radar gauges, improving the measurements in various ways including cost, accuracy, manpower requirement. Sea level measuring instruments are traditionally known as tide gauges. Since 1992, measurement of sea level started from space using instruments known as altimeters onboard satellites. Currently, tide gauge and satellite altimetry-based measurements are two different sea-level measurement methods. Former is in situ measurements while the latter uses remote sensing approach. Over the past, various tide gauges were developed, which vary in their working principle and instrumentation. Besides tide gauges at the coast, there are also bottom pressure recorders deployed in the open ocean which measure sea level.

2.2.1 Tide poles (staffs)

Tide poles (staffs) can be considered as a simple and basic form of a tide gauge. These are vertically mounted and graduated poles on which sea level can be read by an observer. Measurements are relative to a land based reference–‘benchmark’. The

measurement accuracy of tide pole is about 0.02 m in calm conditions (Pugh and Woodworth, 2014). Tide poles are easy to use and cheap. Since tide poles are not automated, they are not suitable for long-term surveys.

2.2.2 Stilling-well gauges

Stilling-well gauges represent the start of a modern era of sea-level measurements with its self-recording system. The first such gauge became functional at Sheerness, the U.K. in 1831 (Pugh and Woodworth, 2014). Fluctuations of a float, sitting inside the stilling well, are recorded on a chart (Figure 2.2). Stilling well filters out the effects of waves and protects float from the weather. Stilling well provides a better sea-level measurement appropriate for scientific research.

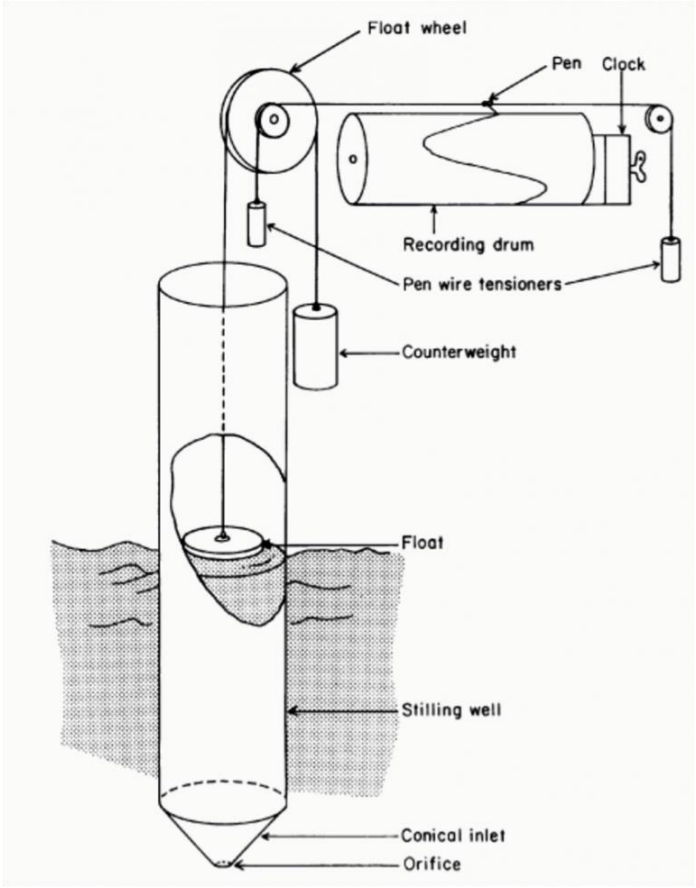

Figure 2.2 A schematic diagram of stilling well tide gauge (Source: IOC, 1985).

2.2.3 Pressure gauges

Pressure gauges measure total pressure at a depth. The measured pressure has atmospheric and water column pressure components. The hydrostatic relationship can be used to convert the measured pressure (P) to sea level (h).

$$P=P_a+h\rho g \quad \textbf{(2.1)}$$

$$h= (P - P_a) / \rho g \quad \textbf{(2.2)}$$

where P_a is the atmospheric pressure at the water surface, ρ is the mean density of overlying water column and g is the acceleration due to gravity. Atmospheric pressure, seawater density and acceleration due to gravity are required to determine the water depth. Pressure based gauges include Pneumatic tide gauges, mechanical strain gauges and quartz gauges. Bottom pressure gauges (BPRs) also work on the same principle, which can be operated at depths of more than 4000 m. BPRs are used for tsunami warning purposes to study the non-tidal signals in the open ocean.

2.2.4 Radar and acoustic gauges

Radar and acoustic gauges measure the travel time of electromagnetic and sound signals respectively from a source to sea surface and back, which is used to determine the distance between the source and sea surface. For acoustic gauges, the velocity of sound is significantly affected by changes in air temperature and humidity, and corrections for the same are necessary for accurate sea-level measurements. Radar gauges are relatively low-cost instruments, reliable and easy to operate and maintain.

2.2.5 GPS buoys

Buoys equipped with global positioning system (GPS) can determine the sea levels. This is a less common approach (Pugh and Woodworth, 2014). The advantages of GPS buoys include portability and they can be used in remote locations. GPS buoys measure the sea level relative to the absolute reference frame. GPS buoys are mainly used for calibrating satellite altimetry measurements. Some practical limitations of

these GPS buoys include battery life, restricted operation in rough seas and data processing issues.

2.2.6 Satellite altimetry

Satellite altimetry is a technique by which sea surface height is measured using altimeters on board. Two measurements are involved in calculating the sea surface height. First, the distance between satellite and sea surface, the satellite range (R). The two-way travel time of radar pulses is used to determine the distance. Second, the precise position of the satellite, the satellite altitude (S) with respect to a reference ellipsoid is needed. Figure 2.3 shows the schematic of satellite altimetry.

Height of sea surface relative to reference ellipsoid is

$$H = S - R \tag{2.3}$$

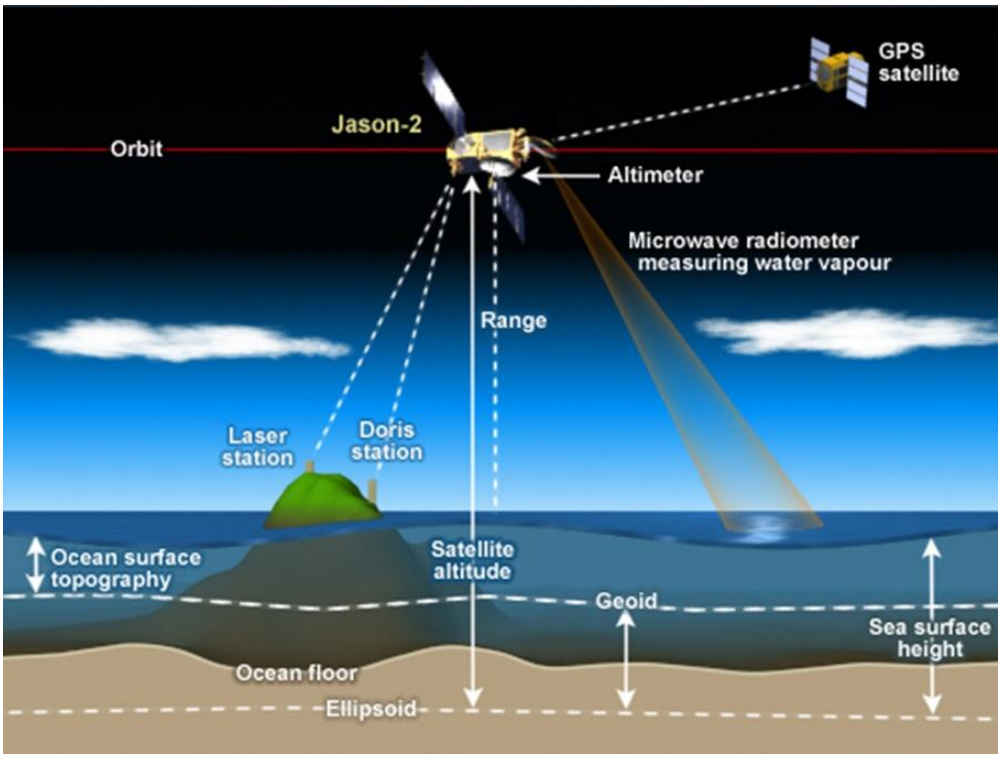

Figure 2.3 The principle of satellite altimetry (Source: https://www.star.nesdis.noaa.gov/sod/lsa/AltBathy/).

2.3 Sea-level components

Sea level at a location can be decomposed into mean sea level (Z_0), astronomical tide (T_t) and residual sea level (R_t).

$$X_t = Z_0 + T_t + R_t \quad \textbf{(2.4)}$$

Z_0 is the average sea level calculated over an extended period such as one month or one year. The astronomical tide at a location can be predicted as the sum of a number of harmonic constituents.

$$T_t = \sum_{i=1}^{n} H_i \cos(\sigma_i t - \phi_i) \quad \textbf{(2.5)}$$

where H_i is the amplitude, σ_i, the frequency and ϕ_i, the phase lag of the constituents ($i=1, 2,.. n$). n is the number of constituents. H_i and ϕ_i are determined through harmonic analysis of sea-level time series, which uses the least-square method. The tidal component is determined first and subtracted from sea level to obtain residual sea level.

2.3.1 Harmonic analysis

Tides can be represented by a set of harmonic constituents (Equation (2.5)). In the harmonic analysis technique which uses least square fitting, sinusoidal components of specific tidal frequencies are extracted. The Equation (2.5) can be rewritten as

$$T_t = \sum_{i=1}^{n} A_i \cos(\sigma_i t) + B_i \sin(\sigma_i t) \quad \textbf{(2.6)}$$

where

$$A_i = H_i \sin(\phi_i) \quad \textbf{(2.7)}$$

$$B_i = H_i \cos(\phi_i) \quad \textbf{(2.8)}$$

and

$$H_i = \sqrt{(A_i^2 + B_i^2)} \quad \textbf{(2.9)}$$

$$\phi_i = tan^{-1}\left(\frac{B_i}{A_i}\right) \quad \textbf{(2.10)}$$

least square requires that

$$\sum R_t^2 = X_t - T_t = 0 \quad \textbf{(2.11)}$$

this is satisfied by

$$\frac{\partial R^2}{\partial A} = 0, \frac{\partial R^2}{\partial B} = 0. \quad \textbf{(2.12)}$$

Finally, this will result in 2n equations and unknowns, which can be solved through matrix method.

2.4 Sea-level data used in the present study

2.4.1 Tide-gauge data

Hourly tide-gauge data from three ports, Chennai, Visakhapatnam and Paradip along the east coast of India and data from the station Hiron Point, at the head of the Bay (Figure 2.4a), were used in the present study. The hourly data along the Indian coast were obtained from the Survey of India (SOI). The Geodetic and Research Branch, SOI maintains tide gauges at various ports along the Indian coast. The oldest sea-level measurements were made at Mumbai since 1877. The gauges operated by SOI are traditional mechanical float gauges, and some are pressure-sensor gauges (Nagarajan et al., 2006). Tide-gauge data at Hiron Point were downloaded from the research quality data archive of the UHSLC. Figure 2.4 gives the tide-gauge location and duration of the data used in the present study. 34 years (1974-2007) of hourly data were used in the present study.

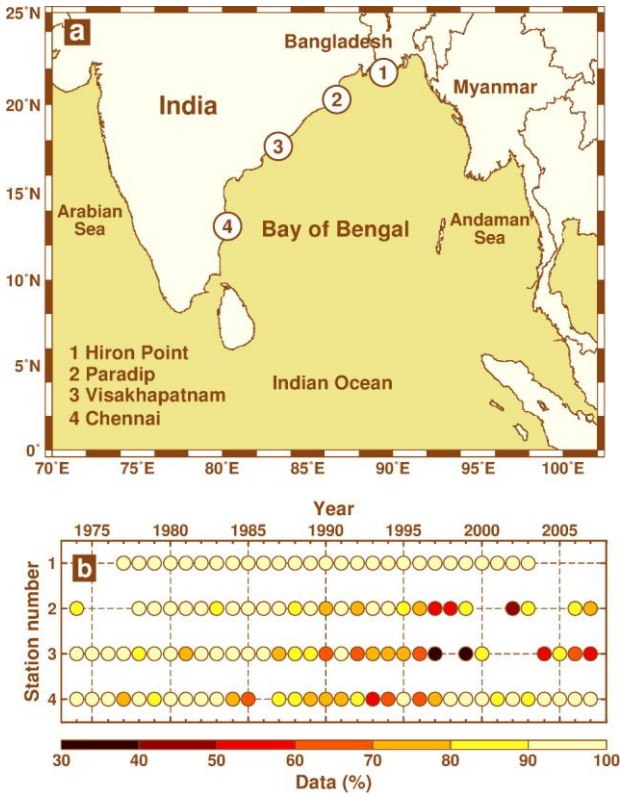

Figure 2.4 a) Locations of tide gauge stations and b) tide-gauge data used in the present study. The data availability (in percentage) is shown in colour code.

2.4.1.1 Data quality checks

Residual sea levels were obtained by removing MSL and astronomical tide components (harmonic analysis) from the measured sea level. The harmonic analysis was done for each year. The residual sea-level data were carefully checked for various errors such as datum shifts, timing errors and spikes (Figure 2.5). Timing error associated with errors in clocks, which results in quasi-tidal oscillations in the residual signal (Figure 2.5c). The raw sea-level data were then corrected for these errors and the harmonic analysis was repeated for the quality checked data. The harmonic analysis was carried out using the Tidal Analysis Software Kit (TASK)(Bell et al., 1999), with a standard set of 62 tidal constituents (Appendix A). These constituents include M_m, M_{sf} and M_f and those having seasonal periods such as S_a and S_{sa}.

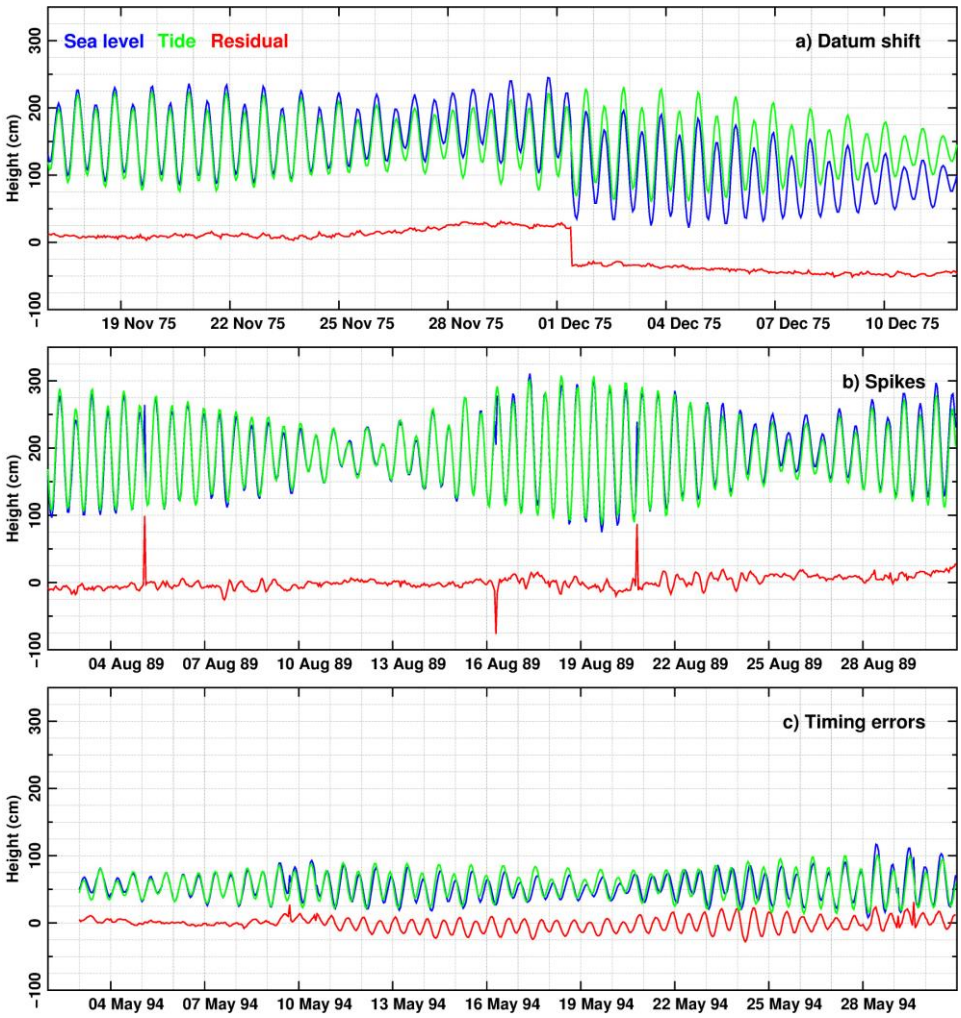

Figure 2.5 Examples of various kinds of errors in the tide-gauge data, a) datum shifts, b) spikes and c) timing errors.

2.4.2 Altimeter data

1 Hz (6–7 km) along-track spatially filtered (20 km–3 points) sea-level anomalies (SLA), distributed by the CTOH, France were used. These data were prepared with the X-TRACK software (Roblou et al., 2007; Roblou et al., 2011). The objective of this processor is to improve both the quantity and quality of altimeter sea surface measurements in coastal regions by minimising the loss of data during the correction phase and by using improved local modelling of tidal and short-period atmospheric forcing. The data have been widely used in several oceanographic studies (Melet et al., 2010; Liu et al., 2012; Birol and Delebecque, 2014). Various geophysical and

environmental corrections include ionospheric, dry tropospheric, wet tropospheric corrections, tides (including solid earth tide, pole tide and loading tide), sea state bias (SSB) and dynamic atmospheric corrections (DAC). SLA is calculated using the formula given below.

$$SLA = SSH - \{iono - dry\ tropo - wet\ tropo - solid\ earth\ tide - pole\ tide - loading\ tide - SSB - tide - DAC\} - MSSH \quad \textbf{(2.13)}$$

where SSH is the sea surface height, observed by the satellite and MSSH is the mean sea surface height.

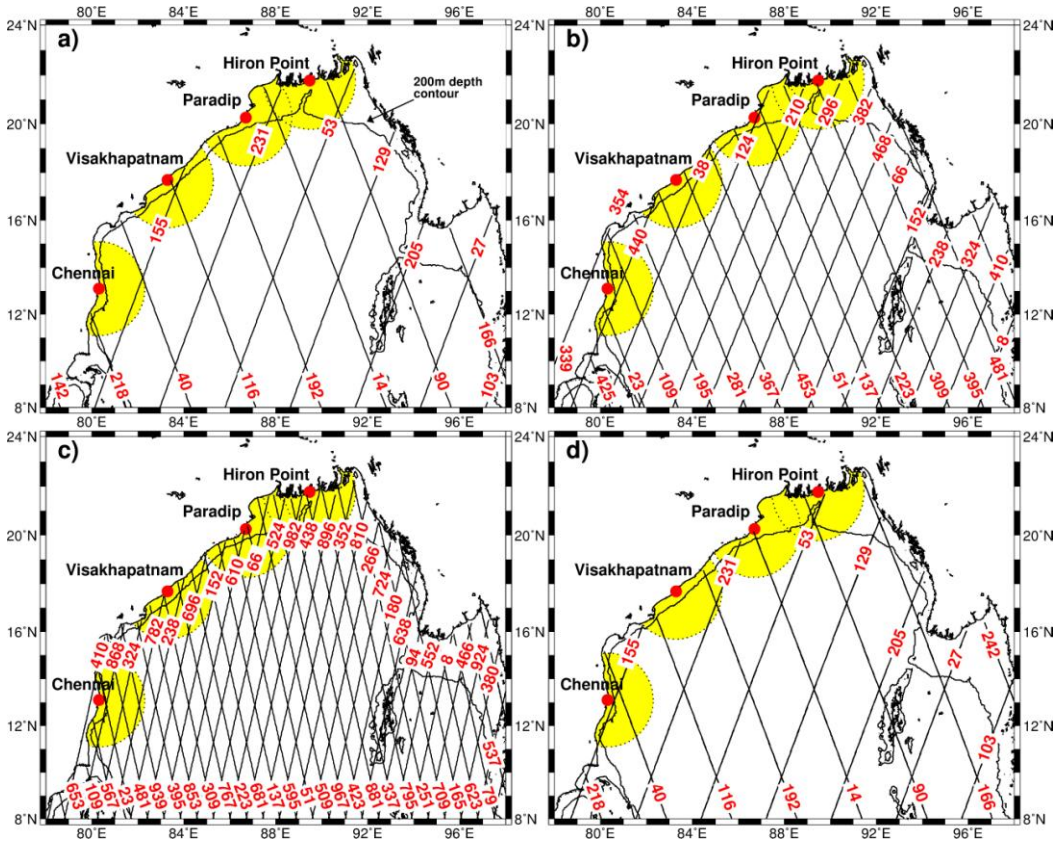

Figure 2.6 Satellite ground tracks of a) TOPEX/Poseidon (same for Jason-1), b) Geosat Follow-On, c) ENVISAT and d) TOPEX/Poseidon interleaved missions. Red circles mark locations of tide gauges used in the present study. Numerals represent satellite track number. 2° circles around the tide-gauge locations are also shown. Satellite tracks within the circle, for respective tide guages, are used for identification of surge events.

Along-track data from T/P+J1+J2 (TOPEX/Poseidon, Jason-1 and Jason-2 merged data), GFO (Geosat Follow-On), ENVISAT (ENVIronmental SATellite) and T/PN (T/P interleaved) missions were used in the present study (Table 2.1). The ground tracks of each satellite over the Bay of Bengal region are shown in Figure 2.6. T/P mission started in 1992. The satellite had a repeat time of nearly 10 days. J-1 was launched in 2001 on the same T/P orbit. The ground tracks of T/P and J-1 are wide, about 315 km at the equator. In 2002, T/P was moved to new ground tracks in tandem with J-1 until the end of the T/P mission in 2006. GFO was launched in 1998, and the mission continued till 2008. The repeat time of GFO was 17 days, and the ground tracks were separated by 160 km at the equator. The ENVISAT mission was carried out from 2002 to 2012. Repeat period of ENVISAT was 35 days and the ground track separation was 90 km.

2.4.2.1 Dynamic atmospheric correction (DAC)

Satellite measurements are affected by the oceans' response to atmospheric pressure and wind forcing. DAC is the correction term which accounts for pressure and wind effects. The high frequency (< 20 days) ocean response to atmospheric pressure and wind is corrected using the T-UGOm 2D shallow water model outputs (Carrère and Lyard, 2003), while the inverse barometric correction is applied for lower frequencies (> 20 days). In the present study, DAC corrections are retained in SLA to get consistent results with tide-gauge measurements.

Table 2.1 Altimeter data used in the present study.

Satellite	Period	Sampling interval (days)
TOPEX/Poseidon (T/P)	1992- 2006	10
Jason-1 (J-1)	2001-2013	
TOPEX/Poseidon Interleaved (T/P)	2002-2006	
Geosat Follow-On (GFO)	1998-2008	17
ENVIronmental SATellite (ENVISAT)	2002-2012	35

2.5 Meteorological data

The tracks of cyclones and depressions formed over the Bay of Bengal were extracted from the Cyclone eAtlas-IMD (online version available at the URL: www.rmcchennaieatlas.tn.nic.in), developed by the India Meteorological Department (IMD). Surface wind fields and mean sea-level pressure from NCEP/NCAR reanalysis (Kalnay et al., 1996) were used to get the evolution of the atmospheric fields during specific storm surge events.

2.6 Numerical model

ADCIRC (Advanced Circulation Model for Oceanic, Coastal, and Estuarine Waters, Two-Dimensional Depth-Integrated) model (Luettich et al., 1992) (Version 50.13) was used in the present study. Various simulations were made to study tide-surge interaction characteristics during the Cyclone Aila at the head of the Bay. ADCIRC uses vertically integrated shallow water equations that are solved in generalised wave continuity equation form. The model uses triangular grids of varying size, which allows using finer resolution near the coast (to better represent the complex coastline) and coarse triangles in the open ocean. This, in turn, increases the model efficiency by being computationally less expensive. ADCIRC has a wide range of application including modelling of tides, storm surges and coastal inundation, etc.

The governing equations of ADCIRC include the continuity equation:

$$\frac{\partial^2 \zeta}{\partial t^2} + \tau_0 \frac{\partial \zeta}{\partial t} + \frac{\partial \tilde{J}_x}{\partial x} + \frac{\partial \tilde{J}_y}{\partial y} - UH \frac{\partial \tau_0}{\partial x} - VH \frac{\partial \tau_0}{\partial y} = 0 \qquad \textbf{(2.14)}$$

where:

$$\tilde{J}_x = -Q_x\frac{\partial U}{\partial x} - Q_y\frac{\partial U}{\partial y} + fQ_y - \frac{g}{2}\frac{\partial \zeta^2}{\partial x} - gH\frac{\partial}{\partial x}\left[\frac{P_s}{g\rho_0} - \alpha\eta\right] + \frac{\tau_{sx,winds} + \tau_{sx,winds} - \tau_{bx}}{\rho_0} + (M_x - D_x) + U\frac{\partial \zeta}{\partial t} + \tau_0 Q_x - gH\frac{\partial \zeta}{\partial x}, \quad \textbf{(2.15)}$$

$$\tilde{J}_y = -Q_x\frac{\partial V}{\partial x} - Q_y\frac{\partial V}{\partial y} + fQ_x - \frac{g}{2}\frac{\partial \zeta^2}{\partial y} - gH\frac{\partial}{\partial y}\left[\frac{P_s}{g\rho_0} - \alpha\eta\right] + \frac{\tau_{sy,winds} + \tau_{sy,winds} - \tau_{by}}{\rho_0} + \left(M_y - D_y\right) + V\frac{\partial \zeta}{\partial t} + \tau_0 Q_y - gH\frac{\partial \zeta}{\partial y}, \quad \textbf{(2.16)}$$

and momentum equations:

$$\frac{\partial U}{\partial t} + U\frac{\partial U}{\partial x} + V\frac{\partial U}{\partial y} - fV = -g\frac{\partial}{\partial x}\left[\zeta + \frac{P_s}{g\rho_0} - \alpha\eta\right] + \frac{\tau_{sx,winds} + \tau_{sx,winds} - \tau_{bx}}{\rho_0 H} + \frac{M_x - D_x}{H}, \quad \textbf{(2.17)}$$

$$\frac{\partial V}{\partial t} + U\frac{\partial V}{\partial x} + V\frac{\partial V}{\partial y} - fU = -g\frac{\partial}{\partial y}\left[\zeta + \frac{P_s}{g\rho_0} - \alpha\eta\right] + \frac{\tau_{sy,winds} + \tau_{sy,winds} - \tau_{xy}}{\rho_0 H} + \frac{M_y - D_y}{H}, \quad \textbf{(2.18)}$$

where $H = \zeta + h$ is the total water depth, ζ is the change in water elevation above mean surface, h is the ocean depth. U and V are depth-averaged currents in the x and y directions. f is the Coriolis parameter. $Q_x = HU$ and $Q_y = HV$ are fluxes per unit

width. g is acceleration due to gravity. P_s is the surface atmospheric pressure. ρ_0 is the density of water. η Newtonian equilibrium tidal potential and α is the effective earth elasticity factor. $\tau_{s,winds}$ and $\tau_{s,waves}$ are surface stresses due to winds and waves. τ_b is bottom stress. M_x and M_y are lateral stress gradients. D_x and D_y are momentum dispersion terms. τ_0 is a numerical parameter that optimizes the phase propagation properties.

2.6.1 Mesh generation and model setup

The ADCIRC requires various sets of inputs for storm surge and total water level simulations (Figure 2.7). These inputs include

- Finite element mesh with bathymetric information
- Boundary conditions, including forcing boundaries and land boundaries
- Meteorological forcing (wind velocities and atmospheric pressures)

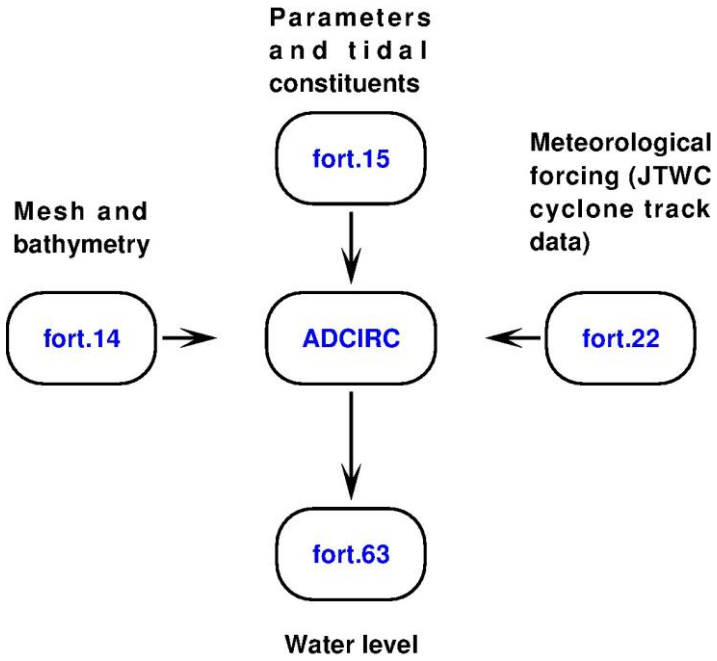

Figure 2.7 A flow chart depicting the steps involved in ADCIRC water level simulation.

Different outputs from ADCIRC model include water elevations and depth-averaged velocities. The SMS (Surface water Modelling System) software (version 11.2.12) was used for creating a triangular mesh for the ADCRIC for the Bay of Bengal. The bathymetric data used in the present research is the new bathymetry data from Krien et al. (2016). The data incorporate digitised data from estuaries and rivers adjoining the head of the Bay. Krien et al. (2016) reported improvements in the simulation of tides using this data. Depths are considered positive and heights are considered negative in ADCRIC. The criteria used to create the mesh were based on Lyard et al. (2006), which includes

- Wavelength criterion

  This mesh size criterion is based on wavelength to grid size ratio. One cycle of the chosen wave will be represented with the number of grid points equal to the ratio. A typical value of this ratio ranges from 15-30. Better resolution can be achieved with a larger ratio. With this criterion, shallow water regions will have a fine resolution.

  $$\Delta x_1 = T\sqrt{gh}/15 \quad \textbf{(2.19)}$$

  where Δx_1 is the mesh size in metre, T the period of smallest wavelength considered (3 hr in the present case) in seconds, g is acceleration due to gravity and h is the depth in metres.

- Bathymetry gradient criterion

  This criterion will account the high bathymetric gradients, with high model resolution over shelf break.

  $$\Delta x_2 = 2\Pi h/15\nabla h \quad \textbf{(2.20)}$$

  where Δx_2 is the mesh size in metre and ∇h is the bathymetry gradient.

Final mesh size function is designed by accounting the required minimum (500 m) and maximum (10000 m) bounds of the mesh size as

$$\Delta x = max\ (500,\ min\ (10000,\ min\ (\Delta x_1,\ \Delta x_2))) \quad \textbf{(2.21)}$$

The mesh created (Figure 2.8a) has approximately 65k elements with grid resolution of about 500 m near the coast and up to 10000 m near the open boundary. The mesh spacing and depths are shown in Figures 2.8b and c. Finally, the finite element mesh and bathymetric information were stored into a file (fort.14) in the standard ADCIRC format. Appendix B gives the fort.14 file used in the present study.

The fort.15 is the standard file for providing various model parameters and boundary conditions. Five major tidal constituents prescribed at the open boundary are M_2 S_2, K_1, O_1 and N_2 (Table 2.2). The amplitude and phase of these constituents were obtained from the output of global tidal model FES2012 (Finite Element Solution) (Carrère et al., 2012). A time step of 10 s was set to run the model. The model was set to be completely non-linear by including advection and finite amplitude terms. The bottom friction relation to drag coefficient is quadratic.

$$\tau_b = C_d \frac{\sqrt{u^2 + v^2}}{H} \quad \textbf{(2.22)}$$

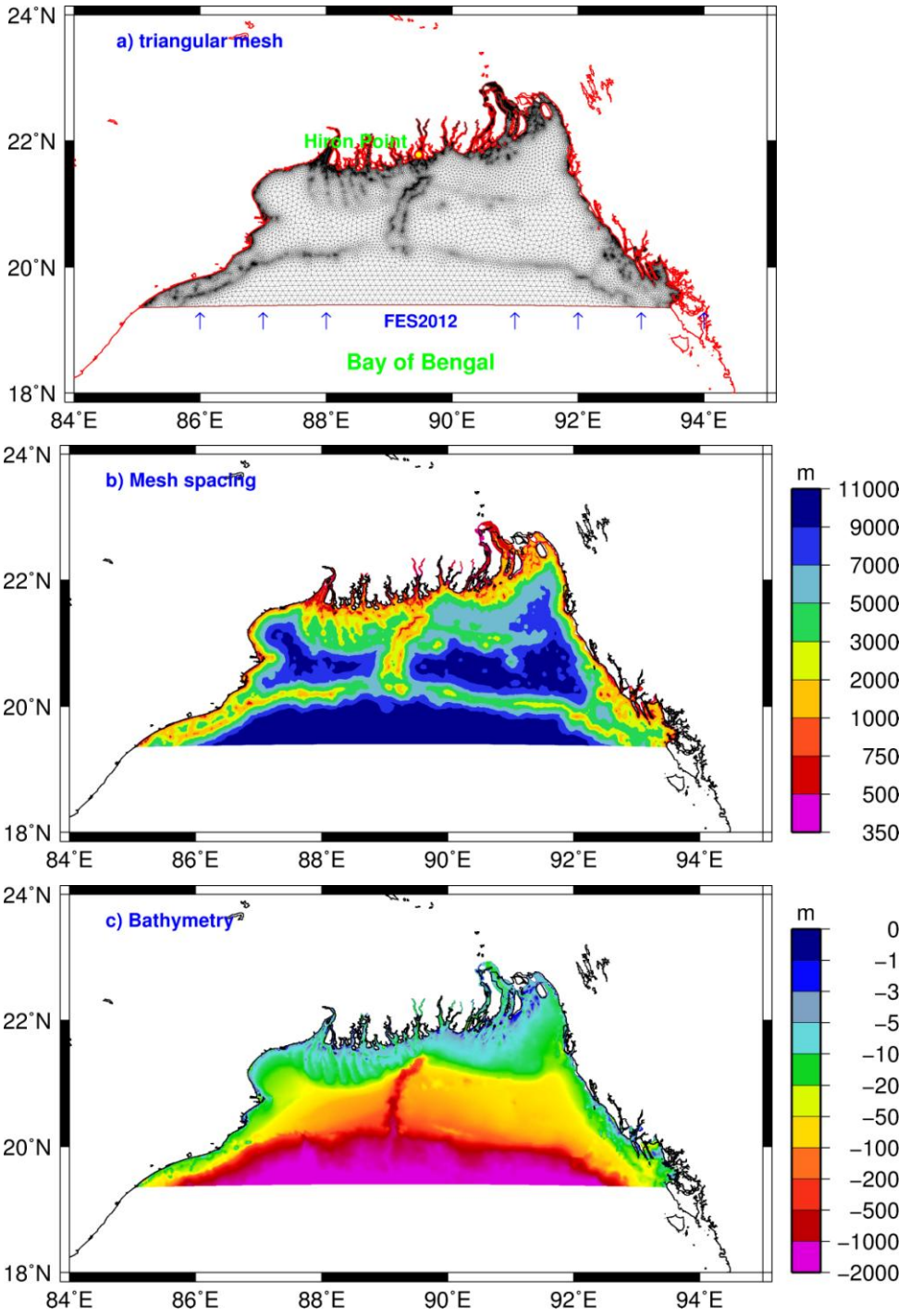

Figure 2.8 a) The unstructured mesh used in the present study, b) mesh resolution and c) bathymetry.

where C_d is the drag coefficient, u and v are depth-averaged velocities and H is the total water depth. Bottom friction coefficient was given as 0.0028. The value of horizontal eddy viscosity was taken as 80 m^2/s. Minimum water depth in the model domain was set to 4 m. Meteorological data required for storm surge simulation can be incorporated with different formats. The format identifier must be set in the fort.15 file and meteorological data can be stored in a standard file, fort.22. In the present study, meteorological data were prescribed in the ATCF (Automated Tropical Cyclone Forecast System) best track format, this corresponds to the format identifier in the fort.15 file as NWS=8. The output data required can be specified in the fort.15 file. Water surface elevations are the output of interest in the present study. The standard file for water surface elevations in ADCIRC is fort.63. Appendix C gives the fort.15 file used in the present study.

Table 2.2 The five tidal constituents, obtained from FES2012, used to force the ADCIRC model.

Constituent		Period (hr)	Frequency (rad/s)
Symbol	Name		
M_2	Principal Lunar Semidiurnal	12.42	0.000140518902509
S_2	Principal Solar Semidiurnal	12.00	0.000145444104333
K_1	Luni-solar diurnal	23.93	0.000072921158358
O_1	Principal Lunar Diurnal	25.82	0.000067597744151
N_2	Larger Lunar Elliptic	12.66	0.000137879699487

In the present thesis, the tide-surge interaction was studied by simulation of surges for the Cyclone Aila, which occurred in May, 2009. A parametric cyclone model by developed by Jelesnianski and Taylor (1973) was used to construct the cyclone winds. Cyclone pressure fields were based on Holland (1980). Jelesnianski model has been widely used for generation of cyclone wind fields in the Bay of Bengal. An improved version of the parametric model (Murty et al., 2016) was used in the present study. The inputs for this parametric model were cyclone core pressure (P_c), maximum wind

speed (V_{max}) and radius of maximum winds (R_{max}). These data were obtained from JTWC (Joint Typhoon Warning Centre, Pearl Harbor, Hawaii) best track archive, in 6 hourly intervals, except R_{max}. R_{max} was calculated using equation given by Knaff and Zehr (2007).

$$R_{max} = 66.785 – (0.09102\ V_{max}) + 1.0619\ (\varphi\text{-}25) \quad \textbf{(2.23)}$$

where φ is the latitude.

Wind speed constructed using the formula

$$W = V_{max}\ \left(2r\ R_{max} / (r^2 + R_{max}^2\ )\right)^{3/5} \quad \textbf{(2.24)}$$

where r is the distance from cyclone centre to a point.
A correction was applied to account forward motion of the cyclone

$$W_f = V_f\ \left(r\ R_{max} / (\ r + R_{max})\right) \quad \textbf{(2.25)}$$

where V_f is the translation velocity of the cyclone.
Wind inflow angle (β) corrections were applied based on Queensland Government's Ocean Hazards Assessment (2001)

$$\beta = \begin{cases} 10\ (r/R_{max}\ ) & 0 \le r < R_{max} \\ 10 + 75((r/R_{max}\ ) - 1) & R_{max} \le r < 1.2\ R_{max} \\ 25 & r \ge 1.2\ R_{max} \end{cases} \quad \textbf{(2.26)}$$

Pressure at a point (P) was calculated using Holland equations (Holland, 1980)

$$P = P_c + (P_{env} – P_c)\ exp\ (-(R_{max}/r)^B) / \rho_w g \quad \textbf{(2.27)}$$

where P_c is the pressure at the centre of the cyclone. P_{env} is the environmental pressure, which is set to 1013 hPa. ρ_w is the density of water. g is then acceleration due to gravity.

B is defined as

$$B = \rho e V^2_{max} / (P_{env} - P_c) \quad \textbf{(2.28)}$$

where ρ is the density of air and e is Euler's number.

2.7 Analysis of extreme high water levels

Extreme sea levels are studied in terms of percentiles of hourly data (Woodworth and Blackman, 2004). For this study, sea-level data from Cox's Bazaar (Figure 2.9a) were also used in addition to the four stations, which are mentioned in Section 2.4.1. Cox's Bazaar data were for the period 1983-2006. The source of Cox's Bazaar data is again the research quality data archive of UHSLC. For all stations, the years that were essentially complete with 50% or more data (Figure 2.9b) were used. A percentile of an ordered data (sorted in the order smallest to largest) represents the value below which certain percentage of data exists. For example, 75% of the data are found below the value which corresponds to the 75th percentile. 50th percentile corresponds to the median of the data. Percentile (N_p) can be calculated as

$$N_p=(p/100)*n \quad \textbf{(2.29)}$$

where n is number of data and p is percent of data. Figure 2.10 demonstrates annual percentile time series derived from hourly sea-level data.

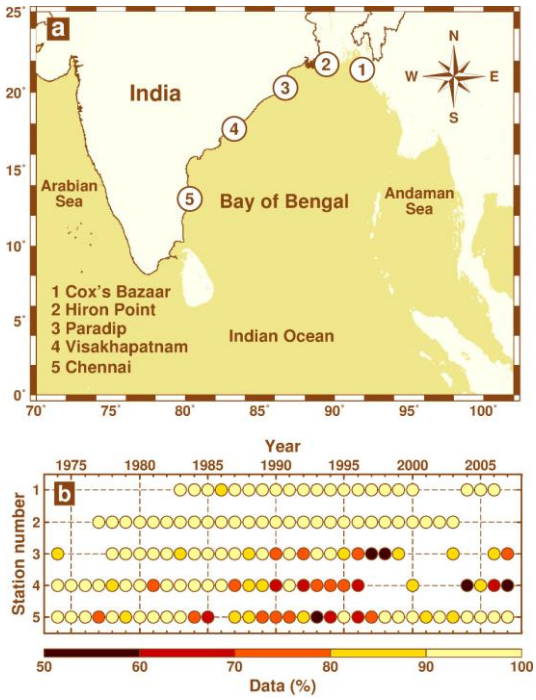

Figure 2.9 a) Locations of tide gauge stations in the Bay of Bengal. b) Tide gauge data used to study extreme sea levels. The colour scale shows the data availability in percentage.

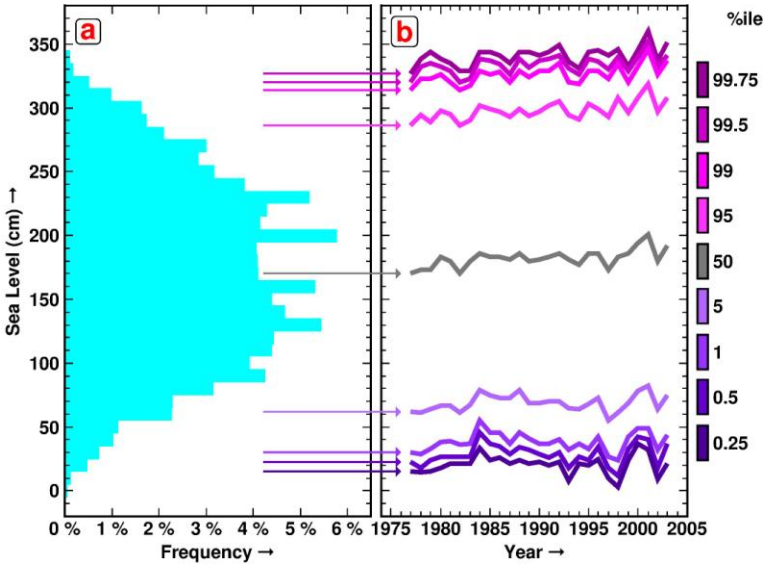

Figure 2.10 a) Frequency distribution of hourly sea-level data. b) Time series of annual percentiles.

Percentile time series were constructed for the 99.9, 99.75, 99.5, 99.0, 95.0 and 50th percentiles for each station by combining corresponding percentiles from each year. A second set of percentile time series were also constructed, which were reduced to their median (50th percentiles subtracted). This reduction corresponds approximately to the removal of MSL for each year. The seasonality in the extreme high waters was studied using percentiles computed month-wise. The mean seasonal cycle was estimated from month-wise percentiles by averaging the percentiles over each month (months with at least 50% data were included). Standard deviations were calculated to represent the month-wise variability.

To study the influence of regional climate on the inter-annual variability of extreme high waters, a linear-correlation analysis was carried out between extreme high waters and the indices of modes of regional climate, such as the Indian Ocean Dipole (IOD) and El Niño Southern Oscillation (ENSO). The Dipole Mode Index (DMI) and the Southern Oscillation Index (SOI) were used as indicators of IOD and ENSO respectively. The DMI and the SOI were obtained from the websites of the Japan Agency for Marine-Earth Science and Technology and the National Oceanic and Atmospheric Administration respectively. The DMI is based on the east-west sea surface temperature anomaly difference across the tropical Indian Ocean (Saji et al., 1999). A positive (negative) DMI is referred as positive (negative) IOD. The SOI is based on sea level pressure difference between Tahiti and Darwin (Trenberth, 1984). During El Niño (La Niña) the SOI is negative (positive). De-trended monthly DMI and SOI, averaged over January–December months were used to construct annual DMI and SOI. De-trended time series of sea level percentiles were used for correlation analysis. The significance of the correlation coefficients was determined through a Student's *t*-test. The correlations mentioned as significant for those values exceed 95% confidence limits in the *t*-test. Serial correlations in the sea level percentiles were observed to be insignificant, in spite of some correlation being expected because of the perigean tidal contribution to extreme high waters in a semi-diurnal environment. It could be possible that the variability in the extremes due to the surge component masks such serial correlation in the data. Hence, the degrees of

freedom for the *t*-test were approximated as *N-2*, where *N* is the sample size. At times the IOD and the ENSO phenomena occur simultaneously, and the indices have an influence on each of them. Partial correlation analysis was to explore the relative impact of each climate index to the extremes. Partial correlation ($R_{SL,DMI \cdot SOI}$) of sea level (SL) and DMI adjusted for SOI can be written in terms of simple correlation coefficients (Saji and Yamagata, 2003).

$$R_{SL,DMI \cdot SOI} = R_{SL,DMI} - R_{SL,SOI}\, R_{DMI,SOI} \Big/ \sqrt{(1 - R^2_{SL,SOI})(1 - R^2_{DMI,SOI})} \qquad \textbf{(2.30)}$$

Subscripts (DMI and SOI) can be interchanged to obtain a partial correlation of sea level and SOI adjusted for DMI. The significance of the correlation coefficient can be evaluated with the same *t*-test with degrees of freedom *N-2-K*, where *K* is the number of variables being partialled out (*K* = 1 for the present case).

The long-term trends in the sea level percentiles were computed using a linear-least square fit. The significance of the trends was examined using the *t*-test at the 95% level of confidence. Results are presented with an emphasis on 99th percentile series as the higher percentiles (for example, 99.9th percentiles) are more likely to be influenced by data errors (Woodworth and Blackman, 2004), but I also discussed annual maximum water levels and examined the consistency among various percentiles.

Chapter 3

Description of storm surges and extreme high waters

The present chapter has four sections. A short description of tropical cyclones during the period of 1974–2007 is presented in Section 3.1. In Section 3.2, storm surges recorded in tide gauges in the Bay of Bengal are described. The storm surges in the Bay of Bengal identified from satellite altimeters are discussed in Section 3.3. The final section (Section 3.4), discusses the characteristics and evolution of extreme high waters along the east coast of India and at the head of Bay of Bengal.

3.1 Tropical cyclones during 1974–2007

Tropical cyclones are intense low-pressure systems formed over the oceans which cause damage to coastal populations due to strong winds, heavy rainfall, storm surges and high waves, caused by them. Tropical cyclones are relatively less intense and less frequent in the Bay of Bengal compared to the systems in other tropical oceanic basins in the Atlantic and Pacific. However, the coastal regions of the Bay of Bengal had experienced some of the heaviest destructions from these natural phenomena. A brief description of tropical cyclone statistics in the Bay of Bengal is presented in this section using data obtained from the Cyclone eAtlas-IMD. The e-Atlas prepared by the IMD provides information on tracks of cyclones and depressions (C and Ds) over the north Indian Ocean during the period from 1891 to the latest year. Two output types from eAtlas are a display of tracks of C and Ds and statistical information on the formation, dissipation, movement, speed, direction of movement, recurvature, coastal crossing and intensification of C and Ds.

The Bay of Bengal experienced 108 tropical cyclones (wind speed 18 m/s and above) during 1974–2007, of which 90 cyclones (83.3%) crossed the coast. 84 out of

the 90 systems had the intensity of a cyclone or more while crossing the coast. A detailed statistics of cyclonic systems are given in Table 3.1. Statistics are presented for the periods 1974–2007 and 1891-2007. The average number of cyclones for 1974–2007 was 3.2, which is less than the long-term average (4.1) of cyclones in the Bay of Bengal. Table 3.1 also shows that the percentage of landfalling cyclones with a minimum intensity of CS was higher during 1974–2007 compared to that of l891-2007.

Table 3.1 Statistics of tropical cyclones in the Bay of Bengal, prepared using the Cyclone eAtlas-IMD.

1974-2007			
	Frequency		
	Total	Landfalling	
		Total	With min. intensity of CS
SCS+CS	108	90	84
Average	3.2	2.65	2.47
% (Total)	-	83.33	77.78
% (Landfalling)	-	-	92.31
1891-2007			
	Frequency		
	Total	Landfalling	
		Total	With min. intensity of CS
SCS+CS	481	425	365
Average	4.1	3.6	3.1
% (total)	-	88.36	75.88
% (Landfalling)	-	-	85.88

Figure 3.1a shows the spatial frequency of cyclones in the Bay of Bengal. Certain regions of high cyclonic activity (southwest and northern regions of the Bay) can be

noticed in the spatial distribution of cyclone frequency. Considering coastal regions, the east coast of India and the coast of Bangladesh experience frequent cyclones. Figure 3.1a also shows the location of four tide gauges in the major cyclone affected coasts. The cyclones have a bimodal structure in the monthly frequency distribution, which is evident during the 1974–2007 period (Figure 3.1b). The month-wise distribution shows cyclones are highest during November followed by October and May (Figure 3.1 b). There is a declining trend (0.08 cyclones/year) in the annual frequency of cyclones during the period 1974-2007 (Figure 3.1c). The decrease in the frequency of cyclones during recent decades has been reported (Niyas et al., 2009) the decrease started since 1960 (Mohapatra et al., 2012). This is attributed to the multi-decadal oscillations in the frequency of cyclones.

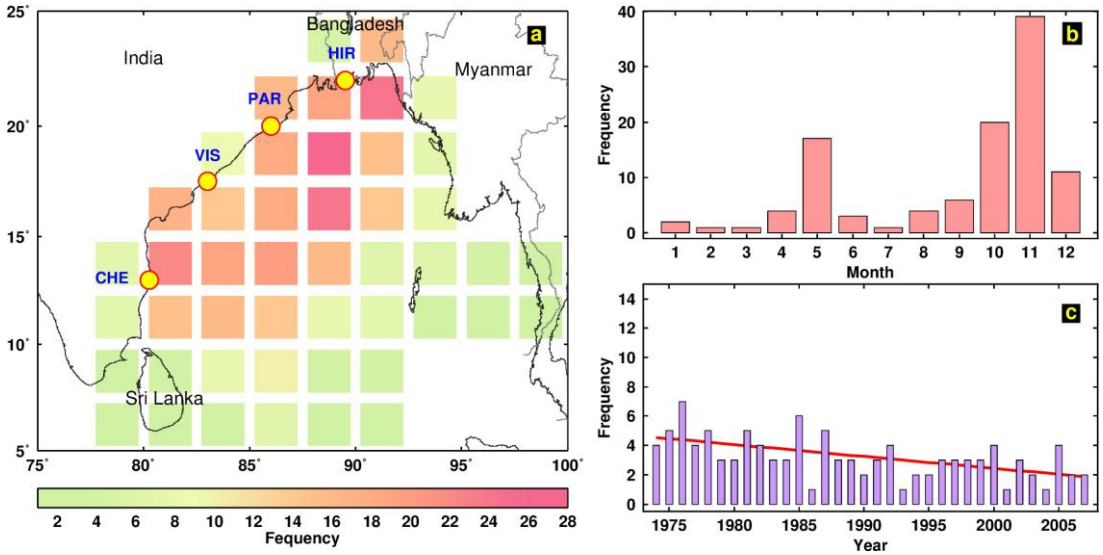

Figure 3.1 a) spatial (2.5°x2.5° boxes), b) monthly and c) annual frequencies of tropical cyclones in the Bay of Bengal during 1974-2007. Tide gauge locations shown in the panel a indicate as HIR (Hiron Point), PAR (Paradip), VIS (Visakhapatnam) and CHE (Chennai). In panel c, the trend is shown. The trend estimate is statistically significant (95% confidence level).

3.2 Storm surges from tide gauges

The present section deals with a description of storm surges, as observed in tide-gauge records. De-tided sea levels (residual sea levels) are used to identify storm surge events. Residual sea levels are the difference between observed sea level and predicted tide. Residual sea levels are caused mostly by the wind and atmospheric pressure forcing. The variability of residual sea level along the east coast of India and at the head of Bay of Bengal is shown in Figure 3.2. Figure 3.2 shows the frequency histogram of residuals at each location. Extreme positive (negative) values of the distribution represent positive (negative) storm surges. Along the western Bay of Bengal, the surge height increases from south to north. The residual sea-level variations are low at Chennai and increases towards Hiron Point. The residual series exhibit a unimodal distribution, and the mode is near to zero. The residual distributions are positively skewed, that is, the existence of large positive surges than large negative surges.

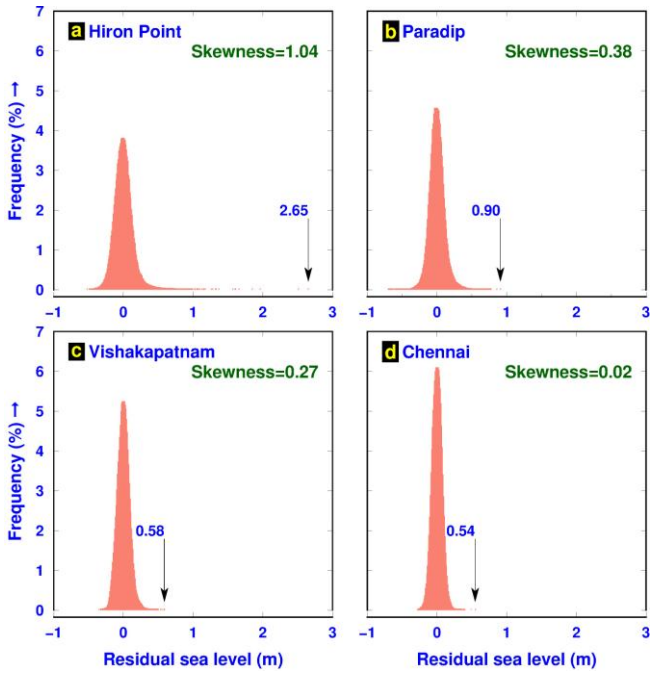

Figure 3.2 Frequency distribution of residual sea levels at a) Hiron Point, b) Paradip, c) Visakhapatnam and d) Chennai. Arrow indicates highest residual sea level or maximum surge height.

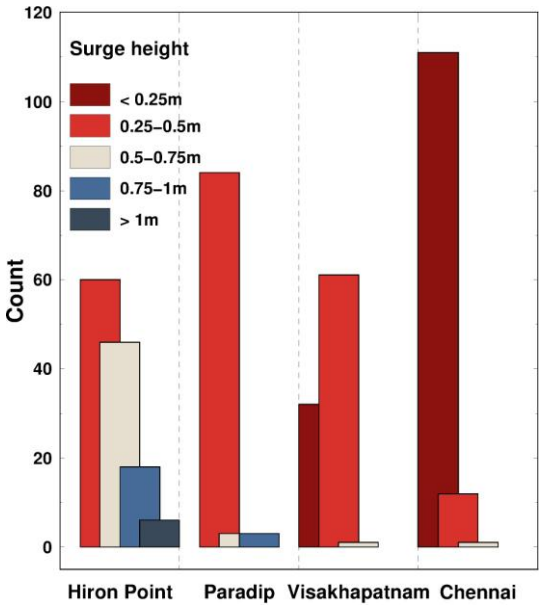

Figure 3.3 Classification of the surge heights above the 99th percentile at Hiron Point, Paradip, Visakhapatnam and Chennai.

Figure 3.3 shows the classification of surge events (above the 99th percentile) based on magnitude. The 99th percentile levels are 38, 28 21 and 15 cm respectively at Hiron Point Paradip, Visakhapatnam and Chennai. Among the four tide gauges, the record at Hiron Point tide gauge is characterised by the presence of storm surge events with large magnitudes (Figures 3.3 and 3.4), several surge events reaching heights above one metre can be found in this record and the highest observed surge has a magnitude of about two and a half metres (Figure 3.4). Observed maximum surge heights for the records at stations Paradip, Visakhapatnam and Chennai are below one metre (Figure 3.4). The highest surge events at all stations, except Visakhapatnam, were associated with a cyclone of the intensity of a SCS (Figure 3.4).

Continental shelf width and depth play an important role in determining surge height (Resio and Westerink, 2008). The shelf widths are about 50 km off Chennai, Visakhapatnam and Paradip. At the head of Bay of Bengal, the shelf is wide (about 200 km), and within the vicinity of Hiron Point, the depth is shallow (below 10 m). Hence, it is observed that surges are higher at Hiron Point compared to those in other stations. This is further illustrated in Figure 3.5, in which a few surges observed at

Paradip and Hiron Point by cyclones crossing between Paradip and Visakhapatnam are shown. Surge heights are found to be higher at Hiron Point than those at Paradip, even though Paradip is close to the cyclone tracks.

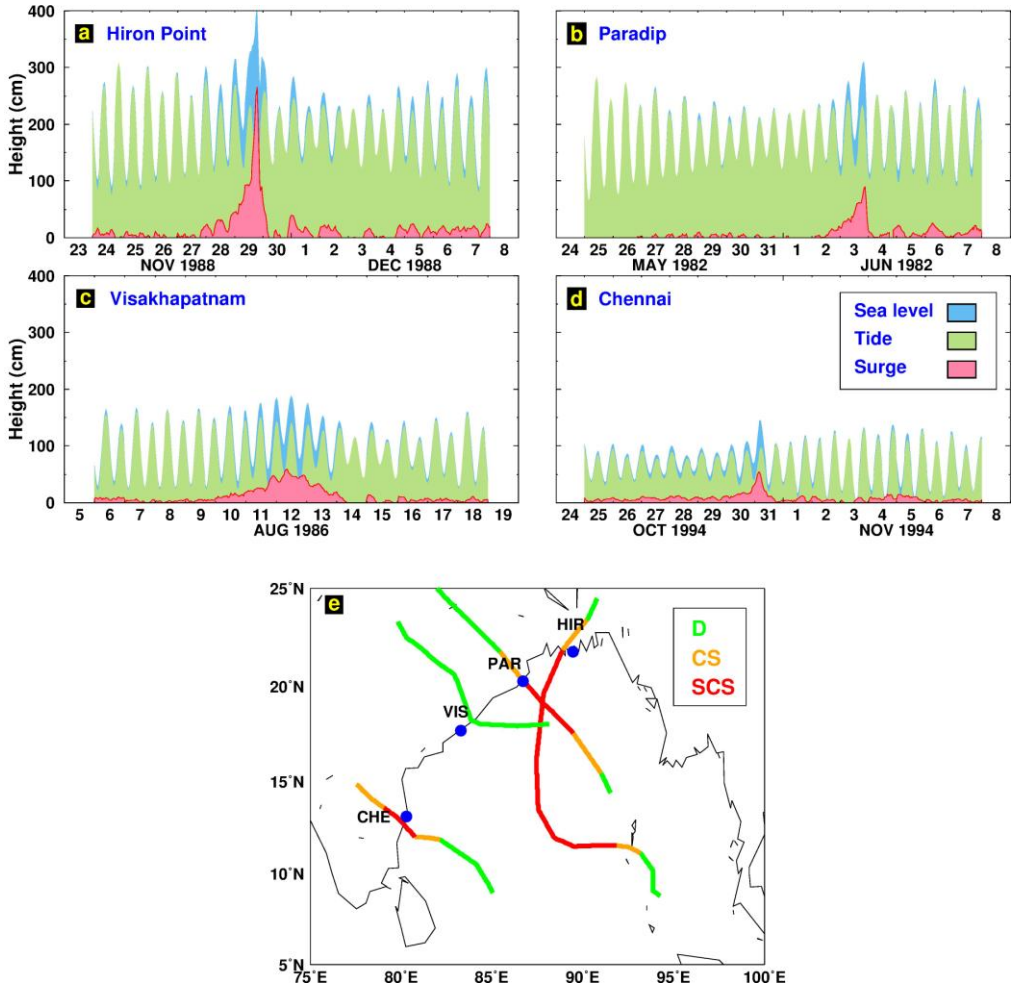

Figure 3.4 The highest storm surge and associated tide and sea level recorded during the period of analysis in a) Hiron Point, b) Paradip, c) Visakhapatnam and d) Chennai tide gauges. e) Tracks of cyclones and depression associated with the highest surge events.

During some of the major cyclonic events, the tide gauges failed to record, which resulted in no data, for example, in the case of Odisha super cyclone in 1999. The proximity of tide gauge to the location of maximum surge is also a factor to record magnitudes close to the actual. Figure 3.6 shows the cyclones crossing close to each tide gauge (within 2°), and resulting surge heights are shown in Figure 3.7. Here also

it is clear that surge heights are relatively higher at Hiron Point compared to those in other stations. Overall, there is an increase in surge heights towards the northern part of the Bay.

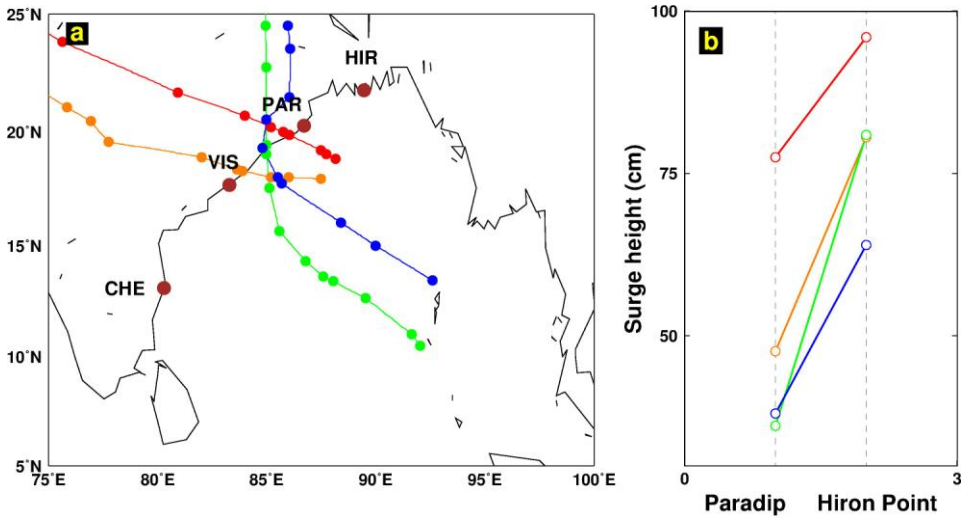

Figure 3.5 a) Examples of cyclones crossing the coast between Paradip and Visakhapatnam and b) associated surge heights at Paradip and Hiron Point.

Surges generated in some of the storms get propagated as coastally trapped waves along the coastline bringing the storm effects to farther locations. A SCS during May 1989 (Figure 3.8b), which crossed north of Paradip and the effect of the same event was found to propagate towards the south (Figure 3.8a). The cyclone was close to Paradip before it turned and crossed the coast, which led to a positive surge of about 50 cm first and followed by a negative surge of about 5 cm as the location was on the left side of the cyclone. The residual time series during the same period at Visakhapatnam and Chennai shows the signature of the cyclone event with a phase delay. The signature has a similar structure that of surge at Paradip but reduced in magnitude. Positive surges were about 25 and 10 cm, and negative surges were about 8 and 9 cm respectively at Visakhapatnam and Chennai. The negative surge appeared on 27 May at Paradip, after about 35 hours, the surge reached Visakhapatnam. Approximate distance between these two stations is about 500 km. The surge propagated with speed of about 4 m/s. The phase speed shown here is similar to those

shown by Sundar et al. (1999) for other surge events along the east coast of India. A few instances of negative surges were also noticed in the tide-gauge records.

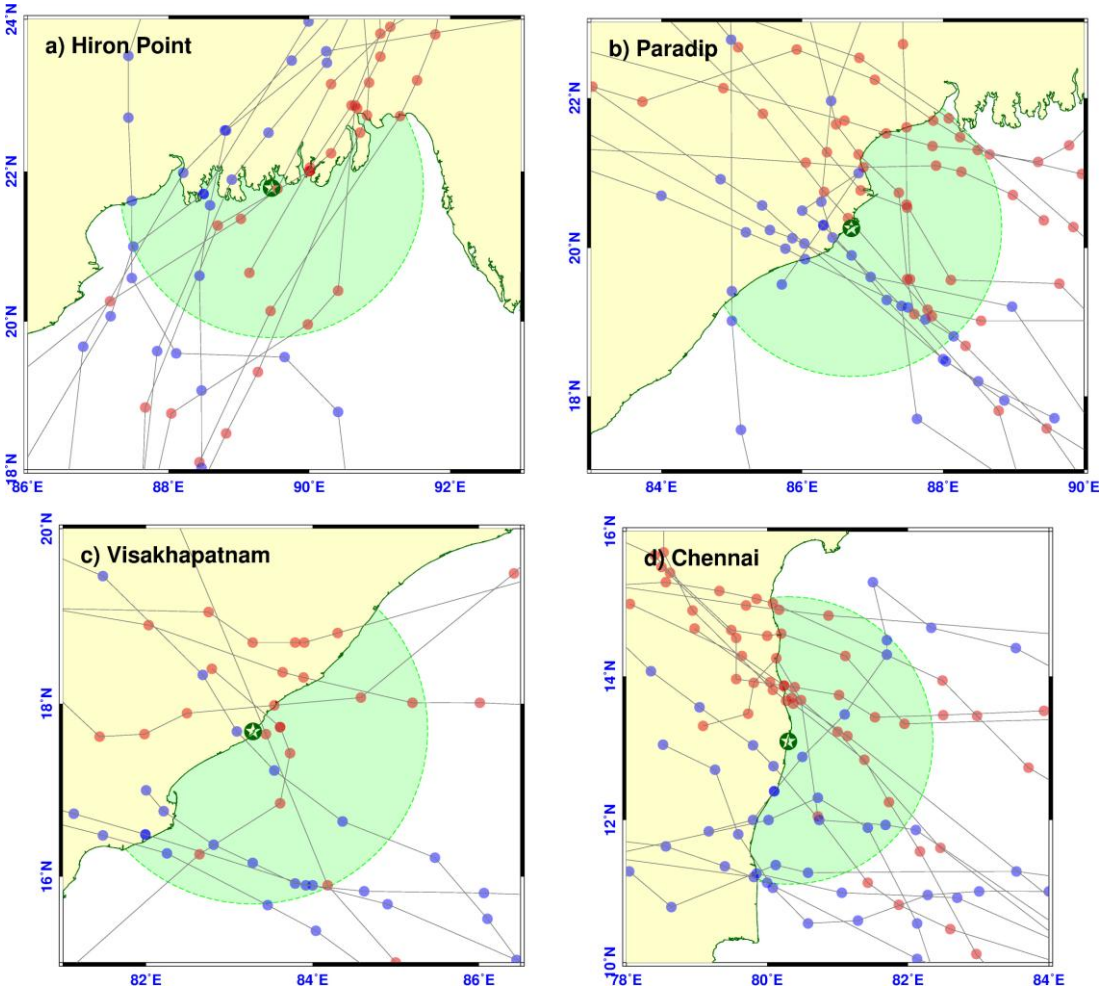

Figure 3.6 Cyclones crossing the coast within 2° radius of tide gauges at a) Hiron Point b) Paradip c) Visakhapatnam and d) Chennai. The red (blue) circle indicates cyclone is on the left (right) side of tide gauge at the time of crossing of the coast.

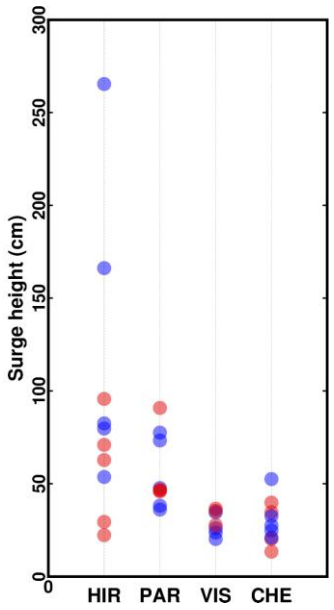

Figure 3.7 Surge heights associated with cyclones shown in Figure 3.6. Circle colour code is the same as in Figure 3.6. In a few cases, surge data was missing and for a few other cases surge was negative. Negative surge events are not shown in the figure.

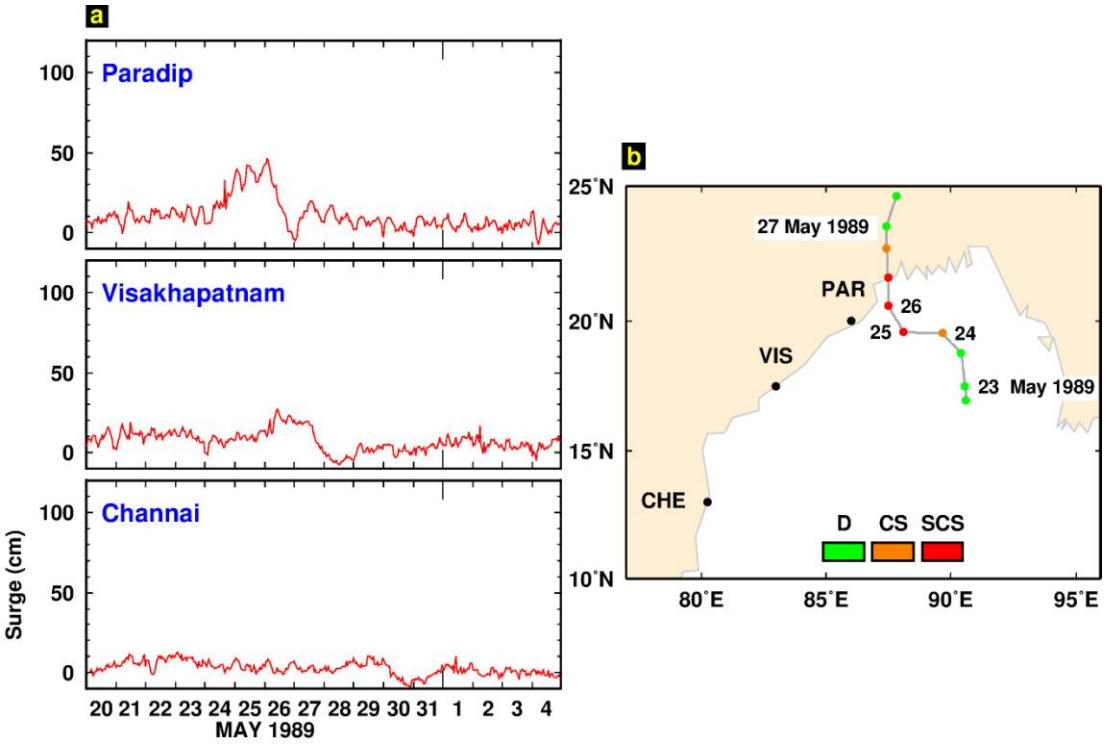

Figure 3.8 a) Storm surge during SCS (23-27 May, 1989) at Pradip, Visakhapatnam and Chennai. b) Cyclone track.

3.3 Storm surges from satellite altimeters

3.3.1 Introduction

Observations from satellites were a breakthrough in the history of oceanography. Satellite observations have given good temporal and spatial coverage of world oceans by measuring many oceanographic parameters. These observations include those from altimetry; which have been available since the launch of TOPEX/Poseidon in 1992. Altimetry provides along-track measurements of sea surface height, wave height and wind speed. Altimeter data have been widely used to describe variability associated with major ocean currents, propagation of planetary-scale waves, such as Rossby waves, meso-scale eddies and for estimating long-term sea level rise trends. Altimeter data are used for assimilation in global tidal models (for instance, Ray (1999) and Lyard et al., (2006)), which are then used for prediction of tides in the open ocean. Various oceanographic applications of satellite altimetry are described in Fu and Cazenave (2001). There have been some rare instances of altimeters capturing tsunami signals, for instance, the Indian Ocean tsunami of 2004 (Gower, 2005). Storm surges are more frequent than tsunamis; therefore, the chances of observing them are higher than those of tsunamis.

The performance of altimeters over the open ocean is good. Moreover, due to various limitations, such as land contamination of the satellite footprints or inaccurate resolution of the corrections of the high-frequency ocean response to tidal and atmospheric loading, the altimetry data near to the coast were discarded within 50km from the land in the past (Cipollini et al., 2017). Past and existing satellite altimetry missions, which have repeat period ranging from 10-35 days, inter-track distance about 90-315 km and narrow swath, were designed for applications in open oceans to capture large-scale sea surface features. Whereas, the dominant dynamical processes in the coastal oceans are complex and have shorter space-time scales than those of the open ocean. Coastal regions are important since a significant portion of the human population resides in these regions. Coastal regions are sensitive to climate change and thus increased flooding and shoreline erosion in a scenario of rising sea level. In

the recent years, there have been significant efforts to recover data in the coastal regions and since then improved coastal altimetry products are available (Vignudelli et al., 2011). It has been shown through various studies (Durand et al., 2009; Birol et al., 2017) that coastal altimetry can provide substantial information to understand the variability of coastal sea levels and currents.

Only very little literature exists on the usage of satellite altimetry for identifying storm surges. Scharroo et al. (2005) reported the records of wind-driven storm surge, associated with the Hurricane Katrina, which affected the Gulf Coast of the U.S.A. in 2005. Geosat Follow-On altimeter measured a surge of about 90 cm during the hurricane Katrina. Han et al. (2012) showed a detailed analysis of Jason-2 satellite observations of sea surface heights combined with tide-gauge data during the passage of the Hurricane Igor that crossed Newfoundland in 2010. For this event, St. John's tide gauge recorded a maximum surge of 94 cm and Jason-2 (the track located 89 km away from the tide-gauge station) showed positive sea-level anomalies of about 60 cm during the storm event. Surge observed by altimeter was extrapolated to the coast was about 1m and close to the observed surge by tide gauge at St. John's. They noted propagation of a shelf wave, generated by the storm, having a phase speed about 10 m/s (from altimetry), consistent with that estimated through tide gauge observations (11-13 m/s). Lillibridge et al. (2013) reported HY-2A altimeter-observed storm surge, generated by the Hurricane Sandy that crossed the northeastern coast of U.S.A. in 2012. In this case, altimeter passed over the region during the maximum surge and the surge height was found to be about 1.5 m from altimeter and about 1.8 m from a nearby (within 55 km) tide gauge. Sirota and Lebedev (2008) reported historical storm surges in the Gulf of Finland and the Neva River, observed from the TOPEX/Poseidon and Jason-1 satellites respectively. The SARAL/Altika altimeter measured storm surge due to the Cyclone Xaver, which affected the coasts of North Sea in 2013 (Scharroo et al., 2014). These studies have shown that satellite measurements provide useful information about storm surges, which can be used for comparison with model results or assimilation in models (Madsen et al., 2007). Most of the earlier studies focused mainly on particular extreme surge events. The present

study is the first attempt to identify storm surges over an extended period of about 15 years in a region using satellite altimetry.

A few studies have made using the coastal altimeter data for various oceanographic studies in the Bay of Bengal. Durand et al. (2008) and Durand et al. (2009) studied the spatiotemporal structure of the East India coastal current using altimeter data from Margins Altimetry Project (MAP), which used various editing strategies to recover data in marginal seas. So far, no studies have reported on the storm surges in the Bay of Bengal using altimeter data. The present study is an attempt to identify storm surges from satellite altimeter data and compare them with those recorded by closest tide gauges. Along-track altimeter data from various missions were analysed to identify storm surges in the Bay. They were compared with storm surges recorded in the hourly data from four tide gauges.

3.3.2 Altimetry data validation

A comparison between X-TRACK SLA and tide-gauge SLA was made by doing a linear correlation between the two and a root-mean-square difference (RMSD) analysis. Figure 3.9 (a, c, e, g) shows RMSD between altimeter SLA and nearest tide-gauge SLA. RMSD varies between 10 and 20 cm in the shelf regions. Figure 3.9 (b, d, f, h) shows the linear correlations between tide-gauge SLA and altimeter SLA. The correlation coefficients within the shelf regions are found to be high (0.5–0.8), indicating that the consistency between the two data is good. Crossover points of various tracks, for example, track 53 and track 90 of T/P, which are separated by about one and half day in time, shows inter-consistency of the data with similar values of correlation coefficients (Figure 3.9b).

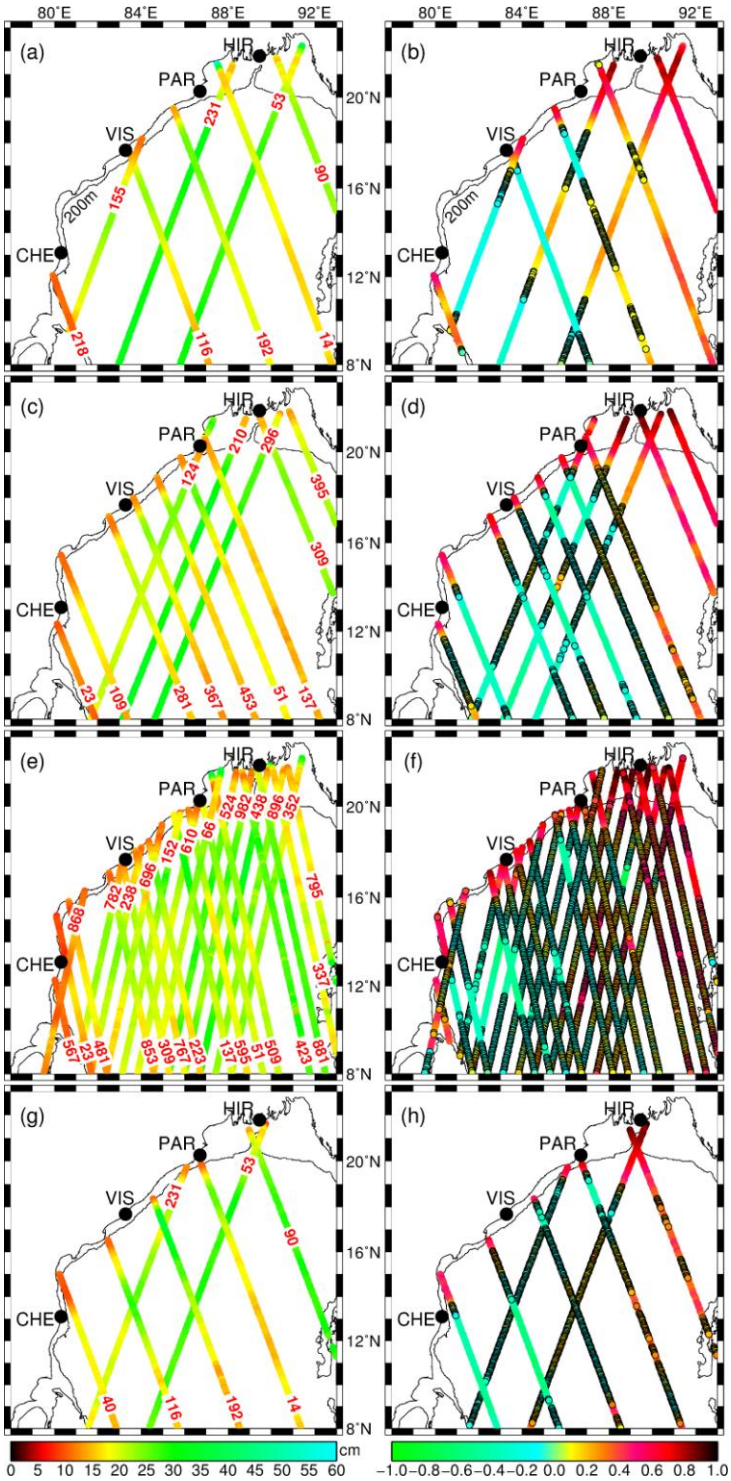

Figure 3.9 Root-mean-square differences (a, c, e, g) and linear correlations (b, d, f, h) between sea-level anomalies of altimeters (T/P – a & b, GFO – c & d, ENVISAT – e & f and T/PN – g & h) and tide gauges. Correlation analysis was performed with the tide-gauge data and the nearest ground tracks. A coloured circle with black border represents correlations, which are not statistically significant (90% significance level). The 200 m depth contour is shown.

3.3.3 Identification of storm surge events

The dates of formation of various low-pressure systems and their tracks in the Bay of Bengal for systems having intensities of depression (wind speed between 9 and 14 m/s) and above were obtained from the e-Atlas. Surge events during the corresponding period with minimum surge height of 25 cm were identified from hourly tide-gauge data. More than half of the events recoded in the tide gauges were found to last 2 days (Table 3.2). About twenty surge events were recorded in two adjacent tide gauges. The satellite tracks within a distance of 2° of tide-gauge location and having a pass within 24 hours of the peak surge, observed in the tide gauge, were considered to identify corresponding surge signals from altimeter data. A minimum surge height of 20 cm was used to identify events in the altimeter data. During the period of study (1993–2007), 30 (19), 21 (09), 09 (07), and 07 (01) storm surge events were identified from tide gauges (altimetry) at Hiron Point, Paradip, Visakhapatnam and Chennai respectively (see Table 3.3 for date and time of surge events recorded in tide gauges and altimeters). The mean surge heights and standard deviations of surge heights from both tide-gauge and altimetry data, and duration of surges are shown in Table 3.2. Mean surge heights tend to decrease from Hiron Point to Chennai. This is evident in the altimetry data also. Figure 3.10 shows a typical surge observed by altimeter and tide gauges at Hiron Point and Paradip. This particular surge event was caused by a depression which crossed at Hiron Point (inset, Figure 3.10a). The time evolution of wind and pressure fields of this depression is shown in Figure 3.10b. T/P satellite (track 231) crossed Hiron Point just 2 hours prior to the occurrence of surge peak. The altimeter recorded a surge of about 65 cm, about 176 km away from the Hiron Point tide gauge. The maximum surge recorded in the tide gauge was 123 cm, and at the time of altimeter pass, the surge in the tide gauge was 86 cm. The wind and pressure fields (Figure 3.10b) show cyclonic circulation in the region extending to Paradip as well. The maximum surge recorded at Paradip was about 51 cm. Tracks 231 and 14 (before and after the event) recorded consistent SLA with respect to Paradip tide gauge. Figure 3.10d shows the total water level (tide + surge) recorded by the altimeter along the track 231. Figure 3.10e shows the total water-level records

from the Hiron Point tide gauge. The peak surge occurred during rising tide (about 4 hours before high tide), and satellite pass was during the low tide. A 15 cm difference in the total water levels between the tide gauge and altimeter was found during satellite's pass.

3.3.4 Discussion and conclusions

Table 3.2 presents the statistics of storm surges identified from altimeter records and events recorded by each tide gauge. 45% of the surge events identified in tide gauges were also recorded by altimeters, with a minimum of 14% for Chennai and a maximum of about 67% for Visakhapatnam. Three events were captured in two altimeters and one event in three altimeters. The storm surges recorded by tide gauges and altimeters were compared (Figure 3.11). The maximum surge recorded in altimeter data during this period is about 93 cm (Figure 3.11). The number of coexisting events is large at Hiron Point due to a large number of adjacent satellite ground tracks (Figure 3.9). In most of the cases, surges observed by altimeters were found to be less than those observed in tide gauges. The values recorded by altimeter were taken from offshore locations. For example, for T/P, closest point of the track 14 is about 16 km away from the coast, whereas closest point on the track 53 is located by about 36 km from the coast. Moreover, the track 116 is close to Visakhapatnam tide gauge by about 15 km, whereas the track 53 is located by about 200 km from Hiron Point tide gauge. Wherever, the distance to the track is large; an exact comparison is not possible. However, the present analysis shows that altimeter is able to capture surge signals and their magnitudes are comparable to those observed by tide gauges. The total water level at the coast is a combination of tide and surge. Storm surges, when combined with high tide results in high sea levels. Total water levels recorded by altimeters are shown in Figure 3.11 with total water levels recorded by tide gauges at the same time. The total water-level measurements by altimeters are comparable to those in tide gauges. The maximum water level recorded in altimeter data during 1993–2007 is about 2 m.

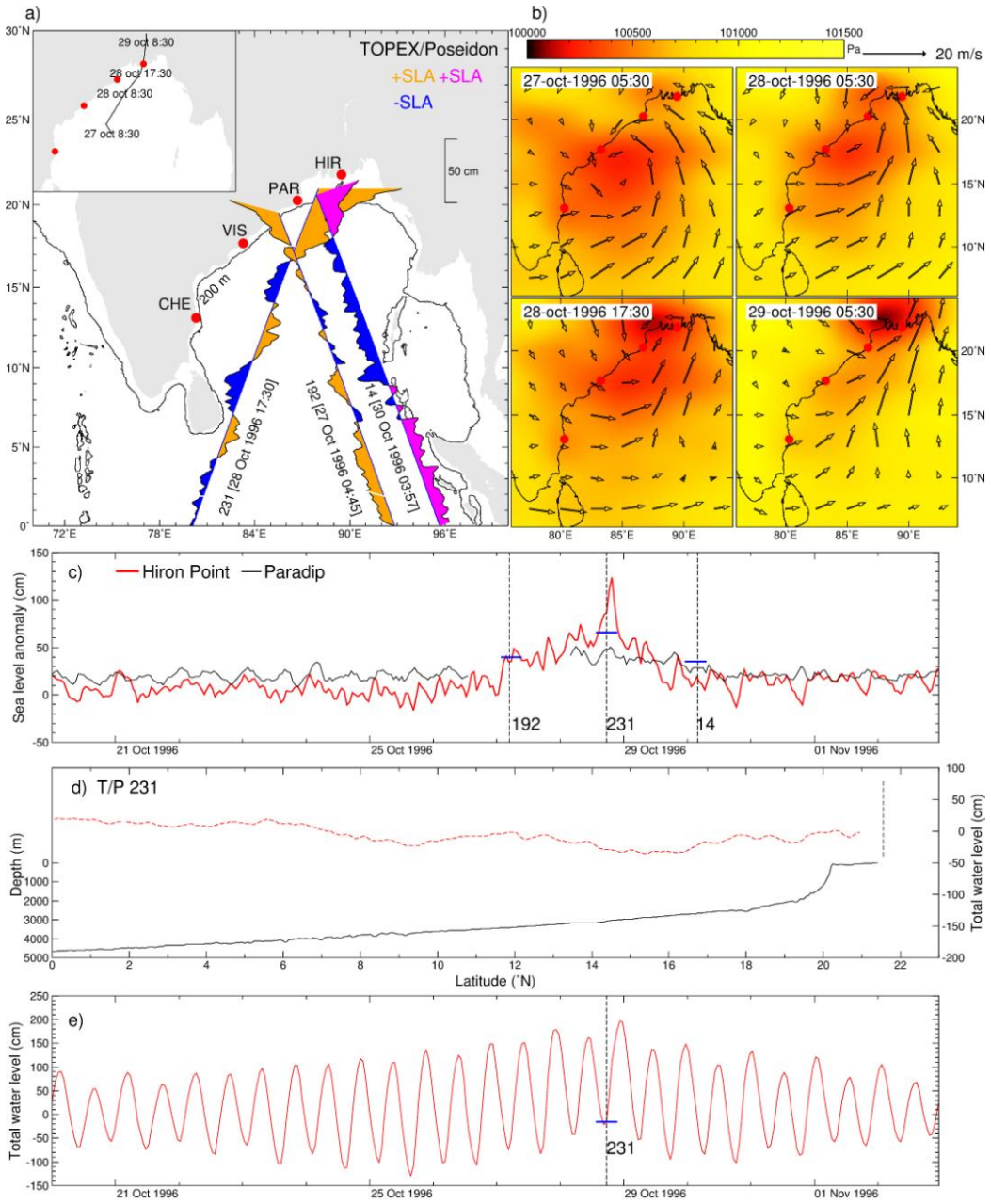

Figure 3.10 a) The track of a depression (inset) which crossed near Hiron Point (HIR) on 28 October 1996 and T/P (231) passed west of the landfall region at around 17:30 IST (Indian Standard Time) on 28 shows surge of about 65 cm. Sea-level anomalies of T/P tracks (192 and 14) during the event is also shown. b) Shows the surface wind fields and mean sea-level pressure taken from NCEP/NCAR reanalysis data to indicate the movement of the depression. c) Shows surge measurements from Hiron Point and Paradip tide gauges. The time of satellite's pass is shown with a vertical line, with the track numbers shown in the *x*-axis and the maximum surge recorded by altimeter is marked with a horizontal line (blue) on this line. d) Shows total water level (tide + surge) profile and bathymetry along sthe track 231 (T/P). The vertical line indicates the coastline. e) Shows total water level measured by Hiron Point tide gauge during the storm event, and the horizontal line indicates total water level recorded by the altimeter.

Table 3.2 Details of storm surge events from tide gauges and altimeters.

Tide gauge stations	No. of events (1993-2007)		Mean surge height (standard deviation) in cm		Surge duration (tide gauge) in days		
	Tide gauge	Altimeter	Tide gauge	Altimeter	< 2	2-4	> 4
Hiron Point	30	19	81.06 (28.37)	51.19 (19.43)	14	14	2
Paradip	21	9	45.21 (14.92)	48.35 (18.95)	10	9	1
Visakhapatnam	9	7	38.79 (7.23)	39.75 (7.93)	2	5	-
Chennai	7	1	36.34 (12.86)	-	3	3	-

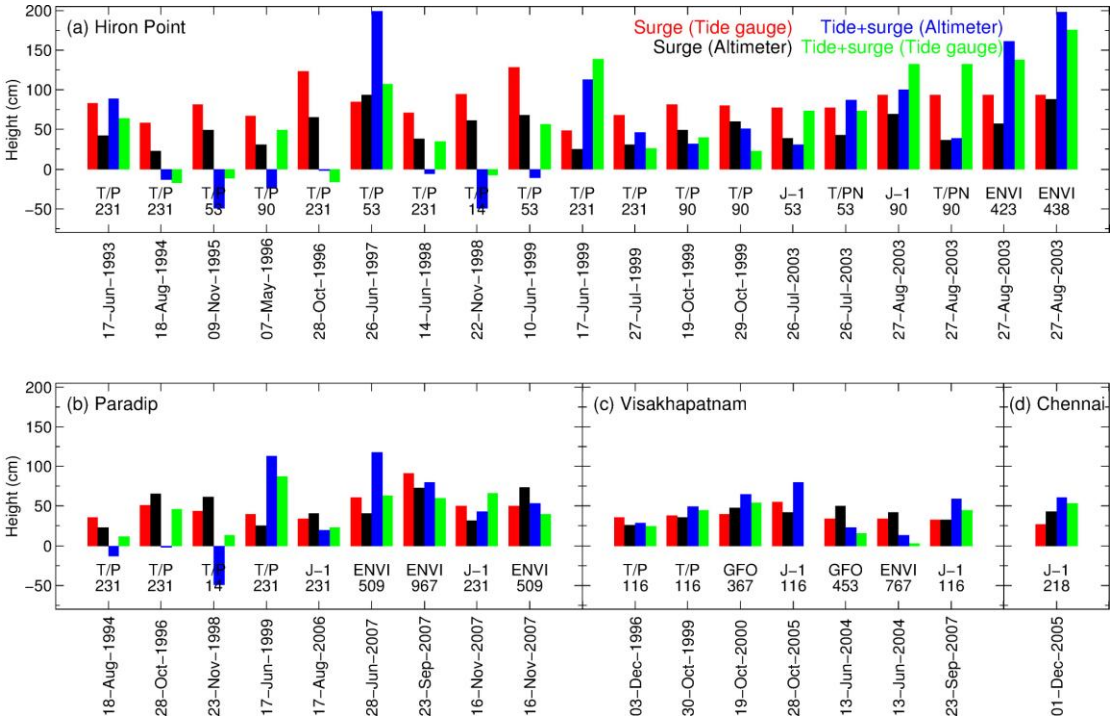

Figure 3.11 Comparison between storm surge heights and total water levels (tide + surge) recorded in tide gauges and altimeters. a) Hiron Point, b) Paradip, c) Visakhapatnam and d) Chennai. Surge heights observed in the tide gauges (altimeters) are represented with red (black) colour bars. Total water level observed in the altimeters and tide gauges during altimeter pass are represented with blue and green colour bars respectively.

During the period of analysis, one super cyclone crossed Paradip on 29 October 1999 (IST), which caused immense loss of life and property. During this event, the tide gauge at Paradip was not functioning, and hardly any data are available to study the event. However, port authorities in Paradip reported a surge of 3 m (Unnikrishnan et al., 2004). However, a strong signature of this event can be seen at Hiron Point tide gauge, which recorded a surge of about 80 cm (Figure 3.12a). T/P, which flew close to Hiron Point (track 90) during this event (28 October), recorded a surge of about 60 cm (Figure 3.12b). The total water level recorded by tide gauge and altimeter are shown in Figure 6a and b respectively. The difference between total water levels measured in tide gauge and altimeter was about 28 cm. 2007 Sidr cyclone was another major event during 1993–2007, which was recorded in altimeters. Cyclone Sidr hit Bangladesh coast in the early hours (IST) of 16 November 2007. Paradip tide-gauge SLA (Figure 3.13a) shows the signature of this event, about 50 cm. On 16 November, J-1 (track 231) and ENVISAT (track 509) recorded SLA about 31 cm and 73 cm respectively. Figure 3.13a, b and c also show the total water-level measurements during the Cyclone Sidr from Paradip tide gauge, J-1 and ENVISAT respectively. The total water-level measurements from J-1 and ENVISAT are in approximate agreement with Paradip tide-gauge measurements with a difference of 23 cm and 13 cm respectively.

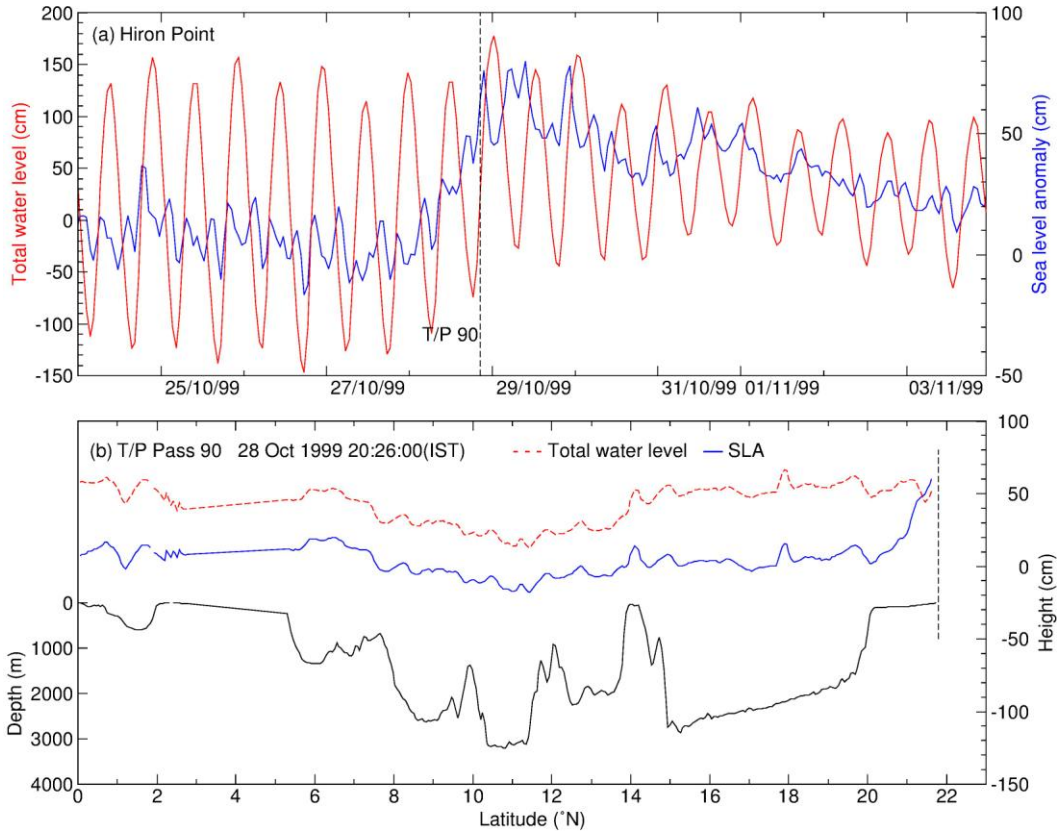

Figure 3.12 a) Tide-gauge measurements of storm surge and total water level (tide + surge) during the 1999 Odisha super cyclone at Hiron Point. The vertical line indicates the time of satellite pass. b) T/P along-track SLA and total water level during pass 90 on 28 October. The vertical line indicates the coastline.

The present study shows that the probabilities of observing storm surge events in altimeter data can be high, especially in regions where multiple tracks of satellites exist. Comparing the data of T/P, J-1, GFO and ENVISAT satellites in the Bay of Bengal with the hourly tide-gauge data, it is illustrated that nearly 45% of surge events are observed both in altimetry and tide gauges on an average in this region during the period of study.

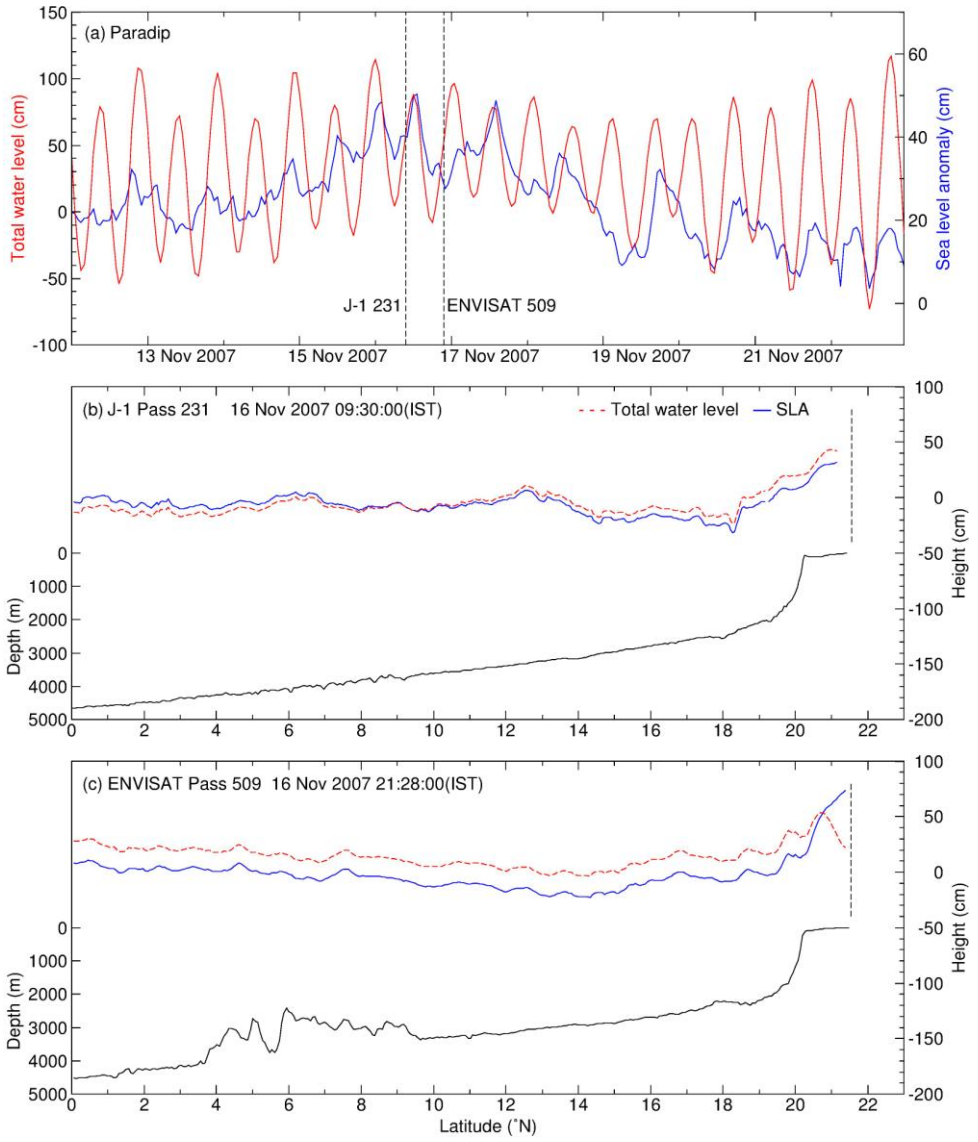

Figure 3.13 a) Tide-gauge measurements of storm surge and total water level (tide + surge) during cyclone Sidr (2007) at Paradip. The vertical line indicates the time of satellite pass. b) J-1 along-track SLA and total water level (tide + surge) during pass 231 on 16 November (IST). (c) ENVISAT along-track SLA and total water level during pass 509 on 16 November (IST). The vertical line indicates the coastline.

During the two decades of satellite altimetry, probably the most challenging task had been to improve usage of altimetry data in the coastal regions. In addition to X-TRACK-processed data, PISTACH (Prototype Innovant de Système de Traitement pour l'Altimétrie Côtière et l'Hydrologie) (Mercier et al., 2010) and COASTALT (ESA development of COASTal ALTimetry) (Gomez-Enri et al., 2008) projects

attempted to recover valuable information of SSH from coastal zones. New initiatives, such as eSurge project (Harwood et al., 2013), promote research in this direction. Vignudelli et al. (2011) detailed the issues, improvements and future of the coastal altimetry. Storm surge studies using altimetry are still in an initial stage of development. Although altimetry is proven to complement tide gauges, a better strategy will be required for routinely monitoring of storm surges in the future. As the repeat period of the orbit is the key factor to increase the probability of observing surges by a satellite, a high repetitive constellation of altimeter satellites can considerably enhance the chances of capturing of surge signals. Classical altimeters of T/P and J-1 measure sea surface height on their nadir. The nadir swath is roughly 2 km, and inter-track distance is about 315 km at the equator. The new proposed SWOT (Surface Water Ocean Topography) (Fu et al., 2009) mission, provide a 2-D map of the sea surface with wide swath (around 120 km). This new mission certainly complements the standard nadir altimeter data with fine spatial coverage and high resolution.

Table 3.3 Date and time of storm surge events from tide gauges and satellites.

Sl No.	Date & time (tide gauge)	Date & time (altimeter)	Tide-gauge stations	Satellite	Track No.	Cycle No.
1	22/11/1998 08:29:00	22/11/1998 18:05:00	Hiron Point	T/P	014	212
2	09/11/1995 17:29:00	09/11/1995 17:37:00	Hiron Point	T/P	053	100
3	26/06/1997 22:30:00	26/06/1997 16:10:00	Hiron Point	T/P	053	160
4	10/06/1999 15:30:00	10/06/1999 14:23:00	Hiron Point	T/P	053	232
5	26/07/2003 01:30:00	26/07/2003 18:36:00	Hiron Point	J-1	053	384
6	07/05/1996 09:30:00	07/05/1996 15:36:00	Hiron Point	T/P	090	118
7	19/10/1999	18/10/1999 22:27:00	Hiron Point	T/P	090	245

	00:30:00					
8	29/10/1999 09:30:00	28/10/1999 20:26:00	Hiron Point	T/P	090	246
9	27/08/2003 15:30:00	26/08/2003 22:58:00	Hiron Point	J-1	090	387
10	17/06/1993 17:30:00	17/06/1993 04:34:00	Hiron Point	T/P	231	011
11	18/08/1994 05:30:00	17/08/1994 13:31:00	Hiron Point	T/P	231	054
12	28/10/1996 19:30:00	28/10/1996 17:31:00	Hiron Point	T/P	231	135
13	14/06/1998 21:30:00	15/06/1998 16:01:00	Hiron Point	T/P	231	195
14	17/06/1999 09:30:00	17/06/199913:07:00	Hiron Point	T/P	231	232
15	27/07/1999 14:29:00	27/07/1999 05:03:00	Hiron Point	T/P	231	236
16	23/11/1998 08:00:00	22/11/1998 18:05:00	Paradip	T/P	014	212
17	18/08/1994 10:00:00	17/08/1994 13:31:00	Paradip	T/P	231	054
18	28/10/1996 06:00:00	28/10/1996 17:31:00	Paradip	T/P	231	135
19	17/06/1999 03:00:00	17/06/1999 13:07:00	Paradip	T/P	231	232
20	17/08/2006 09:59:00	17/08/2006 06:39:00	Paradip	J-1	231	496
21	16/11/2007 12:59:00	16/11/2007 09:30:00	Paradip	J-1	231	542
22	03/12/1996 09:59:00	02/12/1996 21:28:00	Visakhapatnam	T/P	116	139
23	30/10/1999 03:59:00	29/10/1999 20:48:00	Visakhapatnam	T/P	116	246
24	28/10/2005 14:00:00	29/10/2005 05:23:00	Visakhapatnam	J-1	116	467

25	23/09/2007 06:00:00	23/09/2007 07:41:00	Visakhapatnam	J-1	116	537
26	01/12/2005 20:00:00	01/12/2005 22:55:00	Chennai	J-1	218	470
27	26/07/2003 01:30:00	26/07/2003 18:45:00	Hiron Point	T/PN	053	032
28	27/08/2003 15:30:00	26/08/2003 23:03:00	Hiron Point	T/PN	090	035
29	19/10/2000 03:00:00	19/10/2000 13:49:00	Visakhapatnam	GFO	367	016
30	13/06/2004 09:00:00	13/06/2004 12:36:00	Visakhapatnam	GFO	453	094
31	27/08/2003 15:30:00	26/08/2003 21:22:00	Hiron Point	ENVI	0423	010
32	27/08/2003 15:30:00	27/08/2003 09:45:00	Hiron Point	ENVI	0438	010
33	28/06/2007 23:00:00	29/06/2007 21:28:00	Paradip	ENVI	0509	050
34	16/11/2007 12:59:00	16/11/2007 21:28:00	Paradip	ENVI	0509	054
35	23/09/2007 12:59:00	23/09/2007 21:25:00	Paradip	ENVI	0967	052
36	13/06/2004 09:00:00	13/06/2004 21:45:00	Visakhapatnam	ENVI	0767	017

3.4 Extreme high waters

As part of the objective, ‘description of past storm surge events based on tide gauge data’, the variability and long term changes in extreme high waters are addressed in the present section.

3.4.1 Introduction

Rising MSL is one of the climate change phenomena that are of greatest concern. Rising MSL is a pressing concern not only for the small islands but also for the megacities and the villages in the low elevation coastal zones. Over a long span of time, rising MSL has the potential to transform these coastal regions, where a large population resides, impacting upon investments and infrastructures. Accompanying the rising MSL is the increased occurrence of extreme sea levels. Extreme sea levels (Figure 3.14), which arise mostly due to storm surges combined with high tides, above the MSL, cause the abrupt destruction of life and property. Aside from MSL change, causative factors for changing extreme sea levels include changing surge (storminess) and/or tide components. Within long-term trends, extreme sea levels and potential coastal flooding are also found at specific times when the peaks of the nodal and perigean tidal cycles occur (Eliot, 2010; Haigh et al., 2011). Understanding of the variations of extreme sea levels is more complex and difficult than that of MSL, as it depends on various components (Figure 3.14). MSL affects extremes directly and indirectly (Haigh, 2009), direct effects are due to the change in baseline and indirect effects are due to modification of water depth which in turn affect the propagation and dissipation of surge and tide. The difficulty also arises due to lack of access to high-frequency data (Woodworth, 2006), which is essential for identifying true extremes. Another aspect of extreme sea level variability is that how they depend on regional climate variations. Earlier studies have shown that variations in extremes were correlated with regional climate (Woodworth and Blackman, 2004)

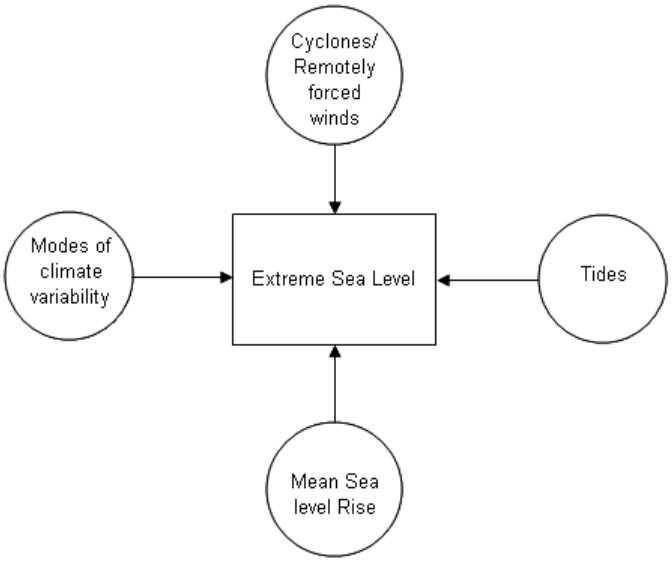

Figure 3.14 Various factors affecting extreme sea level (Source: Unnikrishnan et al, 2011).

The Third Assessment Report of the Intergovernmental Panel on Climate Change (IPCC AR3) (Church et al., 2001) had made only a small note on extreme sea levels, and most of the observational studies on the topic came later. In their study of observed sea level extremes at Liverpool since 1768, Woodworth and Blackman (2002) concluded that the values of annual maximum surge-at-high-water were larger in the late 18th, late 19th and late 20th centuries than for most of the 20th century, and was qualitatively consistent with the variability in storminess from meteorological data and anecdotal information. The first attempt to address changes in extreme sea levels with a reasonable global distribution of data was made by Woodworth and Blackman (2004). They showed a significant increase in extreme sea levels since 1975, which was consistent with changes in MSL.

The IPCC AR4 (Bindoff et al., 2007), noted that "Studies of variations in extreme sea levels during the 20th century based on tide gauge data are fewer than studies of changes in mean sea level". Moreover, only a few literatures can be found therein, which included both extreme sea levels and non-tidal residuals (to assess storminess). A considerable increase in the extreme sea level studies can be found thereafter, especially in the Europe. Ullmann et al. (2007) concluded that annual maximum sea

levels had risen at a rate of 4 mm/yr, which is nearly twice as fast as MSL during the twentieth century in the Camargue (Rhone Delta) region of southern France, rising trends (1.9 mm/year) in positive annual maximum surges were responsible for this rise. Marcos et al. (2009) showed that trends in extremes in the southern Europe were driven MSL changes. Vibilić and Šepić (2010) noted upward trends in storminess and extremes trends over northern Europe. Outside the Europe, Abeysirigunawardena and Walker (2008) showed that highest sea levels of each calendar year were found to have risen at approximately 3.4 mm/year, which was twice the rate for MSL at Prince Rupert in British Columbia, Canada. Lowe et al. (2010) presented a comprehensive review of extreme sea levels. Woodworth et al. (2011) covered, in a short review, the literatures after Lowe et al. (2010). Details of extreme sea level can also be found in IPCC special report (IPCC, 2012). The major scientific works after Lowe et al. (2010) include, Menéndez and Woodworth (2010), Haigh et al. (2010), Letetrel et al. (2010) and Tsimplis and Shaw (2010). These studies have substantiated that the increasing trends in extremes are driven by MSL changes.

Most recently, the Fifth Assessment Report of the Intergovernmental Panel on Climate Change (IPCC AR5) (Church et al., 2013 and Rhein et al., 2013) included a review of extreme sea levels. That report concurred with the view that the recent increase in observed extremes worldwide has been caused primarily by an increase in MSL, although the dominant modes of climate variability (particularly the El Niño Southern Oscillation (ENSO) but including the Indian Ocean Dipole (IOD), North Atlantic Oscillation (NAO) and other modes) also have a measurable influence on extremes in many regions, via variability in MSL and/or mode-related changes in storminess. Since the IPCC AR5, there have been a number of studies relating to extreme sea levels. Wahl et al. (2014) reported rapid changes in the seasonal cycle of MSL along the Gulf coast of the US. Seasonal MSL is found to provide the baseline to which storm surges can be added to provide an overall extreme. Consequently, changes in the seasonal cycle, like changes in annual MSL, can change flood risk.

Among recent regional studies, an investigation of extremes in the Baltic (Ribeiro et al., 2014) found that northernmost stations exhibit larger positive trends in extremes

since 1916, relative to mean values, unlike those of the southern Baltic, where changes in extremes are more in line with those in MSL. Mudersbach et al. (2013) and Dangendorf et al. (2013) examined long records from six stations on the North Sea coast of Germany and concluded that the observed positive trends in extremes are similar to those in MSL prior to the 1950s and for 1990-onwards, but in between the high sea levels rose faster than MSL due to changes in the amplitudes of major tidal constituents and decadal variability of storm surges.

In a study of Caribbean extreme sea levels resulting from tropical storms, Torres and Tsimplis (2014) concluded that the observed trends in extremes are also caused by MSL rise in that region with no evidence of secular changes in the storm activity. Feng and Tsimplis (2014) determined trends in extremes between 1954 and 2012 at 20 tide gauges along the coast of China. They concluded that the trends are primarily driven by changes in MSL, but are also linked with increases in tidal amplitudes at three stations. Neither the Pacific Decadal Oscillation (PDO) nor ENSO is found to be indicators of changes in the magnitude of extremes, but ENSO appeared to regulate the number of tropical cyclones that reach the Chinese coasts. Another study by Feng et al. (2015) concluded that changes in extremes along the coast of China are strongly related to the changes in MSL. Further, they pointed out that these changes are not entirely due to MSL changes, but have contributions due to spatially non-uniform changes in surge and tide components. Increased flooding instances have been reported along the US coasts. Talke et al. (2014) found that increased inter-annual variability together with MSL rise led to the increased flood levels at the New York Harbor. Wahl and Chambers (2015) found significant but small trends in extremes during 1929–2013 along most of the coastline stretches of the US. These trends are primarily due to MSL rise. They also noted multi-decadal variations in extremes which are not related to MSL. Moftakhari et al. (2015) reported an increased frequency of minor flooding instances along the coasts of the US due to sea level rise. Though non-destructive, these floods are capable of causing public inconveniences including frequent road closure, etc. and they signify increased risk during severe floods.

In summary, long-term changes, inter-annual variability and contributing factors in extreme sea levels have been documented globally and in some selected basins (Woodworth and Blackman, 2004, Menéndez and Woodworth, 2010, Merrifield et al., 2013; Marcos et al., 2015). Changes are studied using high-frequency tide-gauge data, usually sampled at a frequency of once per hour. At most of the tide-gauge stations, positive trends in extremes have been found to be due to rising MSL. At inter-annual time scales, extreme sea levels have tended to show a dependence on various modes of climate variability, including ENSO and NAO, depending on the region. Most of these studies have not included a detailed discussion of extreme sea levels in the Bay of Bengal.

Trends in relative MSL, based on long-term tide-gauge data, have been reported for the coasts of the northern Indian Ocean and are consistent with global estimates (1.06 to 1.75 mm/yr during 1878 to 2004 for records having different time spans) (Unnikrishnan and Shankar, 2007). Recent estimates using satellite altimeter observations (Unnikrishnan et al., 2015) have revealed increased sea level rise trends (mean value of 3.28 mm/yr for the north Indian Ocean) during 1993–2012, which are again consistent with findings for trends in global MSL for the same period. Notably, the head of the Bay is characterised by a higher rate of sea level rise than elsewhere (typically 5 mm/yr), which is partly due to the subsidence of Ganga-Brahmaputra-Meghna (GBM) river delta. Modes of climate variability, such as ENSO and IOD, have been found to have a pronounced effect on year-to-year sea level variability in the Bay of Bengal (Singh et al., 2001, Han and Webster, 2002, Srinivas et al., 2005, Singh, 2006, Aparna et al., 2012 and Sreenivas et al., 2012). Sea level along the east coast of India has been found to decrease (increase) during El Niño (La Niña) events (Srinivas et al., 2005). During the positive (negative) phase of the IOD, sea level tends to decrease (increase) along the east coast of India (Aparna et al., 2012).

Knowledge of extreme sea levels, and insight into their future projections, are essential for managing flood risks in the coastal areas. Sea level observations obtained by tide gauges provide the basis of this knowledge. Subsequently, their analysis using statistical techniques can be used to assess changes in future flood risk under different

climate scenarios. Return period and return level estimations of extreme sea levels in the Bay of Bengal have been provided by Unnikrishnan et al. (2004) and Lee (2013) using hourly tide-gauge data and Unnikrishnan et al. (2011) using storm surge models, driven by regional climate models to provide present and future return periods of storm surges and extreme sea levels. Extreme sea level projections for GMB delta (Kay et al., 2015) shows increased likelihood of high water events through the 21st century. A number of other studies related to extreme sea levels in the Bay of Bengal include event-specific numerical modelling of storm surges (Dube et al., 2009; Dube et al., 2013) and tide gauge observations to characterise storm surges (Mehra et al., 2015).

In this section, I investigate and present the spatial patterns and recent changes in extreme high waters in the Bay of Bengal using hourly tide-gauge data available along the east coast of India and at the head of the Bay of Bengal. The study intends to estimate changes in extreme high waters on seasonal, inter-annual to longer time scales.

3.4.2 Results

3.4.2.1 Variation of extreme high waters along the coast

The highest water levels observed among the tide gauge records vary from 170 to 475 cm with the highest water level observed at Cox's Bazaar (475 cm) and the lowest at Chennai (170 cm). The highest water level observed at Hiron Point, Paradip and Visakhapatnam was 404, 356 and 226 cm respectively. The highest water levels at northernmost stations (Cox's Bazaar, Hiron Point and Paradip) were associated with storm surges due to tropical cyclones or depressions (identified using cyclone e-Atlas, IMD). Although mild surge events were found during the highest water levels at Chennai and Visakhapatnam, the e-Atlas shows no cyclones in the vicinity of these stations. However, these surge events were originated due to less-intense low-pressure systems as noticed from the NCEP/NCAR surface wind and MSL pressure data.

Figure 3.15a shows the annual maximum water levels (annual mean removed) at each station plotted as a combination of the corresponding tide and surge. The highest water levels observed were now reduced to 264, 219, 179, 141 and 102 cm at Cox's Bazaar, Hiron Point, Paradip, Visakhapatnam and Chennai respectively. Most of the annual maximum water levels were found to occur in particular period of the year owing to the contribution of seasonal MSL (seasonal cycle of extremes and MSL are discussed in the next section). Figure 3.15b is similar to Figure 3.15a but shows the annual maximum water levels with their monthly mean removed. From Figure 3.15a to b, the mean annual maximum reduced by about 17 to 31 cm from Chennai to Cox's Bazaar indicating the effect of monthly MSL variations. The mean annual maximum tide and surge observed at these stations were marked with triangles (Figure 3.15b). Notably, the annual maximum water levels are largely a combination of moderate or small surges (annual maximum water levels are less frequent towards mean annual maximum surge) and high tides at almost all the stations (as one observes more extremes close to and below the dotted line (75% tide and 25% surge)), although the extremes in several years at Hiron Point and Cox's Bazaar do occur as a combination of extreme surge and low tide (Figure 3.15b). The mean annual maximum reduced to monthly mean ranges from 71 to 195 cm from Chennai to Cox's Bazaar. The average contribution of surge and tide to this mean annual maximum ranges from 13 to 50 cm and from 58 to 144 cm respectively from Chennai to Cox's Bazaar. The mean annual maximum was found to increase from southwestern part of the Bay (Chennai) towards its head (Hiron Point and Cox's Bazaar). A similar increase can be found for mean annual maximum surge and tide.

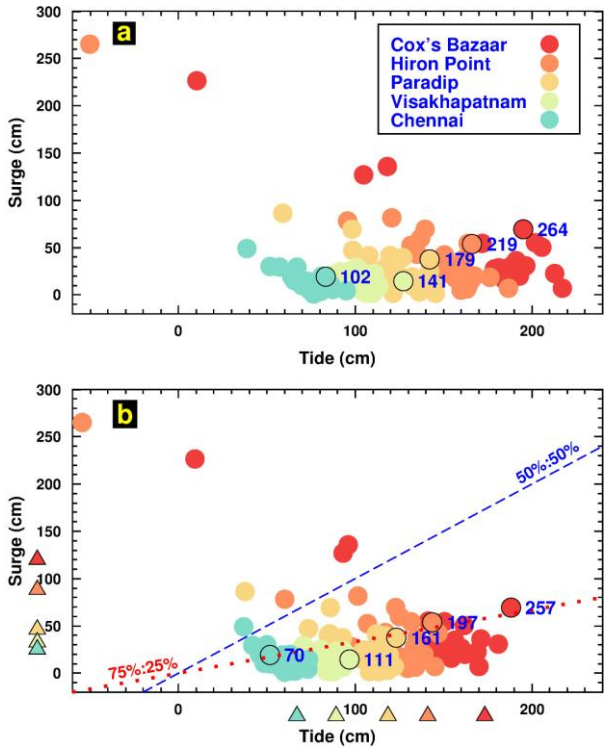

Figure 3.15 a) The annual maximum water levels (annual mean removed), plotted as a combination of tide and surge. The highest water level among the annual maxima is given in centimetres. b) As in a) with the monthly mean removed instead of the annual mean. The mean annual maximum tide and surge for each station are marked on the respective axes with triangles. Reference lines, dashed (dotted), indicate water levels with 50% (75%) tide and 50% (25%) surge contributions.

3.4.2.2 Seasonality of extreme high waters

The mean seasonal cycle in the monthly 99th and 50th percentiles at the five tide gauge locations is shown in Figure 3.16, while Table 3.4 presents their statistics. There is a strong seasonal sea level signal at all the stations for both mean monthly series. Notably, the seasonal changes in sea level are high in the northern part of the Bay and reduce towards the southwest. The seasonal cycle at the northernmost stations is characterised by a strong annual cycle (single high and low) whereas, towards the southwestern part, it is dominated by a semi-annual cycle (double high and low). At Cox's Bazaar, the mean 99th percentiles have a maximum during July and minimum during January and it changes by about 68 cm from its minimum to maximum. At Hiron Point, the mean 99th percentiles have a minimum during January and maximum during August and fluctuate nearly by 67 cm between these months.

Along the east coast of India, seasonality has its minimum during March and maximum during October–November and the range of seasonal change is about 36–48 cm. The shape of the mean seasonal cycle of the monthly 99th and 50th percentiles is similar for most of the stations, with consistency in the range of seasonal change and the month of occurrence of maximum and minimum values, while a one month shift is observed in the occurrence of minimum monthly sea level at Hiron Point and Cox's Bazaar (January to February, Table 3.4) and a notable difference in the range (higher range for 50th percentiles compared to 99th percentiles) for Cox's Bazaar. The range of seasonal sea level change increases towards higher percentiles, except for Cox's Bazaar, where the range of seasonal change towards higher percentiles is about 10 cm lower than that of 50th percentiles.

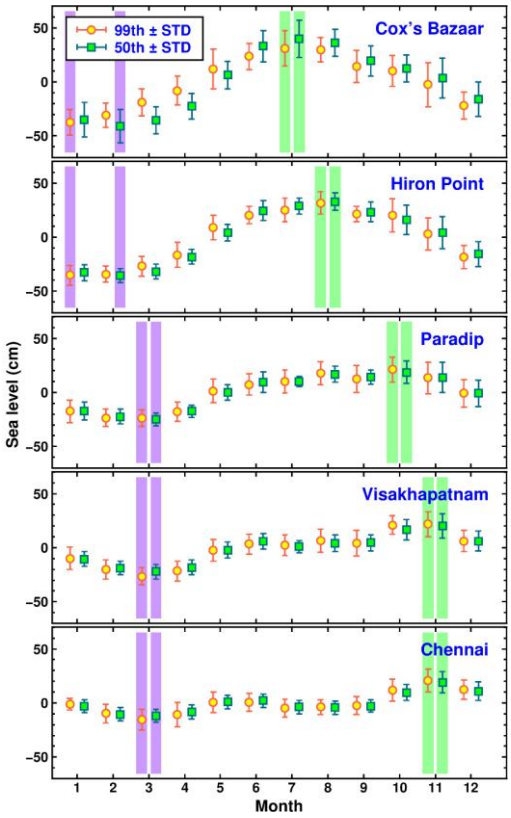

Figure 3.16 Mean seasonal cycle of the 99th and 50th percentiles, together with the standard deviations (STD). Shaded areas represent minimum and maximum of the seasonal cycle.

Table 3.4 Statistics of the mean seasonal cycle of 99th and 50th percentiles.

Station	99th (50th) percentile		Range (cm)
	Month of largest and smallest values		
Cox's Bazaar	Jul (Jul)	Jan (Feb)	68.2(80.5)
Hiron Point	Aug (Aug)	Jan (Feb)	66.7(68.5)
Paradip	Oct (Oct)	Mar (Mar)	45.0(43.5)
Visakhapatnam	Nov (Nov)	Mar (Mar)	48.4(42.0)
Chennai	Nov (Nov)	Mar (Mar)	36.0(30.9)

3.4.2.3 Inter-annual variability of extreme high waters

The de-trended time series of 99th percentiles at each station have standard deviations which are higher than (except for Cox's Bazaar) that of the 50th percentiles (Figure 3.17a), and the correlation between the two percentile time series is positive and significant at all the stations (Figure 3.17b). Standard deviations increase, and the correlations with the 50th percentiles decrease, but are still positive and significant, towards higher percentiles. Also, correlations were calculated for inter-annual sea level percentiles (Figure 3.18) at various stations with one another, finding consistent correlations in all percentiles, which are significant, among stations along the east coast of India. Corresponding correlations after MSL reduction are significant and consistent among various high water percentiles only between Chennai and Visakhapatnam.

Significant correlations are also observed between 99th percentiles (median is not removed) and climate indices (DMI and SOI) for all the stations along the east coast of India (Table 3.5). For the stations at the head of the Bay, a significant correlation is observed between 99th percentiles at Hiron Point and DMI, whereas no significant correlation is found with the SOI. For Cox's Bazaar, there is no significant correlation

of 99th percentiles with the climate indices. The results are mostly the same for other high water percentiles. When the median is removed from the 99th percentiles, the correlations with the DMI and SOI reduced, but a significant correlation is still observed for the 99th percentiles at Paradip and Chennai with the DMI.

The partial correlation analysis, which separates the contributions of DMI and SOI to high waters, shows reduced magnitude of correlation coefficients for both DMI and SOI with median and high water percentiles. Significant correlations persist between DMI (with SOI contribution removed) and 99th percentiles at Hiron Point, Paradip and Chennai. 99th percentiles at Paradip show significant correlations with SOI, after removing the DMI contribution. These results are largely consistent for other percentiles also. For the median removed percentiles, significant correlations with DMI are observed for Paradip. Overall, the results show a wider impact of IOD on extremes compared to that of SOI.

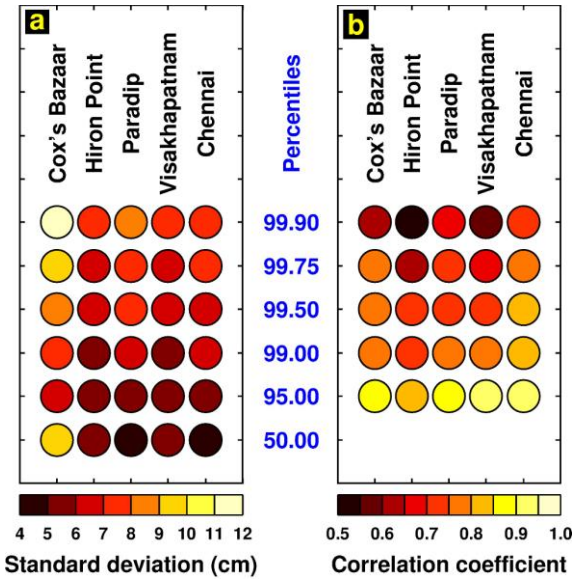

Figure 3.17 a) Standard deviations of various sea level percentile time series. b) Linear correlation coefficients between the 50th percentiles and various high water percentiles.

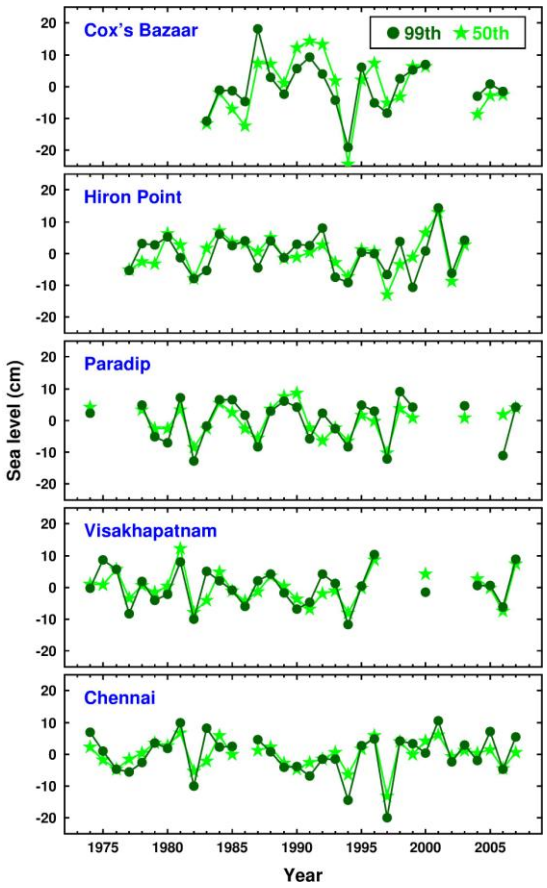

Figure 3.18 Time series of de-trended 99th (median is not removed) and 50th percentiles.

Table 3.5 Correlation coefficients between climate indices (DMI and SOI) and sea level percentiles (99th and 99th–50th).

Station	DMI		SOI	
	99th	99th–50th	99th	99th–50th
Cox's Bazaar	−0.16	0.31	0.16	−0.17
Hiron Point	**−0.56**	−0.07	0.30	−0.18
Paradip	**−0.69**	**−0.48**	**0.59**	0.10
Visakhapatnam	**−0.44**	−0.18	**0.43**	−0.10
Chennai	**−0.58**	**−0.35**	**0.42**	0.28

Statistically significant correlations are shown in bold.

3.4.2.4 Trends in extreme high waters

Figure 3.19 shows the annual 99.9, 99.75, 99.5, 99.0, 95.0 and 50th percentile time series of hourly sea level fitted with linear trend lines for the stations Cox's Bazaar, Hiron Point, Paradip, Visakhapatnam and Chennai. Table 3.6 shows linear trends and standard errors (SEs) in 50th, 99th percentiles as well in 99th percentiles reduced to median for different stations. The high water percentiles at Hiron Point show significant positive trends at 95% confidence level. The trends in the various high water percentiles at Hiron Point are between 4.3 and 5.8 mm/yr, which are generally slightly lower than that of the 50th percentiles (5.4 mm/yr), except for 95th percentiles. The SE estimates for various percentiles at Hiron Point are small compared to respective trends and range between 1.4 and 1.9 mm/yr. Although trends up to 4.3 mm/yr are observed in high water percentiles at Cox's Bazaar, these trends are not statistically significant due to the large SEs, about 2.2–3.8 mm/yr. Along the east coast of India, decreasing trends are observed in the high water percentiles at Paradip Visakhapatnam and Chennai (Table 3.6). Their high water trends are relatively small compared to those at stations at the head of the Bay and range between 0.1 and – 2 mm/yr. These trends are not significant, due to their large SEs. To detect the contribution of MSL change to the observed extreme high water trends, high waters at these locations were reduced to their median values (50th percentiles). The higher MSL trend at Hiron Point resulted in small decreasing trends (not significant) in most of its high water percentiles after MSL reduction. The increasing trends (up to 1.9 mm/yr) in high water percentiles at Cox's Bazaar are not significant since their SEs are even larger than the trends themselves. For the east coast stations, the MSL reduction resulted in minor changes in trends of high water percentiles since the MSL trend itself is relatively small, about ± 1 mm/yr. The trends are not significant for almost all the high water percentiles.

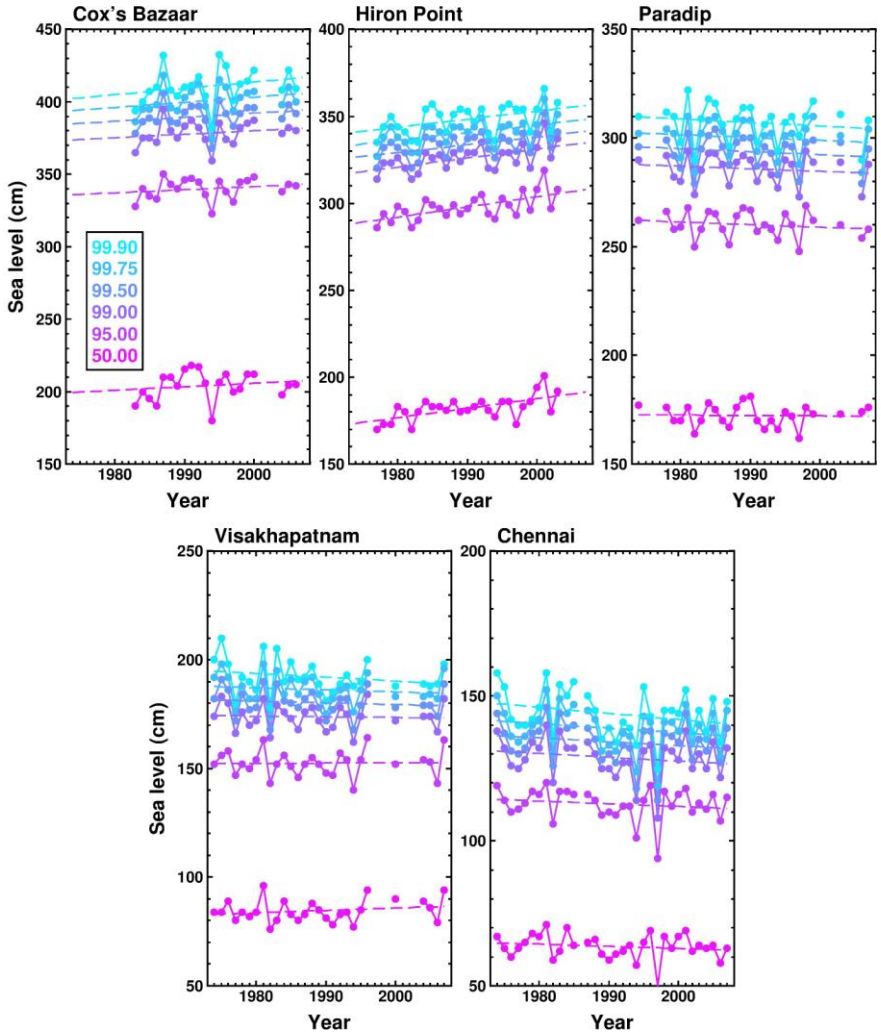

Figure 3.19 Annual 99.9, 99.75, 99.5, 99.0, 95.0 and 50th percentile time series at Cox's Bazaar, Hiron Point, Paradip, Visakhapatnam and Chennai. The dashed lines represent linear trend fits.

Table 3.6 Linear trend and standard error (mm/yr) estimates for 99th, 50th and 99th–50th percentiles.

Station	Period	99th	50th	99th–50th
Cox's Bazaar	1983–2006	2.47±2.60	2.42±3.18	0.05±1.99
Hiron Point	1977–2003	**5.17±1.49**	**5.44±1.39**	−0.27±1.07
Paradip	1974–2007	−1.18±1.54	−0.19±1.13	−0.99±1.01
Visakhapatnam	1974–2007	−0.32±1.16	1.06±1.00	−1.38±0.72
Chennai	1974–2007	−1.34±1.18	−0.74±0.74	−0.60±0.69

Trends statistically significant at 95% confidence level are shown in bold.

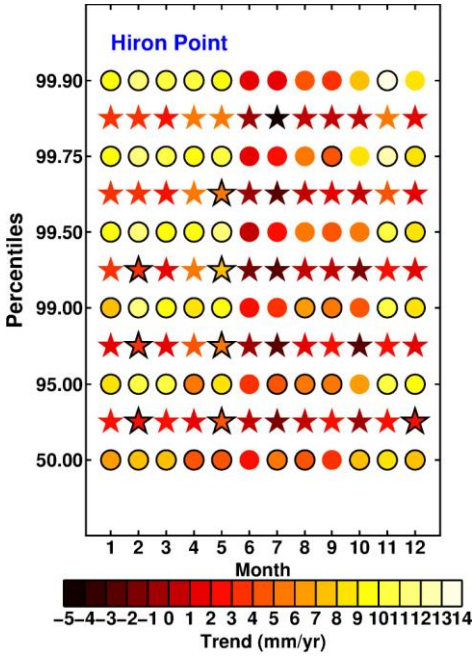

Figure 3.20 Month-wise trends in various sea level percentiles (circle) and high water percentiles reduced to the median (star) at Hiron Point. Statistically significant trends are shown with a black border.

Also, the trends in percentile time series derived from each month were used to see month-wise distribution and whether these trends are confined to specific months. Significantly increasing trends (0.6–13 mm/yr) are observed for most of the months and for the various percentile levels only at Hiron Point (Figure 3.20). Significant increasing trends are found consistently from January to May, and in November and December, for various percentiles. The trends in the months June–October, when the seasonal sea level is mostly at its peak, are also positive, although small, but are less consistent (in terms of trend significance) among the various percentiles. Further, reduction of high water percentiles to median values results in the significance of most of these trends being further reduced (Figure 3.20).

3.4.3 Discussion and conclusions

The magnitude of extreme high waters relative to MSL along the coasts of the western Bay of Bengal increases from the southwestern part of the Bay to the head of the Bay.

This is largely in accordance with the spatial distribution of the tides, which increases from south to north (Murty and Henry, 1983; Sindhu and Unnikrishnan, 2013). The mean of the surge heights which contributes to the annual maximum sea levels ranges from 13 to 50 cm from Chennai to Cox's Bazaar, whereas the mean of the annual maximum surges range from 25 to 120 cm. This asserts the fact that the low and moderate surges contribute to the extreme high waters. Tide-surge interaction is significant in the Bay of Bengal, and towards the head of the Bay the occurrence of surge peaks at high tide is reduced there, the surges may not usually result in extremes. Tide-surge interaction will be discussed in detail in Chapter 4. Recently, Feng et al. (2015) showed that tides are also an important factor for extreme sea levels in regions where tide-surge interaction is large.

The historical record based on anecdotal information and sources in the literature makes clear that there have occurred surges and high water levels, all along the western Bay of Bengal, much higher than those shown in the available tide gauge data. In addition, numerical modelling suggests that there is indeed a potential for much larger events than what available for study here (Dube et al., 1997 and Dube et al., 2009). Moreover, the tide gauges used in the present study are separated from their neighbours by about 250–600 km and this spatial coverage is inadequate to sample surges caused by all tropical cyclones. Therefore, especially severe events may not be always recorded. Also, during certain occasions, such as the 1999 Odisha super cyclone, the tide gauge instrument itself may have failed and will not have provided suitable measurements. Although some of these very extreme events may be missing from the present data set, it should be noted that the tide gauges will have recorded the bulk of major events such as those considered in the present study.

The seasonal changes in the MSL in the Bay of Bengal are prominent. In their study, Tsimplis and Woodworth (1994) noted annual amplitudes exceeding 1000 mm in the Ganges delta (northern Bay of Bengal) and large semi-annual amplitudes along the east coast of India. Shankar (1998), Shankar (2000) and Wijeratne et al. (2008) discussed more on the spatial variability and causes of the seasonal cycle of MSL in the Bay of Bengal and adjacent regions and pointed out the importance of wind-

driven coastal currents and river runoff in seasonal sea level changes, in addition to the atmospheric pressure effects. Seasonal changes in the extreme high waters in the Bay of Bengal are mostly similar to the seasonality in the MSL. Slight difference is observed at northernmost stations, especially Cox's Bazaar, where seasonality observed other than that in MSL. The seasonality peaks during July to August owing to the large river discharge during the south-west monsoon period (June–September) at the head of the Bay of Bengal, whereas it peaks during October–November along the east coast of India. The sea level peak during October–November along the east coast of India has contributions from salinity changes (Shankar, 1998). For the Bay of Bengal, October and November months are observed to have higher cyclone frequencies compared to other months (Li et al., 2013). The combined effect of peak seasonal sea level along with high cyclone risk poses a relatively high risk of extreme sea levels for the east coast of India. Additionally, since the Bay of Bengal is characterised by large changes in sea level between seasons, any change in the seasonality, the baseline over which storm surges occur, may cause potential impact to the flood risk.

The inter-annual variability of extreme high waters observed in the Bay of Bengal closely resembles that of the MSL. The SOI and DMI indices are correlated with high waters at gauges along the east coast of India and Hiron Point. The significant negative correlations with DMI show that extremes are smaller (higher) during positive (negative) IOD events. A direct relationship (positive correlations) is observed between extremes and the SOI indicating lower (higher) extreme sea levels during El Niño (La Niña) events. Most of the correlations reduced when MSL effect is removed, but significant correlations exist between extreme high waters reduced to median and the DMI for the stations Paradip and Chennai, suggesting that the IOD also impact the extreme high waters in an additional way to that due to MSL. An analysis on the impact of ENSO and IOD on sea level variations in the Bay of Bengal by Aparna et al. (2012) showed that sea level change signatures are relatively stronger during positive IOD and El Niño events compared to negative IOD and La Niña events. They further analysed the forcing mechanism for the sea level variations

during IOD and ENSO events, and the model solutions suggest that remote influence of equatorial winds as a reflection of equatorial Kelvin waves from the eastern boundary as Rossby waves and direct wind forcing from winds in the interior of the Bay as the two important forcing processes. During ENSO events the sea level variations are remotely forced from the equator via reflected Rossby waves and a minor contribution from direct wind forcing by interior winds within the Bay, whereas both processes are important during positive IOD events.

The high water percentiles at Hiron Point tide gauge are characterised by significant increasing trends. Trends in high water percentiles reduced to median shows decreasing trends but not significant indicating that much of the changes are due to MSL. Increasing trends in extremes at Hiron Point are not specifically restricted to any season rather found in most of the months although I notice increasing trends which are relatively small and not significant during June–October period for higher high water percentiles due to comparable SEs. In a recent study, Pethick and Orford (2013) reported a rapid rise in high water maxima in the Sundarban area of south-west Bangladesh. They present evidence for tidal amplification, based on three estuarine tide gauge records, as being the predominant cause of this high rate. They found increasing rates of 7.9, 10.7 and 19.5 mm/yr respectively for MSL, monthly mean high water and annual maximum high water at Hiron Point over their period of study from 1990 to 2011. A significant part of the MSL at Hiron Point was considered to be contributed by subsidence of the delta, and in the case of high water change, there is an additional contribution from tidal amplification. According to Pethick and Orford (2013), the tidal amplification at Hiron Point, "an undisturbed environment", must have taken place due to natural processes. The changes in extreme high waters found in the present study are far less compared to the rates reported in Pethick and Orford (2013). Trends are calculated using monthly percentiles for the high waters at Hiron Point and observe trends about 8 mm/yr and in either case (annual and monthly) it should be noted that the period of study in the present study spans 1977–2003. The difference in the period of study as

well as the presence of high water levels towards the end of the record may affect the trend estimates.

In conclusion, the present section discusses the spatial distribution, seasonal pattern, long-term changes and inter-annual variability of extreme high waters along the east coast of India and at the head of the Bay of Bengal during the recent past (1974–2007). The major finding is that the high water changes are mostly in line with MSL change. The results are presented with limitations that emerge from the spatial coverage, length and completeness of the observed data. As the understanding of past extremes is crucial for projection of future extremes, the present study points out the need for an extensive network of tide gauges, as this coastline is among the most vulnerable and densely populated region of the globe. In spite of these data limitations, the results do provide some insight into the reasons for changes in high waters that may be of use to coastal engineers working in this important section of the world coastline and form a basis for the future studies.

Chapter 4

Tide-surge interaction

4.1 Introduction

The storm surge problem in the Bay of Bengal has gained much scientific attention due to the large impacts caused by the surges. The coastal regions adjoining the Bay are densely populated, which results in a massive loss of life and property during the storm surges. The non-linear interaction between tides and surges forms an integral part of storm surge studies. It is crucial to understand and incorporate tide-surge interaction for the precise forecasting of total water levels.

Conventionally, the total water level during a storm is considered as the superposition of tide and surge. However, at certain locations, in particular, in shallow seas and estuaries, significant interaction occurs between tides and surges, which produce changes in propagation characteristics of tides and surges. Interaction studies started in the Thames river estuary with the pioneering works of Proudman (1955). In his theoretical investigation, he considered surge, coming from the open ocean, propagating into an estuary as a progressive wave, Proudman concluded that surge peak close to low tide is higher than that of a surge, which peaks close to high tide. This predominant occurrence of large surges near low tide water is due to friction terms in the equation that represent surge. As tidal range increases, surge maxima close to high tide tend to decrease. As the surge continues for duration and includes tidal high water, the resulting surge time series has two peaks, each on either side of the high tide. Rossiter (1961) found statistically significant tide-surge interaction based on observations on storm surges in the river Thames. Interaction tends to amplify surge heights on rising tides. Rossiter put forward mutual phase alteration as the physical mechanism behind interaction. He confirmed Proudman's theoretical

results on interaction in estuaries. In his investigation on storm surges recorded in the ports along the east coast of Great Britain, Keers (1968) noticed that the degree of interaction correlated with tidal range for ports under the same amphidrome. Moreover, correlation with surge height was noticed to be less significant. Prandle and Wolf (1978) tried to estimate the role quadratic friction in tide-surge interaction in the Thames estuary through numerical modelling approach. The Numerical modelling study by Wolf (1978) made further advancement stating that the largest interaction effects are produced by quadratic friction followed by shallow water terms and convective terms. Walden et al. (1982) noted negligible tide-surge interaction at Portsmouth and prominent interaction at Southampton. Horsburgh and Wilson (2007) put forward a simple mathematical explanation for surge clustering at rising tide, observed along the east coast of the U.K. According to them, phase modification of the tide signal and water depth dependence of surge production are the two processes which contribute to the surge clustering at rising tide. Numerical experiments by Jones and Davies (2007) showed significant interaction effects in coastal regions of the eastern Irish Sea that modified surge elevation and tidal amplitude. Idier et al. (2012) noted interaction heights reaching up to 74 cm during large storm surge events in the eastern part of the English Channel. Shallow water depths and strong tidal currents in the region cause the strong interactions.

Along the coastline of U.K. it has been found that larger surges occur more frequently at rising tide or in the lower tidal bands (Prandle and Wolf, 1978; Dixon and Tawn, 1994; Horsburgh and Wilson, 2007). The non-linear interaction between tides and surges has been reported in many other regions such as, off the east coast of Canada, northeastern U. S. A. (Bernier and Thompson, 2007), north Queensland coast of Australia (Tang et al., 1996), Gulf of Suez (Rady et al., 1994) and Taiwan Strait (Zhang et al., 2010). Bernier and Thompson (2007) noted that interaction effects can reach 20 cm during extreme events at Northumberland Strait. Their sensitivity experiments with numerical model showed non-linear bottom friction contributed significantly to the interaction effects. Rego and Li (2010), in a case study of the Hurricane Rita showed peak water levels were lower than expected for a landfall at

high tide due to interaction. Numerical investigations by Tang et al. (1996) for the north Queens land coast showed that water level from a coupled tide-surge model was lower than that resulted from addition of tide and surge, indicating the interaction effect. Further, authors demonstrated that interaction effect was due to quadratic friction. Oscillations of surge due to tide-surge interaction were observed during the Typhoon Dan (1999) along the western bank of Taiwan Strait (Zhang et al., 2010). Numerical experiments showed non-linear bottom friction has significant role in predicting these oscillations. Park and Suh (2012) noted storm surges are higher at high tide during neap tide than those at spring tide in their numerical investigation of tide-surge interaction in the seas around Korean peninsula. Liu et al. (2016) noticed similar effects along the Taiwan coast. Interaction effects up to 58 cm were observed during extreme events along the coast of Bohai Sea (Xu et al., 2016). Feng et al. (2016) observed semidiurnal signals in the surge series along the east coast of U.S.A. due to tide-surge interaction. Delay and damping of tides resulted in these signals. Authors identified the significant role of bottom friction and Coriolis acceleration causing changes to tides. Tide-surge interaction magnitudes during extreme events tend to reach up to 1m along the southern coast of China (Zhang et al., 2017). Bottom friction is noticed to be the main contributor to the interaction.

4.2 Tide-surge interaction studies in the Bay of Bengal

The tide-surge interaction studies commenced in the Bay of Bengal with numerical modelling experiments by Johns and Ali (1980). They used a non-linear model to determine the interaction between tides and surges at the head of the Bay and the associated river systems. Some general interaction characteristics observed are: the surge elevation due to interaction of tide and surge (ζ_{S+IST}) is less than the elevation due to surge alone (ζ_S) at times of high tide and greater than ζ_S at times of low tide, and the peak values of total water level ($\zeta_{S+T+IST}$) consistently occur after the time of high tide. As surge reaches inside the river, the interaction effects changes and ζ_{S+IST} was less than ζ_S at all stages of the tide. Later, Johns et al. (1985) studied the tide-

surge interaction in the Bay of Bengal by simulating two storm surge events that affected the coasts of Odisha and Andhra (Figure 4.1). They found significant interaction along the Odisha coast and relatively weak interaction along the Andhra coast. Sinha et al. (2008), through numerical modelling experiments of the 1999 Odisha cyclone, found an additional rise in sea level due to tide-surge interaction from 0.2 m to 0.6 m for selected stations along the Odisha coast. There have been some studies on tide-surge interaction in the estuaries bordering the Bay. Sinha et al. (1996) performed numerical experiments in the Hooghly estuary (Figure 4.1) and concluded that the storm surges influence the arrival of tidal high and low waters by as much as 1 h. As-Salek and Yasuda (2001), through numerical modelling studies in the Meghna estuary (Figure 4.1) found that peak surges can develop during any tidal phase, and the one that develops around the time of local peak tide, travels faster than the surge that develops in any other tidal phase. Kim et al. (2008) showed that interaction can increase or decrease the surge height. By studying two major cyclones, which made landfall in the Bangladesh coast, Hussain and Tajima (2017) concluded that during ebb tide, water level due to tide-surge interaction was higher compared to that during high tide. Investigating storm surge during cyclone Sidr, Krien et al. (2017) showed that interaction changed water level by more than one metre, close to the landfall area, in rivers and in the north-eastern part of the Bay. The tide-surge interaction studies in the Bay of Bengal were based on numerical modelling, which concentrate on a selected number of events. However, no efforts have been made so far to analyse hourly tide-gauge data to study the nature of tide-surge interaction. In the present study, I analysed nearly 34 years of hourly tide-gauge data from four stations (Figure 4.1), three along the east coast of India and one in the head of the Bay of Bengal.

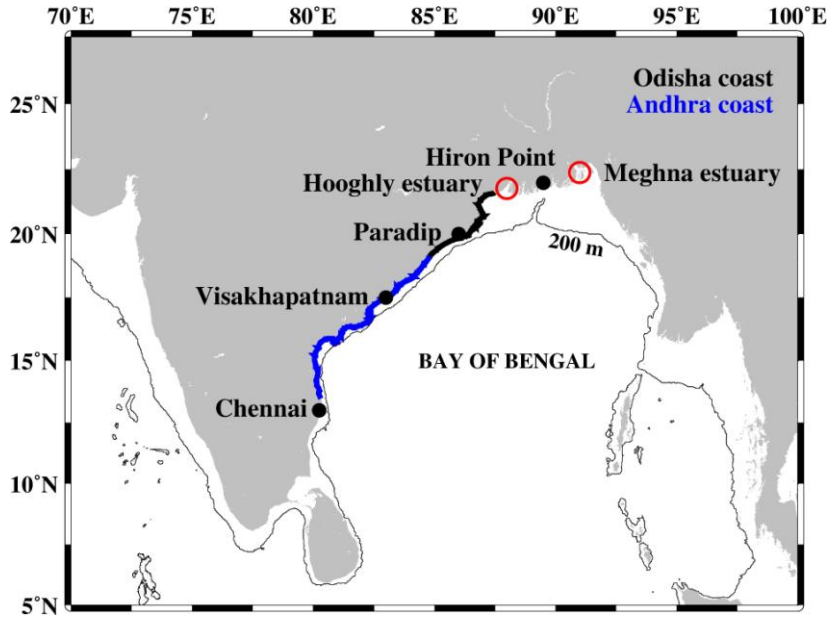

Figure 4.1 A map showing the locations of the tide-gauges used for present study. The 200 m depth contour is shown using improved bathymetry data of Sindhu et al. (2007). Coastline marked in black (blue) represent Odisha (Andhra) coast.

4.3 Tide-surge interaction from observations

4.3.1 Statistical analysis

Several statistical methods are available to estimate tide-surge interaction using tide-gauge observations of storm surges. For the present study, the method put forward by Dixon and Tawn (1994) was used. This method detects the dependency of residuals on the magnitude of the tide. Along with this, a modified version of the above method (Haigh et al., 2010), which identifies the dependency of residuals on the different phases of tide, was also used. Both the methods are described briefly below.

In the first method, the astronomical tidal range was split into five equal bands (each twenty percent of sorted tide data forms a band). If the surge and tide were independent processes, the number of surges per tidal band expected to exceed a threshold, *u*, would be the same for all the bands. On the contrary, if interaction is present, then the number of surges per tidal band which exceed *u* would be expected to differ from one tidal band to another. The level *u* is taken to be the 99th percentile

of the residual series. The peak surge value associated with individual surges separated by 48 hours (to avoid counting of an event twice) above the 99th percentile and corresponding tide magnitudes were identified. This data was plotted over the five equal tidal bands to obtain the observed surge peak distribution. A chi-square test was performed to compare observed distribution with the distribution expected. The test statistic is

$$\chi^2 = \sum_{i=1}^{5} [(N_i - e)^2 / e] \quad \textbf{(4.1)}$$

where N_i is the observed number of surges per tidal band, e is the expected number of surges per tidal band, which is equal to the number of events above the level u , divided by the number of bands. At the 95% significance level, the test statistic is, $\chi^2_{4,0.95} = 9.5$ (critical chi-square from theoretical distribution), where the degrees of freedom are four. Interaction is significant if the computed chi-square value exceeds the critical chi-square at 95% significance level.

In the second method, the timing of the surge peaks relative to the nearest high tide is noted. The tide is then divided into thirteen hourly bands with respect to the timings of high tide (see Figure 4.2b). Each surge above the level u will have equal chance of falling in any of these bands. The interaction is tested with the same statistics (Equation (4.1)) as in the previous method, except that chi-square values are summed over thirteen bands. At the 95% significance level, the test statistic is, $\chi^2_{12,0.95} = 21$ (critical chi-square), where the degrees of freedom are twelve.

4.3.2 Results

Figure 4.2a shows the frequency distribution of surge peaks above 99th percentile against the tide level for each station. Chennai is characterised by small surges and low tidal range (up to 1.5 m). A gradual increase in surge height and tidal range are found towards north and at Hiron Point surge height and tidal range (up to 4 m) become large. At Hiron Point, surge peaks are found to occur largely on mid and low tide levels and their occurrence are hardly noticed on high tide levels. At Paradip,

Visakhapatnam and Chennai, the occurrence of surge maxima is more on mid and high tide levels, with less surge peaks on low tide levels. The chi-square test statistic values indicate statistically significant tide-surge interaction in all the stations. Hiron Point has the highest degree of interaction. For the rest of the stations, the degree of interaction is found to be less.

In Figure 4.2b, the frequencies of surge peaks above 99th percentile were plotted with respect to the timings of high tide for each station. The surge peak frequency pattern has multiple peaks, with each peak on rising and falling tides. Chi-square statistic shows that estimations are statistically significant in all the stations. Hiron Point has the highest degree of interaction. Some features to be noted here are, the surges tend to peak more frequently on the rising tide (4 hours before high tide). A less dominant peak at 5 hours after the high tide is also observed at this location. It may also be noted that none of the surge peaks occur at high tide and only a few of them occur closer to high tide. Though there is a frequent peaking of surges at 4 hours before high tide at Paradip, it is not as pronounced as that in Hiron Point. The degree of interaction here is less than that at Hiron Point. The degree of interaction further decreases towards Visakhapatnam and Chennai. The occurrence of surge peaks is high at 2 hours before and 3 hours after high tide in Visakhapatnam, whereas it is 3 hours before and 4 hours after high tide in Chennai.

Surge heights and tidal ranges increase from Chennai to Hiron Point; accordingly, an increase in surge dependency on tide magnitude and phase is also noticed. I repeated the analysis for surge distributions above 99.5th percentile and found that the surge characteristics were similar to those described earlier. Both the methods show significant interaction at all the locations and the results are found to be consistent.

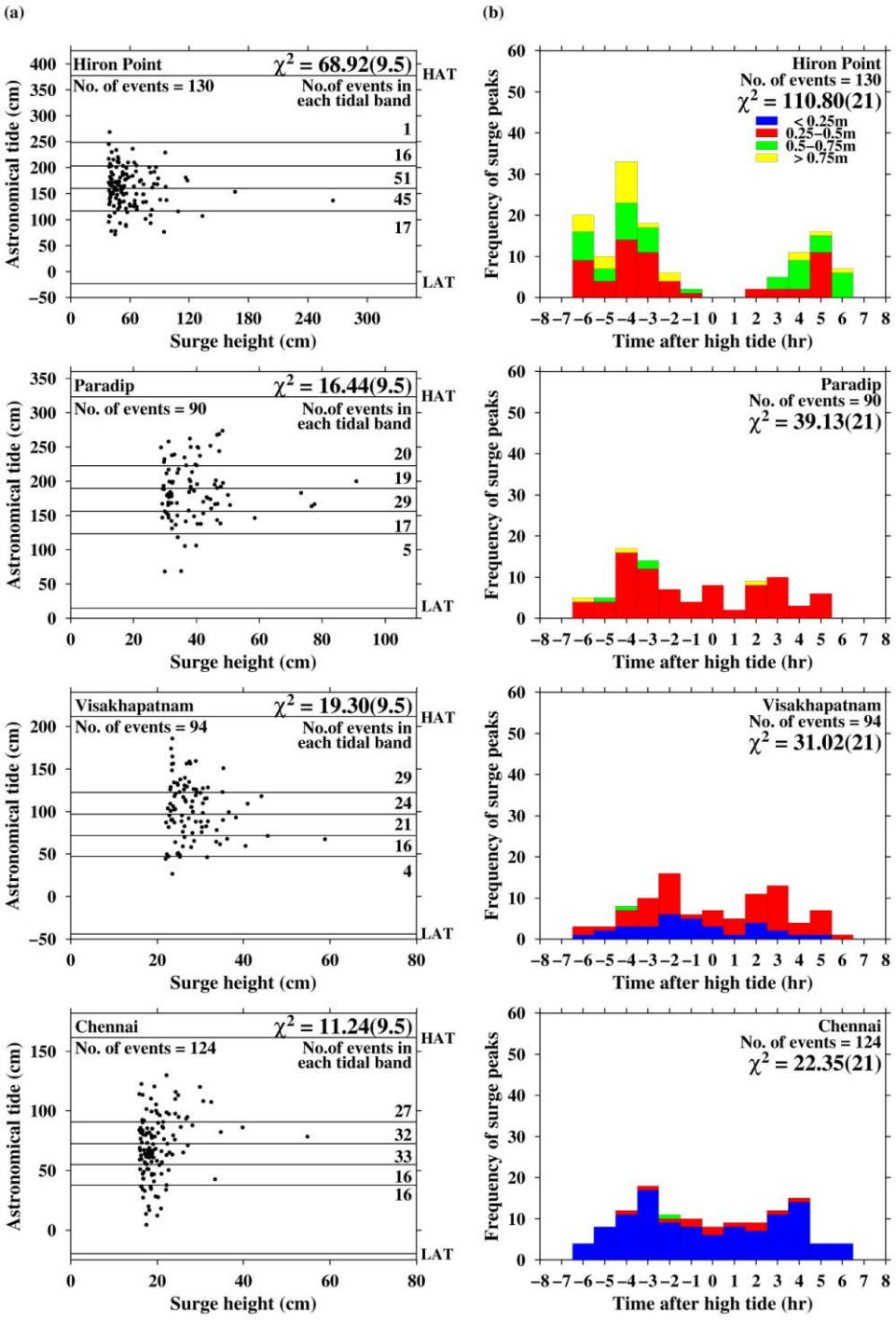

Figure 4.2 Surge peaks above 99th percentile plotted a) with respect to tidal heights (in cm). The horizontal lines on the plots separate equal tidal bands. Lines of HAT (Highest Astronomical Tide) and LAT (Lowest Astronomical Tide) are shown. b) With respect to timing of the high tide (in hours) for the four stations. Surges peaks are classified depending on the magnitudes and different colours represent each magnitude range. The computed chi-square and critical chi-square (in brackets) are presented for each station.

4.3.3 Discussion

To examine the features of clustering of surges during some particular phases of tides, the approach described in Horsburgh and Wilson (2007) was followed. They gave an explanation for the unique clustering of surges on the rising tide through a very simple model and found that phase alteration of the tidal signal, due to surge causes preferential clustering of residuals on rising tide. An observed sea level may be represented by $O = A\ cos(\omega t)$ and the predicted tide as $T = Acos(\omega t-\varphi)$, where A and ω are the amplitude and frequency respectively and φ is the phase shift. The residual, $R = O-T$, which may be deduced as

$$R = Bcos(\omega t+\theta) \quad \textbf{(4.2)}$$

where B and θ are the amplitude and phase, given by

$$B = A(2-2cos\varphi)^{1/2} \quad \textbf{(4.3)}$$

$$\theta = tan^{-1}[sin\varphi/(1-cos\varphi)] \quad \textbf{(4.4)}$$

For small values of φ, a good approximation is that θ will advance observations by close to 90°. This causes the residual peak to be at rising tide. Now, the residual peak will be on falling tide when observation lags the prediction. Earlier, Rossiter (1961) had arrived at a similar conclusion but in a qualitative sense. Tide and surge propagate as shallow water waves, with phase speed of $\sqrt{gh}$, where h is the water depth and g is the acceleration due to gravity. Phase shift occurs when a positive surge increases the phase speed of both tide and surge and hence the observed sea level will lead the predicted tide (opposite effect for a negative surge). Moreover, reduced bottom friction, caused by increased total sea level, will accelerate the surge and tide during a positive surge (opposite effect for negative surge). In addition, there is another mechanism that takes place. A tidally modulated surge production, in which surge is notably higher at low tide and lower at high tide. The steady state effect of wind stress on sea surface (ζ) slope may be written (Pugh, 1996) as

$$\partial\zeta/\partial x = C_D \rho_A W^2/g\rho D \quad \textbf{(4.5)}$$

where C_D is the Drag coefficient, ρ_A is the density of air, W is the wind speed, g is the acceleration due to gravity, ρ is the density of water and D is the water depth. Equation (4.5) shows that the effects of wind stress on sea level gradient increases inversely with the water depth. Hence, the surge generated by the strong winds associated with cyclones, blowing over a large area and for a few hours, is expected to be higher at low tide than high tide. Horsburgh and Wilson (2007) demonstrated this tidally modulated surge production through numerical experiments, which was consistent with Equation (4.5). They showed using residual time series, obtained from model simulations, that surge is prevented from peaking at high tide even at strongest meteorological forcing. The surge modulation by tide is incorporated by modifying the Equation (4.4). The residual peak with respect to high tide is now given by

$$(\theta+\varphi) = \tan^{-1}[\sin\varphi/(1-\cos\varphi+k)]-\pi \quad \textbf{(4.6)}$$

where k is the ratio of local surge modulation to the tidal amplitude. Horsburgh and Wilson (2007), using Equation (4.6), showed theoretically that how small phase shift combined with moderate surge modulation causes surges to peak at rising tide. They applied the theory for the surge data at Sheerness, a tide-gauge station along the U.K. coast, where phase alteration and surge modulation are present.

To test the above theories, I analysed the surges at Hiron Point. Thirty one surge events were identified above a threshold of 99.9 percentile at Hiron Point (Figure 4.3a). These surges were grouped into (1) phase altered, (2) long duration surges, (3) surges at low water and (4) surges at high water, following the classification by Horsburgh and Wilson (2007). Characteristics of each surge type are described in Table 4.1 along with their number of occurrence. Figure 4.3b shows a phase altered event. Thirteen surge events belong to this category, in which there is a phase shift between observed sea level and predicted tide. Figure 4.3c represents a long-duration surge with a characteristic dip at the time of high tide (category 2).

There were twelve such events in this category, which are caused by modulation of surges by tides. These observations indicate that clustering of surges at Hiron Point could be due to a combination of surge modulation and phase alteration of tides. From Chennai, where lowest interaction is observed, to Hiron Point, where interaction is highest, the tidal range and surge heights increase gradually. Earlier studies in the North Sea (Prandle and Wolf, 1978) noticed that interaction increases in direct proportion to both surge height and tidal range.

Table 4.1 Category of surges above 99.9th percentile at Hiron Point.

Type	Characteristics	Number of occurrences
Phase altered	Phase alteration between sea level and predicted tide	13
Long duration	Surge is significant for two or more high tide. A dip in surge during high tide.	12
Low water	No phase alteration. Surge is significant at low tide.	4
High water	No phase alteration. Surge is significant at high tide.	-

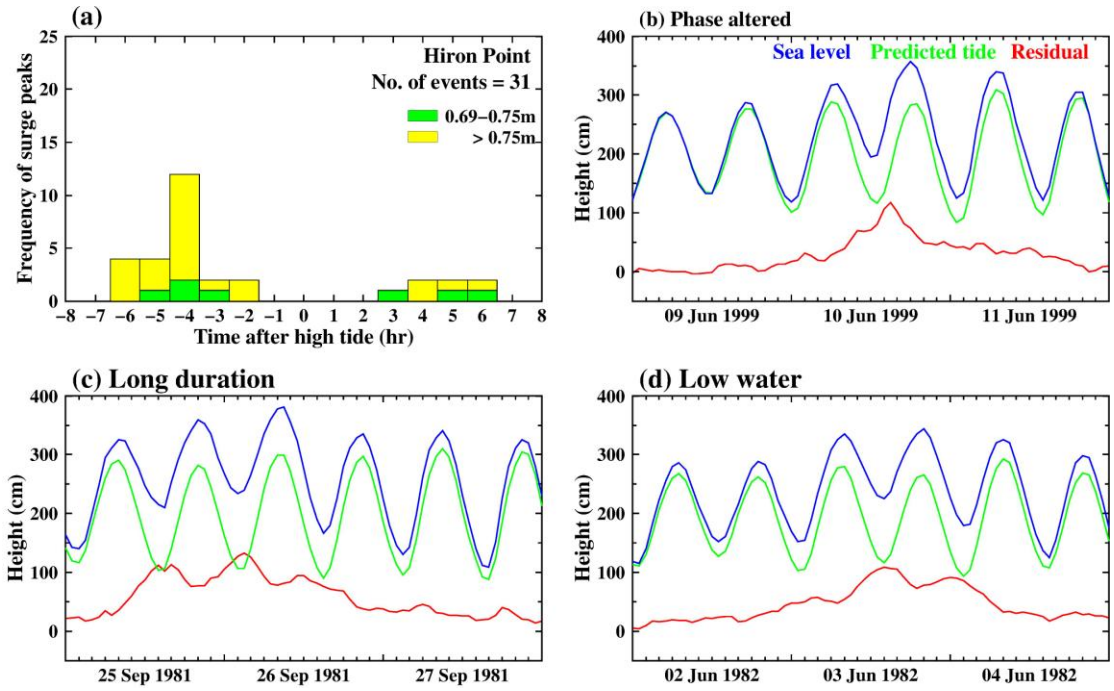

Figure 4.3 a) Surges above 99.9th percentile with respect to timing of high tide at Hiron Point. b-d) Surges representing each category (Table 4.1) at Hiron Point.

4.4 Numerical study of tide-surge interaction at the head of the Bay of Bengal

In the previous sections (Section 4.1 to 4.3), earlier studies on numerical modelling to study tide-surge interaction in the Bay of Bengal and observed interaction characteristics were presented. In this section, interaction processes at the head Bay is studied using simulations from the ADCIRC model. Storm surge during the Cyclone Aila was chosen as the event of interest. A few studies have attempted to simulate the storm surge during the Cyclone Aila (Paul et al., 2016; Gayathri et al., 2016). Even though these studies used coupled tide surge models, their primary interests were towards coastal inundation (Gayathri et al., 2016) and air bubble effects (Paul et al., 2016) found during the Cyclone Aila. In the present work, I investigate in detail, tide-surge interaction effects on water level during the Cyclone Aila.

4.4.1 Cyclone Aila

The Cyclone Aila formed as a tropical depression at 88.8°E and 16.9°N in the central Bay of Bengal (Figure 4.4a) on 22 May 2009 at 18:00:00 hrs (JTWC). The system advanced northward and made landfall at the West Bengal coast (India). Aila developed to a category 1 cyclone before its landfall with maximum sustained 10 m wind speed reaching up to 65 knots (Figure 4.4b). The minimum pressure at the centre of the storm was about 974 mb (Figure 4.4b). The storm surge during this event reached heights of about 3 m (IFNet, 2009; Roy et al., 2009). Water level (including MSL) and Surge observed at Hiron Point (Figure 4.4c), approximately 130 km away on the right side of the cyclone, reached up to 4.5 m and 1.7 m respectively. The observed water level was about one metre higher than the highest astronomical tide for the same year (Figure 4.4c).

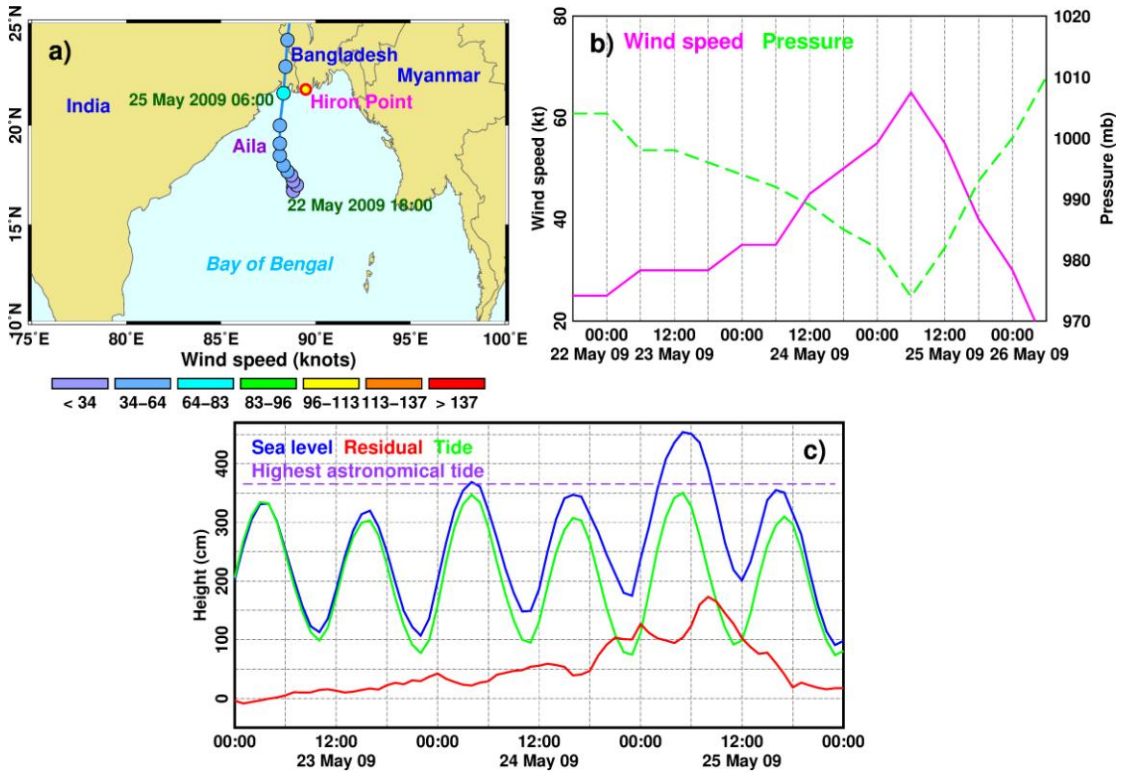

Figure 4.4 a) The Cyclone Aila track (JTWC) with wind intensity shown in Sarrif-Simpson Scale. Location of Hiron Point tide gauge is also shown. b) Time evolution of JTWC maximum wind (1-minute average) and minimum pressure at the surface (10 m) during the Cyclone Aila. c) Water level, tide and storm surge observed by tide gauge at Hiron Point during the Cyclone Aila. The height of the highest astronomical tide for the year 2009 is shown with a dashed line.

4.4.2 Storm surge simulation during the Cyclone Aila

The storm surge and water level simulation results are shown in Figure 4.5. The observed maximum surge was about 1.75 m at Hiron point. Model simulations show a surge of about 1.32 m at Hiron Point. The model performance is satisfactory considering the aspects like, temporal resolution of wind data and wave setup is not included in the present study. The observed surge was much longer (lasts for about 18 hours above 1m) compared to modelled surge. This could be due to the quality of meteorological data. The primary goal of the present study is to study tide-surge interaction; therefore, very fine tuning is not attempted. Observed total water level with mean removed was about 2.65 m and the modelled water level was about 2.33 m (Figure 4.5). The spatial distribution of maximum surge, simulated by the model for the head of the Bay region is shown in Figure 4.6. Simulations show that the Cyclone Aila surge reached above 3 m inside the river channels near to the landfall location. Surge heights reached above half metre along the shallow coastal waters, extending about 400 km, on the right side of landfall location. The simulated storm surge and water level of the present study are comparable to those reported in the previous study (Gayathri et al., 2016). Unlike the earlier study, in the present study drying and wetting scheme was not used. Instead, prescribed the minimum depth to 4 m.

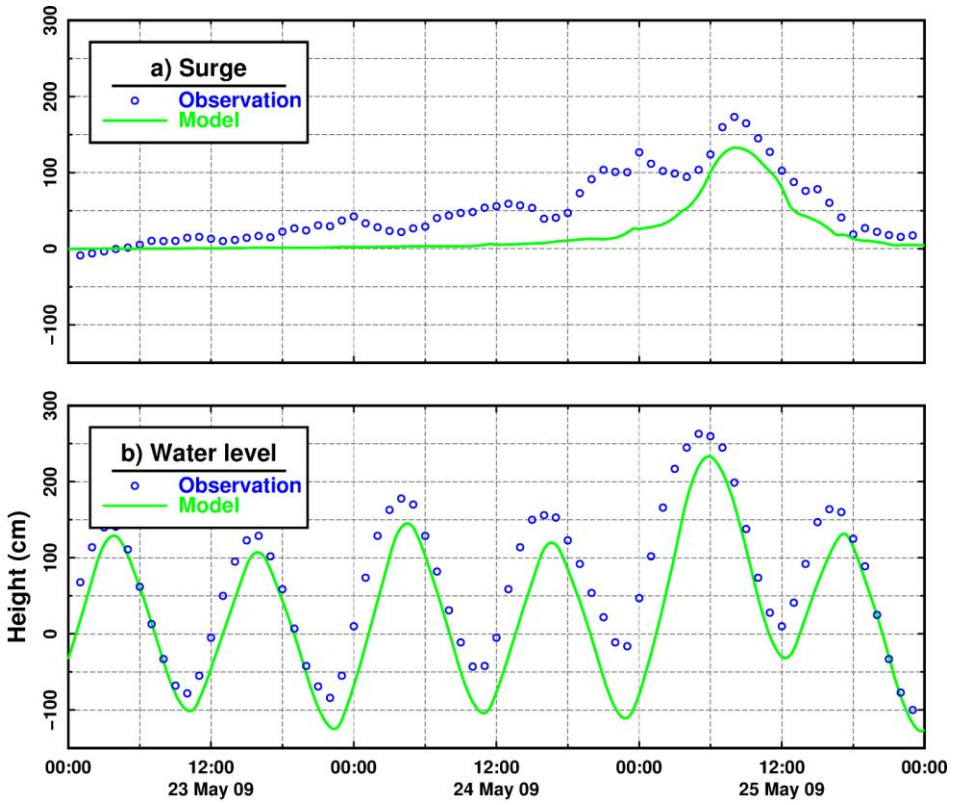

Figure 4.5 Time series of observed (circle) and modelled (line) a) storm surge and b) water level at Hiron Point during the Cyclone Aila. Modelled surge is the practical surge (including interaction effects). Observed water level (with mean removed) is shown.

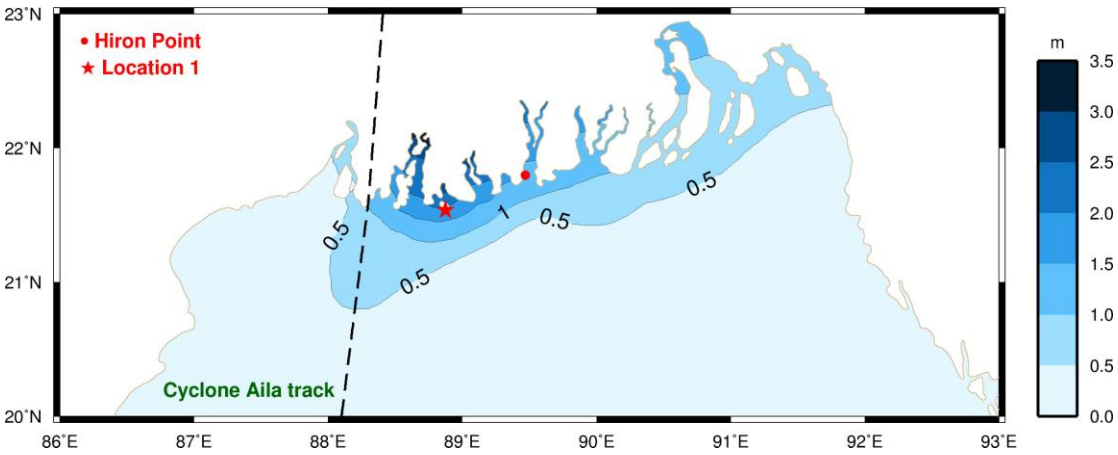

Figure 4.6 Maximum values of storm surge at model grid points. Track of the Cyclone Aila is shown with a dashed line. Location 1, marked with a star, is located near the region of maximum winds.

4.4.3 Tide-surge interaction during the Cyclone Aila

Tide-surge interaction component (ζ_{IST}) can be given as

$$\zeta_{IST} = \zeta_{S+T+IST} - (\zeta_S + \zeta_T) \quad \textbf{(4.7)}$$

This is the difference between the water level in a coupled tide-surge ($\zeta_{S+T+IST}$) and the sum of the tide (ζ_T) and pure surge (ζ_S) simulations. A practical storm surge (ζ_{S+IST}) is defined as the surge including the interaction heights (Idier et al., 2012).
Hence, the following simulations were carried out.

- Forced with tide only
- Forced with surge only
- Forced with both tide and surge

Figures 4.7a and b show the various components of water level during the Cyclone Aila at Location 1 (L1, near the region of maximum winds) and Hiron Point respectively. The water level as the sum of tide and surge (ζ_{S+IST}) was higher than that from a coupled tide-surge simulation ($\zeta_{S+T+IST}$). The change in peak water level was 17 cm and 14 cm at L1 and Hiron Point respectively. The difference in heights between $\zeta_{S+T+IST}$ and $\zeta_{S+IST,}$ the interaction component (ζ_{IST}), is represented by a red line. The interaction was noticed to be high towards low tides reaching values of about 0.35 m and 0.20 m at L1 and Hiron Point respectively. Interaction heights were noticed to be negative ($\zeta_{IST} < 0$) at the time of high tide. Interaction magnitude at L1 was higher than that at Hiron point. Absolute maximum (maximum of $|\zeta_{IST}|$) of this interaction component over the entire study domain is shown in Figure 4.8. Interaction heights were high near the maximum surge and northeastern corner of the head Bay, reaching above 0.4 m. This maximum of absolute interaction tends to follow the bathymetry of the head Bay, which again similar to tidal amplitudes of the region.

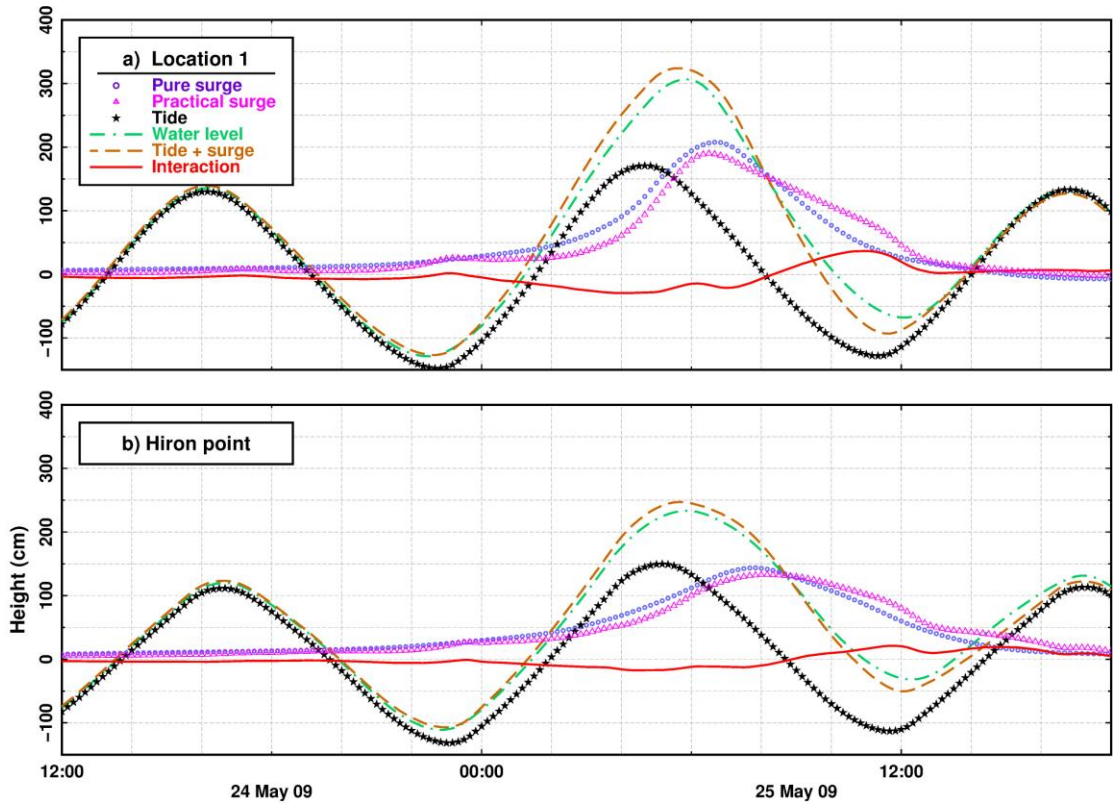

Figure 4.7 Time series of various components of water level at a) Location 1 and b) Hiron Point during the Cyclone Aila. Pure surge is the surge from a surge only simulation and practical surge is the surge including tide-surge interaction.

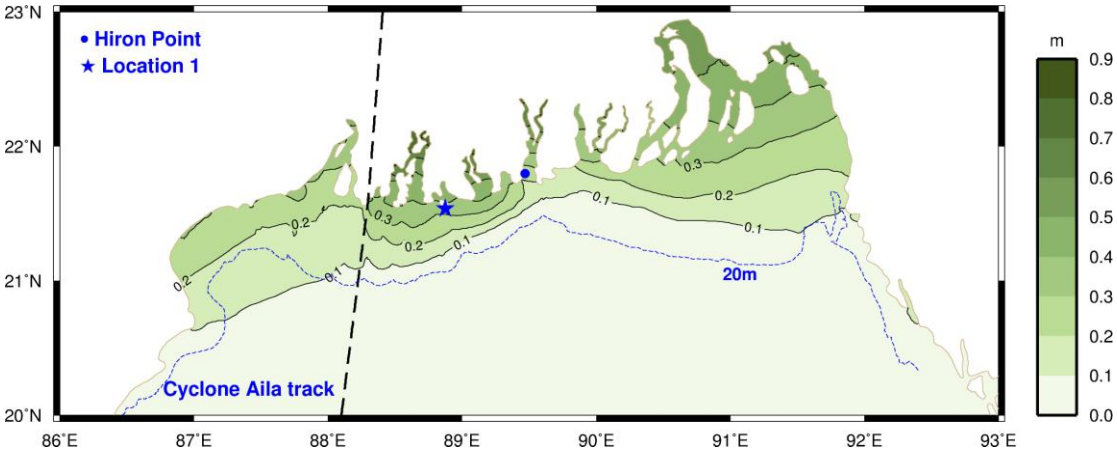

Figure 4.8 Spatial distribution of absolute maximum ($|\zeta_{IST}|$) of interaction component for the Cyclone Aila. Blue dashed line represents the 20 m depth contour.

4.4.4 Numerical experiments

In the previous section, I discussed the tide-surge interaction during the Cyclone Aila. In order to explore further, the influence of tidal phase, tidal range and surge height on interaction, a set of experiments were carried out for the Cyclone Aila event.

i) The storm was made to landfall at different phases of the tide by shifting its time of landfall (Figures 4.9a and b). Time shifting was done for one hour intervals, covering high, low, rising and falling tides.

ii) Cyclone wind speeds (V_{max}) were increased by 10%, 20% and 30% to see the changes in interaction heights with changes in surge heights.

iii) Simulations were carried out during spring and neap tides to examine their effects on interaction.

4.4.5 Influence of tidal phase on interaction

Time series of pure and practical surges for cyclone landfall at various tidal phases are shown in Figure 4.9 at L1 and Hiron Point. It is clear from this figure that for a given surge, at different tidal phases, the resulting practical surge has increased surge height towards low tides. Practical surges close to the high tide were smaller than their pure surge (ζ_S) counterparts.

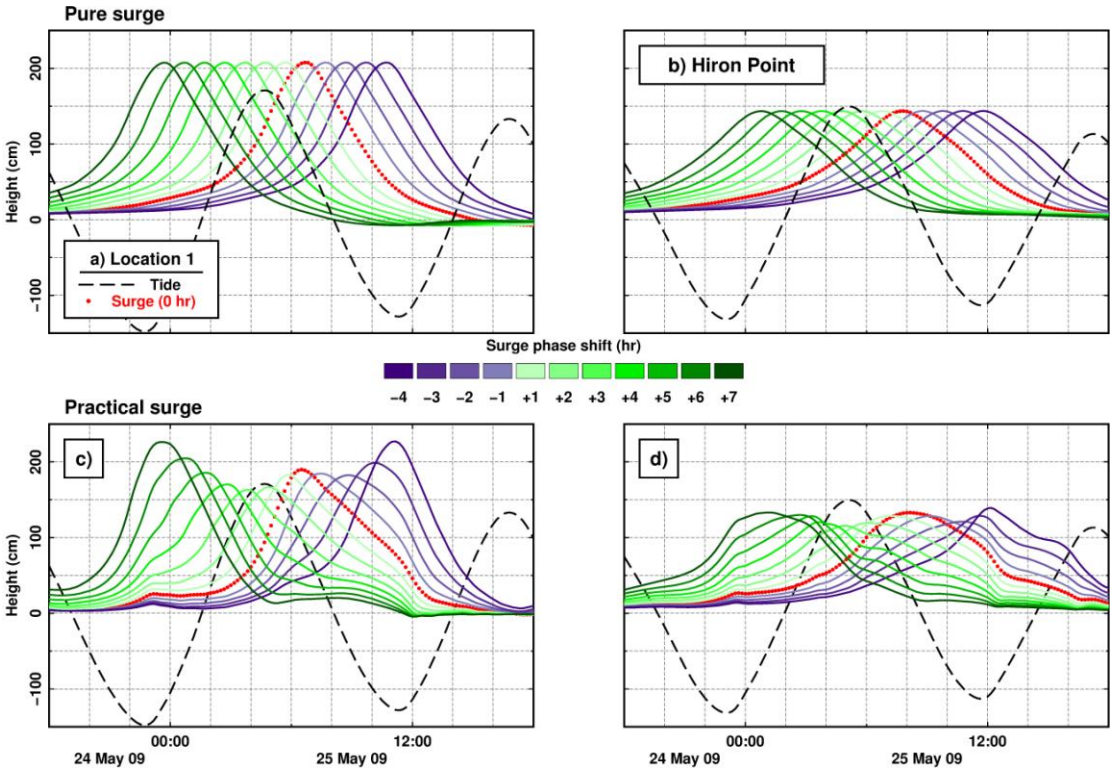

Figure 4.9 a) and b) Pure surges for various time shifted landfalls of Aila at Location 1 and Hiron Point respectively. Positive (negative) phase shift indicates surge leading (lagging) the original surge simulation (red dotted curve with 0 hour phase shift). The lead/lag between the curves is one hour. c) and d) Practical surges (surges due to interaction) at L1 and Hiron Point respectively.

4.4.6 Influence of surge height on interaction

Storm surge simulations with 10%, 20% and 30% increments in wind speed were done and corresponding interaction heights are shown in Figure 4.10. It can be noted that interaction heights increased as the surge height increased and the increase was almost linear.

4.4.7 Spring-neap variations of tide-surge interaction

Figure 4.11 shows the spring-neap variations in tide–surge interaction at L1 and Hiron Point. The tidal amplitudes for spring and neap tides are about 1.5 m and 0.5 m for both the locations respectively. The interaction profiles during spring and neap tides were not different, but their magnitudes differed significantly. Interaction effects were

higher during spring tide compared to that during neap tide. Surge height reductions were about 40 cm and 16 cm at spring and neap tides respectively for L1. At Hiron Point surge height reductions were about 27 cm and 8 cm at spring and neap tides respectively.

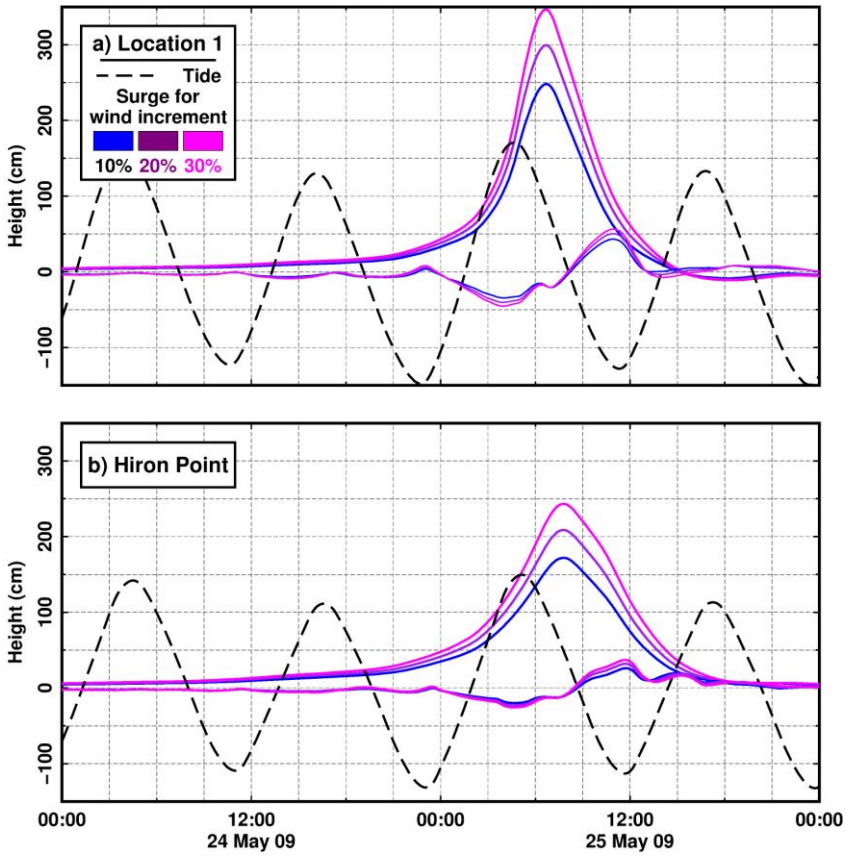

Figure 4.10 Pure surge and interaction time series obtained for the Cyclone Aila with wind speed (Vmax) increased by 10%, 20% and 30% at (a) Location 1 and (b) Hiron Point.

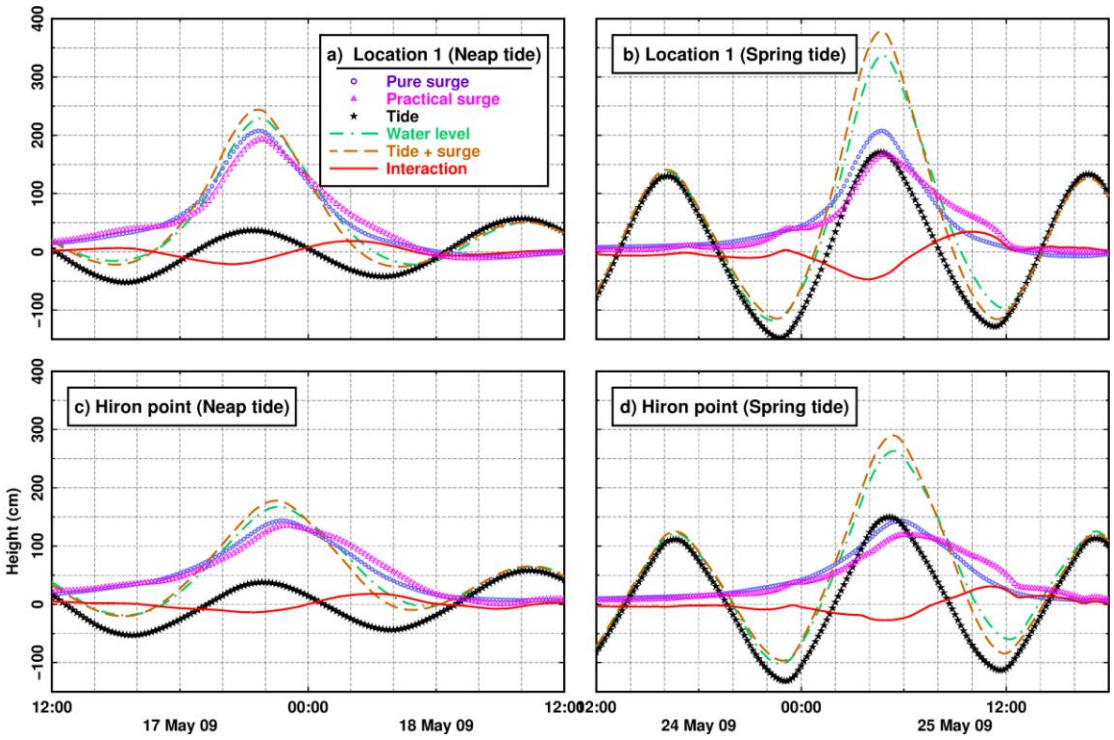

Figure 4.11 Time series of various components of water level at Location 1 and Hiron Point for cyclone landfall during spring and neap tides.

4.4.8 Discussion

The Cyclone Aila storm surge simulations show that practical surge maximum occurring at high tide were lower than those occurring at low tide. This is in accordance with Equation (4.5), which says, wind generated surge is inversely proportional to the depth of water. The reduced (increased) heights of a practical surge during high (low) tides were shown previously by Johns and Ali (1980) and Johns et al. (1985) in the head Bay region. Recent numerical instigations by Krien et al. (2017) and Hussain and Tajima (2017) on tide-surge interaction in the head of the Bay region also confirmed this tendency. This reduced surge production has been reported in various other regions (Horsburgh and Wilson, 2007; Ideir et al., 2012; Zhang et al., 2017). Our observational evidence (Section 4.3.2) has already confirmed the occurrence of surge peaks away from high tide at Hiron Point.

Simulations show that tide-surge interaction was significant in the shallow waters of head Bay and negligible in deep waters (depths greater than 20 m). Extensive area

covering the northeastern part of the head of the Bay is shallow water (below 10 m). Interaction effects can be significant when both tide and surge interact over a large distance in shallow water. Obvious high interaction effect was noticed in this region during the Cyclone Aila. Besides northeastern part of the head Bay, regions close to maximum surge had high tide-surge interaction during the Cyclone Aila. This is similar to the conclusion by Rego and Li (2010), who observed significant interaction between landfall position and within a distance of 2.5 times radius of maximum winds. The spatial distribution of maximum interaction shows that tide-surge interaction was relatively low at Hiron Point. Shallow water regions are more towards the northeast and northwest corners of the Bay and such is the nature of tidal amplitude, they are high towards the corners. The central part of the head Bay, the region including Hiron Point is characterised by relatively low tidal amplitudes and large bathymetric gradient (due to the presence of submarine canyon). These features can probably explain the relatively low interaction effects at Hiron Point.

Numerical experiments show that interaction increases proportionately with surge height. This is similar to the conclusion by Prandle and Wolf (1978). Spring-neap interaction experiment shows that interaction is directly proportional to tidal range. An increase in practical surge height at high tide during neap tide is observed compared to that during spring tide, which is again consistent with Prandle and Wolf (1978), who argued that interaction depends directly on tidal range.

Tide-surge interaction phenomenon has important practical application because of its role in determining the total water level. The tide-surge interaction effect is remarkable in the head of the Bay region, which needs to be taken into account for numerical modelling simulations.

Chapter 5

Conclusions and future perspectives

The cyclone disasters along the coasts of the Bay of Bengal are of serious concern. Especially at the head of the Bay, a large population gets affected by the cyclones and surges. Geographical features of the head Bay, such as, wide continental shelf, shallow water, converging nature of the coast and the presence of numerous estuarine channels, enhance surges and their penetration into coastal regions resulting in inundation. Most of the literature available on storm surges in the Bay of Bengal is based on numerical modelling research. Tide gauges functioning along the coast record the sea level changes, typically at hourly or even higher intervals. These records also have sea level signatures during storm surges. When such long-term records are available, they can be subjected to scientific analysis to understand features of storm surges. The present thesis is an effort to study storm surges and extreme sea levels in the Bay of Bengal using long-term (34 years) tide gauge observations.

5.1 Major findings and conclusions

In Chapter 3, the first two sections describe tropical cyclone and storm surges in the tide gauge records during the period 1974-2007. Storm surges in the Bay of Bengal are forced by cyclones. The semi-enclosed nature of the Bay leads to high rates of landfall of tropical cyclones, which are formed in the Bay. Cyclone frequency is observed to be high towards the northern part of the Bay, which is among the densely populated coasts of the world. Analysis of 34 years of storm surge observations derived from sea level data reveals that the northern part of the Bay experienced highest storm surges compared to the southwestern part. As noticed, the northern part

of the Bay has the highest frequency of cyclones, also, this part of the Bay is characterised by a wide continental shelf, shallow depths and converging coast. These factors have contributed to the high surge heights in the region. The surge distributions are positively skewed indicating the presence of large positive surges than negative surges.

Section 3 of Chapter 3 deals with use of satellite altimetry data for storm surge studies. Signatures of many storm surges have been found in the altimeter data. Though their magnitudes are not expected to match with those observed by nearest tide gauges, the magnitudes are found to be comparable. A close match is not expected because the surges identified are slightly offshore and at the coast in altimeter and tide gauge records respectively. This study offers a few possibilities; coastal altimetry can provide nearly 25 years data for under-explored and extremely vulnerable coastlines of the Bay of Bengal. This in turn offers a good possibility for comparison with model simulations and assimilation in storm surge models. Moreover, it is also shown that multiple missions could enhance the possibilities of capturing storm surges.

In the final section of Chapter 3, characteristics of extreme sea levels are presented. An assessment of the recent evolution of extreme high waters along the severe cyclone-risk coasts of the Bay of Bengal (the east coast of India and Bangladesh) shows that the highest water levels above MSL have the greatest magnitude towards the northern part of the Bay, which decreases towards the southwest region. Extreme high waters observed are a combination of moderate, or even small, surges with large tides at these stations in most of the cases. Seasonal changes in the extremes are remarkable, especially at the northernmost stations where it reaches more than 30 cm in amplitude. Seasonal distribution has a single peak at the northern stations, and it has bimodal nature towards the southwest. The nature of seasonality in extremes is similar to that of MSL. Changes in extreme high waters in the Bay of Bengal are found to be influenced by the El Niño Southern Oscillation and the Indian Ocean Dipole. Long-term increasing trends, which are significant, have been observed in the extreme high waters at Hiron Point, at the head of the Bay. For the other stations,

Paradip, Visakhapatnam and Chennai, no significant trends have been observed. Overall, the nature of variability in extremes is in line with MSL variability.

Chapter 4 entirely addressed the tide-surge interaction phenomenon in the Bay of Bengal. Observed nature of interaction is presented in the third section of the chapter. The surge peak distribution with respect to the tidal phase at Hiron Point, at the head of the Bay of Bengal, shows a clear interaction pattern. It is observed that many of the surges peak four hours before the high tide at Hiron Point. Further, the distribution has asymmetric bimodal character with peaks on rising and falling tides and only a few of the surge peaks occurring close to high tide. The phase alteration of tides with respect to the sea level explains the observed surge peaking at rising.

Further, in the fourth section of Chapter 4, the interaction phenomenon is addressed through a numerical modelling study. A nonlinear numerical model (ADCIRC) has been used to investigate tide-surge interaction process at the head of the Bay of Bengal during the Cyclone Aila. The results show noticeable interaction effects. It is also found that high tides lead to reduced surge heights and interaction heights increased in proportion to surge height. Interaction heights are found to be higher during spring tide than those during neap tide. The model has been configured without river and wave effects in it. This might have some implications to the results. However, general conclusions can be the same.

Present thesis has explored the characteristics of surge and extreme sea levels along the coasts of the Bay of Bengal. Even though many instances of storm surges are recorded in the tide gauges, some of them are missing due to inadequate spatial coverage of the tide gauges. Hence, it is desirable to have a close network of tide gauges, which will improve capturing of storm surges and obtaining peak surge heights.

5.2 Future perspectives

Long-term tide-gauge data do not have a good spatial coverage along the coasts of the Bay of Bengal. To derive detailed spatial features of storm surges and extreme sea levels, numerical modelling studies can be carried out. It has been noticed that sea-level rise trends are quite high in the head of the Bay owing to various factors, including delta subsidence. Understanding changes in storm surge dynamics in such a scenario is important. It is also a subject of interest to study the remotely forced storm surges in the Bay of Bengal. Positive surges, which tend to increase the sea level, bring much threat to coastal communities compared to negative surges. Significantly reduced sea levels during negative surges are also capable of bringing some risk. Negative storm surge are relatively less studies in the Bay.

Capabilities of altimetry to identifying storm surges in the Bay have been explored in a preliminary manner. The present research explored the altimeter surges for 15 years of period. Recent altimeter data spanning for about a decade are still need to be used. Further, the scope of altimeter data can be extended through comparison of altimeter-observed storm surges with numerical models and assimilation of altimeter observations into numerical models. It is also possible to explore the usefulness of these altimeter observations to study the extreme sea levels related to the storm surges and mesoscale variability.

Tide-surge interaction patterns have been studied only for the selected stations. There is need to understand this phenomenon at other high tide and shallow water regimes in the head of Bay of Bengal. Further, the numerical modeling study discussed in the present thesis can be improved by incorporating river and wave forcings.

Appendices

Appendix A

Tidal constituents used for de-tiding sea-level data

No	Constituent	Speed (deg/hour)
1	SA	0.0410686
2	SSA	0.0821373
3	MM	0.5443747
4	MSF	1.0158958
5	MF	1.0980331
6	2Q1	12.8542862
7	SIG1	12.9271398
8	Q1	13.3986609
9	RO1	13.4715145
10	O1	13.9430356
11	MP1	14.0251729
12	M1	14.4920521
13	CHI1	14.5695476
14	PI1	14.9178647
15	P1	14.9589314
16	S1	15.0000000
17	K1	15.0410686
18	PSI1	15.0821353
19	PHI1	15.1232059
20	TH1	15.5125897
21	J1	15.5854433
22	SO1	16.0569644
23	OO1	16.1391017
24	OQ2	27.3416965
25	MNS2	27.4238337
26	2N2	27.8953548
27	MU2	27.9682084
28	N2	28.4397295
29	NU2	28.5125831
30	OP2	28.9019669
31	M2	28.9841042
32	MKS2	29.0662415
33	LAM2	29.4556253
34	L2	29.5284789
35	T2	29.9589333

36	S2	30.0000000
37	R2	30.0410667
38	K2	30.0821373
39	MSN2	30.5443747
40	KJ2	30.6265120
41	2SM2	31.0158958
42	MO3	42.9271398
43	M3	43.4761563
44	SO3	43.9430356
45	MK3	44.0251729
46	SK3	45.0410686
47	MN4	57.4238337
48	M4	57.9682084
49	SN4	58.4397295
50	MS4	58.9841042
51	MK4	59.0662415
52	S4	60.0000000
53	SK4	60.0821373
54	2MN6	86.4079380
55	M6	86.9523127
56	MSN6	87.4238337
57	2MS6	87.9682084
58	2MK6	88.0503457
59	2SM6	88.9841042
60	MSK6	89.0662415
61	MA2	28.9430356
62	MB2	29.0251728

Appendix B

ADCIRC input: Fort.14

```
Aila
123733  65904
         1   90.5073888369   22.6116590641    0.8973369960
         2   90.5074554143   22.6071952085   -0.7744544314
         3   90.5115572660   22.6089861750    7.2446689873
         ...
         ...
     65902   88.1346249671   22.1869577821    6.9746181764
     65903   88.1338358295   22.1949990521   15.8525953243
     65904   88.1324007655   22.1909056958    8.1637075520
    1    3     5     1     3
    2    3     1     2     3
    3    3     5     6     1
    ...
    ...
123729    3 65898 65902 65899
123730    3 65898 65901 65902
123731    3 65901 65900 65903
123732    3 65901 65904 65902
123733    3 65903 65904 65901
1 = Number of open boundaries
138 = Total number of open boundary nodes
138 = Number of nodes for open boundary 1
21131
21623
...
...
33822
33240
```

```
20 = Number of land boundaries
7994 = Total number of land boundary nodes
69 1 = Number of nodes for land boundary 1
64883
64839
...
...
64923
64883
42 1 = Number of nodes for land boundary 2
47927
47926
...
...
47928
47927
...
...
5736 0 = Number of nodes for land boundary 9
21131
20652
...
...
33239
33240
```

Appendix C

ADCIRC input: Fort.15

```
02-05-2009-18:00                          ! 32 CHARACTER
ALPHANUMERIC RUN DESCRIPTION
ibtype0&1-tide-aila                       ! 24 CHARACTER
ALPHANUMERIC RUN IDENTIFICATION
1                                         ! NFOVER - NONFATAL
ERROR OVERRIDE OPTION
0                                         ! NABOUT - ABREVIATED
OUTPUT OPTION PARAMETER
1                                         ! NSCREEN - OUTPUT TO
UNIT 6 PARAMETER
68                                        ! IHOT - HOT START
OPTION PARAMETER
2                                         ! ICS - COORDINATE
SYSTEM OPTION PARAMETER
0                                         ! IM - MODEL RUN TYPE:
0,10,20,30 = 2DDI, 1,11,21,31 = 3D(VS), 2 = 3D(DSS)
1                                         ! NOLIBF - NONLINEAR
BOTTOM FRICTION OPTION
1                                         ! NOLIFA - OPTION TO
INCLUDE FINITE AMPLITUDE TERMS
1                                         ! NOLICA - OPTION TO
INCLUDE CONVECTIVE ACCELERATION TERMS
1                                         ! NOLICAT - OPTION TO
CONSIDER TIME DERIVATIVE OF CONV ACC TERMS
0                                         ! NWP - Number of nodal
attributes.
1                                         ! NCOR - VARIABLE
CORIOLIS IN SPACE OPTION PARAMETER
```

```
1                                       ! NTIP - TIDAL POTENTIAL
OPTION PARAMETER
8                                       ! NWS - WIND STRESS AND
BAROMETRIC PRESSURE OPTION PARAMETER
1                                       ! NRAMP - RAMP FUNCTION
OPTION
9.80665                                 ! G - ACCELERATION DUE
TO GRAVITY - DETERMINES UNITS
0.00100                                 ! TAU0 - WEIGHTING
FACTOR IN GWCE
10.00000                                ! DT - TIME STEP (IN
SECONDS)
0.00000                                 ! STATIM - STARTING
SIMULATION TIME IN DAYS
0.00000                                 ! REFTIME - REFERENCE
TIME (IN DAYS) FOR NODAL FACTORS AND EQUILIBRIUM ARGS
2009 05 02 18     1         0.800000    !
YYYY,MM,DD,HH24,StormNumber,BLAdj
23.50000                                ! RNDAY - TOTAL LENGTH
OF SIMULATION (IN DAYS)
5.00000                                 ! DRAMP - DURATION OF
RAMP FUNCTION (IN DAYS)
0.350000 0.300000 0.350000              ! TIME WEIGHTING FACTORS
FOR THE GWCE EQUATION
4.000000                                ! H0 - MINIMUM WATER
DEPTH
89.721703 20.566036                     ! SLAM0, SFEA0 -
LONGITUDE AND LATITUDE ON WHICH THE CPP COORDINATE PROJECTION IS
CENTERED
0.002800                                ! FFACTOR - 2DDI BOTTOM
FRICTION COEFFICIENT
80.000000                               ! ESLM - SPATIALLY
CONSTANT HORIZONTAL EDDY VISCOSITY FOR THE MOMENTUM EQUATIONS
0.000100                                ! CORI - CONSTANT
CORIOLIS COEFFICIENT
```

```
5                                       ! NTIF - NUMBER OF TIDAL
POTENTIAL CONSTITUENTS
K1                                      ! TIPOTAG - NAME OF
TIDAL POTENTIAL CONSTITUENT
0.14156500 0.000072921158358 0.736 1.074 47.472    ! TPK, AMIGT,
ETRF, FFT, FACET - CONSTITUENT PROPERTIES
M2                                      ! TIPOTAG - NAME OF
TIDAL POTENTIAL CONSTITUENT
0.24233400 0.000140518902509 0.693 0.979 343.429   ! TPK, AMIGT,
ETRF, FFT, FACET - CONSTITUENT PROPERTIES
N2                                      ! TIPOTAG - NAME OF
TIDAL POTENTIAL CONSTITUENT
0.04639800 0.000137879699487 0.693 0.979 306.633   ! TPK, AMIGT,
ETRF, FFT, FACET - CONSTITUENT PROPERTIES
O1                                      ! TIPOTAG - NAME OF
TIDAL POTENTIAL CONSTITUENT
0.10051400 0.000067597744151 0.695 1.119 293.172   ! TPK, AMIGT,
ETRF, FFT, FACET - CONSTITUENT PROPERTIES
S2                                      ! TIPOTAG - NAME OF
TIDAL POTENTIAL CONSTITUENT
0.11284100 0.000145444104333 0.693 1.000 180.000   ! TPK, AMIGT,
ETRF, FFT, FACET - CONSTITUENT PROPERTIES
5                                       ! NBFR - NUMBER OF
PERIODIC FORCING FREQUENCIES ON ELEVATION SPECIFIED BOUNDARIES
K1                                      ! BOUNTAG - FORCING
CONSTITUENT NAME
0.000072921158358 1.074 47.472
M2                                      ! BOUNTAG - FORCING
CONSTITUENT NAME
0.000140518902509 0.979 343.429
N2                                      ! BOUNTAG - FORCING
CONSTITUENT NAME
0.000137879699487 0.979 306.633
O1                                      ! BOUNTAG - FORCING
CONSTITUENT NAME
```

```
0.000067597744151 1.119 293.172
S2                                      ! BOUNTAG - FORCING
CONSTITUENT NAME
0.000145444104333 1.000 180.000
K1                                      ! EALPHA - FORCING
CONSTITUENT NAME AGAIN
0.144962 242.529                        ! EMO, EFA
0.144948 242.520                        ! EMO, EFA
...
...
0.130766 252.632                        ! EMO, EFA
0.130750 252.637                        ! EMO, EFA
M2                                      ! EALPHA - FORCING
CONSTITUENT NAME AGAIN
0.748358 76.922                         ! EMO, EFA
0.747755 76.939                         ! EMO, EFA
...
...
0.548183 79.293                         ! EMO, EFA
0.548154 79.296                         ! EMO, EFA
N2                                      ! EALPHA - FORCING
CONSTITUENT NAME AGAIN
0.154713 72.896                         ! EMO, EFA
0.154595 72.886                         ! EMO, EFA
...
...
0.110820 75.198                         ! EMO, EFA
0.110817 75.198                         ! EMO, EFA
O1                                      ! EALPHA - FORCING
CONSTITUENT NAME AGAIN
0.051802 229.557                        ! EMO, EFA
0.051784 229.563                        ! EMO, EFA
...
...
0.046119 244.840                        ! EMO, EFA
```

```
0.046117 244.842                          ! EMO, EFA
S2                                        ! EALPHA - FORCING
CONSTITUENT NAME AGAIN
0.349603 108.609                          ! EMO, EFA
0.349207 108.585                          ! EMO, EFA
...
...
0.245990 108.021                          ! EMO, EFA
0.245962 108.027                          ! EMO, EFA
90                                        ! ANGINN - MINIMUM ANGLE
FOR TANGENTIAL FLOW
-1 20.000000 23.500000 60                 ! NOUTE, TOUTSE, TOUTFE,
NSPOOLE - FORT 61 OPTIONS
8                                         ! NSTAE - NUMBER OF
ELEVATION RECORDING STATIONS, FOLLOWED BY LOCATIONS ON PROCEEDING
LINES
89.4684421974   21.7841091633             ! Hiron Point  1.36
31488
...
...
-1 20.000000 23.500000 60                 ! NOUTV, TOUTSV, TOUTFV,
NSPOOLV - FORT 62 OPTIONS
8                                         ! NSTAV - NUMBER OF
VELOCITY RECORDING STATIONS, FOLLOWED BY LOCATIONS ON PROCEEDING
LINES
89.4684421974   21.7841091633             ! Hiron Point  1.36
31488
...
...
-1 20.000000 23.500000 60                 ! NOUTM, TOUTSM, TOUTFM,
NSPOOLM - METEOROLOCIAL OUTPUT INFO
8                                         ! NSTAM - NUMBER OF
METEOROLOGICAL RECORDING STATIONS, FOLLOWED BY LOCATIONS ON
PROCEEDING LINES
```

```
89.4684421974   21.7841091633           ! Hiron Point  1.36
31488
...
...
-1 21.750000 23.500000 60               ! NOUTGE, TOUTSGE,
TOUTFGE, NSPOOLGE - GLOBAL ELEVATION OUTPUT INFO (UNIT 63)
0 21.750000 23.500000 60                ! NOUTGV, TOUTSGV,
TOUTFGV, NSPOOLGV - GLOBAL VELOCITY OUTPUT INFO (UNIT 64)
0 21.750000 23.500000 60                !
NOUTGM,TOUTSGM,TOUTFGM,NSPOOLGM  - GLOBAL METEOROLOGICAL OUTPUT
INFO (UNIT 73/74)
0                                       ! NHARF - NUMBER OF
FREQENCIES IN HARMONIC ANALYSIS
20.000000 80.000000 360 0.000000        ! THAS,THAF,NHAINC,FMV -
HARMONIC ANALYSIS PARAMETERS
0 0 0 0                                 !
NHASE,NHASV,NHAGE,NHAGV - CONTROL HARMONIC ANALYSIS AND OUTPUT TO
UNITS 51,52,53,54
0 360                                   ! NHSTAR,NHSINC - HOT
START FILE GENERATION PARAMETERS
1 0 1e-010 50                           ! ITITER, ISLDIA,
CONVCR, ITMAX - ALGEBRAIC SOLUTION PARAMETERS
&timeBathyControl  !NDDT, BTIMINC, BCHGTIMINC -- BATHYMETRY TIME
RECORDS (IN SECONDS) AND TRANSITION TIME
    NDDT = 0
    BTIMINC = 0
    BCHGTIMINC = 43200
/
```

References

Abeysirigunawardena, D.S., Walker, I.J., 2008. Sea level responses to climatic variability and change in northern British Columbia. Atmosphere-ocean, 46(3), pp.277-296.

Agardy, T., Alder, J., Dayton, P., Curran, S., Kitchingman, A., Wilson, M., Catenazzi, A., Restrepo, J., Birkeland, C., Blaber, S.J.M., Saifullah, S., Branch, G.M., Boersma, D., Nixon, S., Dugan, P., Davidson, N., Vorosmarty, C., 2005. Hassan, R., Scholes, R., Ash, N. (Eds.), Coastal systems. In: Ecosystems and human well-being: Current state and trends, Volume 1. Findings of the Condition and Trends Working Group of the Millennium Ecosystem Assessment. Island Press, pp.513-549.

Agnihotri, N., Chittibabu, P., Jain, I., Sinha, P.C., Rao, A.D., Dube, S.K., 2006. A bay–river coupled model for storm surge prediction along the Andhra coast of India. Natural hazards, 39(1), pp.83-101.

Aparna, S.G., McCreary, J.P., Shankar, D., Vinayachandran, P.N., 2012. Signatures of Indian Ocean Dipole and El Niño–Southern oscillation events in sea level variations in the Bay of Bengal. Journal of Geophysical Research: Oceans, 117(C10).

Appelquist, L.R., Halsnæs, K., 2015. The Coastal Hazard Wheel system for coastal multi-hazard assessment & management in a changing climate. Journal of Coastal Conservation, 19(2), pp.157-179.

As-Salek, J.A., 1997. Negative surges in the Meghna estuary in Bangladesh. Monthly Weather Review, 125(7), pp.1638-1648.

As-Salek, J.A., Yasuda, T., 2001. Tide-surge interaction in the Meghna estuary: most severe conditions. Journal of Physical Oceanography, 31(10), pp.3059-3072.

Bechle, A.J., Wu, C.H., Kristovich, D.A., Anderson, E.J., Schwab, D.J., Rabinovich, A.B., 2016. Meteotsunamis in the Laurentian Great Lakes. Scientific Reports, 6, 37832.

Bell, C., Vassie, J.M., Woodworth, P.L., 1999. POL/PSMSL Tidal Analysis Software Kit 2000 (TASK-2000). Permanent Service for Mean Sea Level. CCMS Proudman

Oceanographic Laboratory, Bidston Observatory, Birkenhead, Merseyside CH43 7RA, UK.

Bernier, N.B., Thompson, K.R., 2007. Tide-surge interaction off the east coast of Canada and northeastern United States. Journal of Geophysical Research: Oceans, 112(C6).

Bhaskaran, P.K., Gayathri, R., Murty, P.L.N., Bonthu, S., Sen, D., 2014. A numerical study of coastal inundation and its validation for Thane cyclone in the Bay of Bengal. Coastal Engineering, 83, pp.108-118.

Bindoff, N.L., Willebrand, J., Artale, V., Cazenave, A., Gregory, J.M., Gulev, S., Hanawa, K., Le Quéré, C., Levitus, S., Nojiri, Y., Shum, C.K., Talley, L.D., Unnikrishnan, A. S., 2007. Observations: oceanic climate change and sea level. In: Solomon, S., Qin, D., Manning, M., Chen, Z., Marquis, M., Averyt, K.B., Tignor, M., Miller, H.L. (Eds.), Climate change 2007: the physical science basis. Contribution of Working Group I to the Fourth Assessment Report of the Intergovernmental Panel on Climate Change. Cambridge University Press, Cambridge, UK.

Birol, F., Delebecque, C., 2014. Using high sampling rate (10/20 Hz) altimeter data for the observation of coastal surface currents: a case study over the northwestern Mediterranean Sea. Journal of Marine Systems, 129, pp.318-333.

Birol, F., Fuller, N., Lyard, F., Cancet, M., Niño, F., Delebecque, C., Fleury, S., Toublanc, F., Melet, A., Saraceno, M. and Léger, F., 2017. Coastal applications from nadir altimetry: example of the X-TRACK regional products. Advances in Space Research, 59(4), pp.936-953.

Blier, W., Keefe, S., Shaffer, W. A., Kim, S. C., 1997. Storm surges in the region of western Alaska. Monthly Weather Review, 125(12), pp.3094-3108.

Carrère, L., Lyard, F., 2003. Modeling the barotropic response of the global ocean to atmospheric wind and pressure forcing - comparisons with observations. Geophysical Research Letters, 30 (6), 1275.

Carrère, L., Lyard, F., Cancet, M., Guillot, A., Roblou, L., 2012. FES2012: A new global tidal model taking advantage of nearly 20 years of altimetry. Paper presented at The Symposium 20 Years of Progress in Radar Altimetry, Venice, Italy.

Church, J.A., Gregory, J.M., Huybrechts, P., Kuhn, M., Lambeck, K., Nhuan, M.T., Qin, D., Woodworth, P.L., 2001. Changes in sea level. In , in: Houghton, J. T., Ding, Y., Griggs, D. J., Noguer, M., van der Linden, P. J., Dai, X., Maskell, K., Johnson, C. A.(Eds.), Climate Change 2001: The Scientific Basis: Contribution of Working Group I to the Third Assessment Report of the Intergovernmental Panel, pp.639-694.

Church, J.A., Clark, P.U., Cazenave, A., Gregory, J.M., Jevrejeva, S., Levermann, A., Merrifield, M.A., Milne, G.A., Nerem, R.S., Nunn, P.D., Payne, A.J., Pfeffer, W.T., Stammer, D., Unnikrishnan, A.S., 2013. In: Stocker, T.F., Qin, D., Plattner, G.-K., Tignor, M., Allen, S.K., Boschung, J., Nauels, A., Xia, Y., V., Bex, Midgley, P.M. (Eds.), Sea Level Change. In: Climate Change 2013: The Physical Science Basis. Contribution of Working Group I to the Fifth Assessment Report of the Intergovernmental Panel on Climate Change. Cambridge University Press, Cambridge, United Kingdom and New York, NY, USA, pp.1137-1216.

Cipollini, P., Calafat, F.M., Jevrejeva, S., Melet, A., Prandi, P., 2017. Monitoring sea level in the coastal zone with coastal altimetry and tide gauges. Surveys in Geophysics, 38(1), pp.33-57.

Creel, L., 2003. Ripple effects: population and coastal regions. Population Reference Bureau, Washington, DC, pp.1-7.

Dangendorf, S., Mudersbach, C., Jensen, J., Anette, G., Heinrich, H., 2013. Seasonal to decadal forcing of high water level percentiles in the German Bight throughout the last century. Ocean Dynamics. 63 (5), pp.533-548.

Das, P.K., 1972. Prediction model for storm surges in the Bay of Bengal. Nature, 239, pp.211-213.

Das, P.K., Sinha, M.C., Balasubramanyam, V., 1974. Storm surges in the Bay of Bengal. Quarterly Journal of the Royal Meteorological Society, 100(425), pp.437-449.

Dixon, M.J., Tawn, J.A., 1994. Extreme Sea-levels at the UK A-class Sites: Site-by-site Analysis. Proudman Oceanographic Laboratory. Internal Document No. 65.

D'Onofrio, E. E., Fiore, M. M., Pousa, J. L., 2008. Changes in the regime of storm surges at Buenos Aires, Argentina. Journal of Coastal Research, 24(1A), pp.260-265.

Dube, S.K., Sinha, P.C., Roy, G.D., 1985. The numerical simulation of storm surges along the Bangladesh coast. Dynamics of atmospheres and oceans, 9(2), pp.121-133.

Dube, S.K., Sinha, P.C., Roy, G.D., 1986. Numerical simulation of storm surges in Bangladesh using a bay-river coupled model. Coastal Engineering, 10(1), pp.85-101.

Dube, S.K., Rao, A.D., Sinha, P.C., Murty, T.S., Bahulayan, N., 1997. Storm surges in the Bay of Bengal and Arabian Sea: the problem and its prediction. Mausam, 48, 283-304.

Dube, S.K., Chittibabu, P., Sinha, P.C., Rao, A.D., Murty, T.S., 2004. Numerical modelling of storm surge in the head Bay of Bengal using location specific model. Natural Hazards, 31(2), pp.437-453.

Dube, S.K., Jain, I., Rao, A.D., Murty, T.S., 2009. Storm surge modeling for the Bay of Bengal and Arabian Sea. Natural Hazards, 51(1), pp.3-27.

Dube, S.K., Poulose, J., Rao, A.D., 2013. Numerical simulation of storm surge associated with severe cyclonic storms in the Bay of Bengal during 2008-11. Mausam 64, pp.193-202.

Durand, F., Shankar, D., Birol, F., Shenoi, S.S.C., 2008. Estimating boundary currents from satellite altimetry: A case study for the east coast of India. Journal of Oceanography, 64(6), pp.831-845.

Durand, F., Shankar, D., Birol, F., Shenoi, S.S.C., 2009. Spatiotemporal structure of the East India Coastal Current from satellite altimetry. Journal of Geophysical Research: Oceans, 114(C2).

Ekman, M., 1988. The world's longest continued series of sea level observations. Pure and Applied Geophysics, 127(1), pp.73-77.

Eliot, M., 2010. Influence of interannual tidal modulation on coastal flooding along the Western Australian coast. Journal of Geophysical Research: Oceans, 115 (C11).

Ellis, J., Sherman, D.J. (Eds.), 2014. Coastal and marine hazards, risks, and disasters. Academic Press.

El-Sabh, M. I., Murty, T. S., Briand, J. M., 1988. Negative Storm Surges on Canada's East Coast. Natural and Man-Made Hazards, Springer Netherlands, pp. 305-316.

Feng, J., von Storch, H., Jiang, W., Weisse, R., 2015. Assessing changes in extreme sea levels along the coast of China. Journal of Geophysical Research: Oceans, 120 (12), pp.8039-8051.

Feng, X., Olabarrieta, M., Valle-Levinson, A., 2016. Storm-induced semidiurnal perturbations to surges on the US Eastern Seaboard. Continental Shelf Research, 114, pp.54-71.

Feng, X., Tsimplis, M.N., 2014. Sea level extremes at the coasts of China. Journal of Geophysical Research: Oceans, 119 (3), pp.1593-1608.

Finkl, C. W., 2013. Coastal hazards. Springer, Dordrecht.

Flather, R.A., 1994. A storm surge prediction model for the northern Bay of Bengal with application to the cyclone disaster in April 1991. Journal of Physical Oceanography, 24(1), pp.172-190.

Flierl, G.R., Robinson, A.R., 1972. Deadly surges in the Bay of Bengal: Dynamics and storm-tide tables. Nature, 239(5369), pp.213-215.

Frank, N. L., Husain, S. A., 1971. The deadliest tropical cyclone in history. Bulletin of the American Meteorological Society, 52(6), pp.438-445.

Fu, L.L., Cazenave, A., 2001. Satellite Altimetry and Earth Science: A Handbook of Techniques and Applications. Academic Press, San Diego, pp. 624.

Fu, L.L., Alsdorf, D., Rodriguez, E., Morrow, R., Mognard, N., Lambin, J., Vaze, P., Lafon, T., 2009. The SWOT (Surface Water and Ocean Topography) Mission: spaceborne radar interferometry for oceanographic and hydrological applications. In: OCEANOBS'09 Conference.

Gayathri, R., Murty, N., Bhaskaran, P.K., Kumar, T.S., 2016. A numerical study of hypothetical storm surge and coastal inundation for AILA cyclone in the Bay of Bengal. Environmental Fluid Mechanics, 16(2), pp.429-452.

Glejin, J., Kumar, V.S., Nair, T.M., Singh, J., Nherakkol, A., 2014. Freak waves off Ratnagiri, west coast of India. Indian Journal of Geo-Marine Sciences, 43(7), pp. 1339-1342.

Gomez-Enri, J., Cipollini, P., Gommenginger, C., Martin-Puig, C., Vignudelli, S., Woodworth, P., Beneviste, J., Villares, P., 2008. COASTALT: improving radar altimetry products in the oceanic coastal area. In: Bostater, C.R., Mertikas, S.P., Neyt, X., Velez-Reyes, M. (Eds.), Proceedings of SPIE-remote Sensing of the Ocean, Sea Ice, and Large Water Regions, 15 September 2008, 7105. SPIE, Cardiff, Wales, Bellingham WA, 71050J.

Goodbred, S.L., Kuehl, S.A., 2000. The significance of large sediment supply, active tectonism, and eustasy on margin sequence development: Late Quaternary stratigraphy and evolution of the Ganges–Brahmaputra delta. Sedimentary Geology, 133(3), pp.227-248.

Gower, J., 2005. Jason 1 detects the 26 december 2004 tsunami. Eos, Transactions, American Geophysical Union, 86(4), pp.37-38.

Gratiot, N., Anthony, E.J., Gardel, A., Gaucherel, C., Proisy, C., Wells, J.T., 2008. Significant contribution of the 18.6 year tidal cycle to regional coastal changes. Nature Geoscience, 1(3), pp.169-172.

Gray, W.M., 1975. Tropical cyclone genesis. Atmospheric science paper, No. 234.

Haigh, I.D., 2009. Extreme sea levels in the English Channel 1900 to 2006. Doctoral dissertation, University of Southampton, UK.

Haigh, I., Nicholls, R., Wells, N., 2010. Assessing changes in extreme sea levels; application to the English channel, 1900-2006. Continental Shelf Research, 30, pp.1042-1055.

Haigh, I.D., Eliot, M., Pattiaratchi, C., 2011. Global influences of the 18.61 year nodal cycle and 8.85 year cycle of lunar perigee on high tidal levels. Journal of Geophysical Research: Oceans, 116(C6).

Hallegatte, S., Green, C., Nicholls, R.J., Corfee-Morlot, J., 2013. Future flood losses in major coastal cities. Nature Climate Change, 3, pp.802-806.

Han, G., Ma, Z., Chen, D., deYoung, B., Chen, N., 2012. Observing storm surges from space: Hurricane Igor off Newfoundland. Scientific Reports, 2, 1010.

Han, W., Webster, P.J., 2002. Forcing mechanisms of sea level interannual variability in the Bay of Bengal. Journal of Physical Oceanography, 32 (1), pp.216-239.

Harwood, P., Cipollini, P., Snaith, H., Høyer, J., Dwyer, N., Dunne, D., Stoffelen, A., Donlon, C., 2013. Earth observation in aid of surge monitoring and forecasting: ESA's eSurge project. EGU General Assembly Conference Abstracts, 15, pp.11942.

Holgate, S.J., Matthews, A., Woodworth, P.L., Rickards, L.J., Tamisiea, M.E., Bradshaw, E., Foden, P.R., Gordon, K.M., Jevrejeva, S., Pugh, J., 2013. New data systems and products at the permanent service for mean sea level. Journal of Coastal Research, 29(3), pp.493-504.

Holland, G.J., 1980. An analytic model of the wind and pressure profiles in hurricanes. Monthly Weather Review, 108(8), pp.1212-1218.

Holligan, P. M., Boois, H. D., 1993. Land ocean interactions in the coastal zone (LOICZ). Science plan. Global Change Report (Sweden).

Horsburgh, K. J., Wilson, C., 2007. Tide-surge interaction and its role in the distribution of surge residuals in the North Sea. Journal of Geophysical Research: Oceans, 112(C8).

Hussain, M.A., Tajima, Y., 2017. Numerical investigation of surge–tide interactions in the Bay of Bengal along the Bangladesh coast. Natural Hazards, 86(2), pp.669-694.

Ichinose, G.A., Anderson, J.G., Satake, K., Schweickert, R.A., Lahren, M.M., 2000. The potential hazard from tsunami and seiche waves generated by large earthquakes within Lake Tahoe, California-Nevada. Geophysical Research Letters, 27(8), pp.1203-1206.

Idier, D., Dumas, F., Muller, H., 2012. Tide-surge interaction in the English Channel. Natural Hazards and Earth System Sciences, 12(12), pp.3709-3718.

IFNet, 2009. International Flood Network secretariat/ Infrastructure Development Institute-Japan, June 24, 2009. http://www.internationalfloodnetwork.org/aila.htm

IOC, 1985. Manual on sea-level measurement and interpretation, Volume 1, Basic procedures. IOC Manuals and Guides, 14, 8.

IPCC, 2012. Managing the Risks of Extreme Events and Disasters to Advance Climate Change Adaptation. A Special Report of Working Groups I and II of the Intergovernmental Panel on Climate Change, Field, C.B., V. Barros, T.F. Stocker, D. Qin, D.J. Dokken, K.L. Ebi, M.D. Mastrandrea, K.J. Mach, G.-K. Plattner, S.K. Allen, M. Tignor, and P.M. Midgley (Eds.). Cambridge University Press, Cambridge, United Kingdom and New York, NY, USA, pp.582.

Jain, I., Chittibabu, P., Agnihotri, N., Dube, S.K., Sinha, P. C., Rao, A.D., 2006. Simulation of storm surges along Myanmar coast using a location specific numerical model. Natural Hazards, 39, pp.71-82.

Jain, I., Rao, A.D., Jitendra, V., Dube, S.K., 2010. Computation of expected total water levels along the east coast of India. Journal of coastal research, 26(4), pp.681-687.

Jelesnianski, C.P., Taylor, A.D., 1973. A Preliminary View of Storm Surges before and after Storm Modifications. NOAA Technical Memorandum. ERL WMPO-3, National Oceanic and Atmospheric Administration, U.S. Department of Commerce, pp.33.

Johns, B., Ali, M.A., 1980. The numerical modelling of storm surges in the Bay of Bengal. Quarterly Journal of the Royal Meteorological Society, 106(447), pp.1-18.

Johns, B., Dube, S.K., Mohanty, U.C., Sinha, P.C., 1981. Numerical simulation of the surge generated by the 1977 Andhra cyclone. Quarterly Journal of the Royal Meteorological Society, 107(454), pp.919-934.

Johns, B., Rao, A.D., Dube, S.K., Sinha, P.C., 1985. Numerical modelling of tide-surge interaction in the Bay of Bengal. Philosophical Transactions of the Royal Society A: Mathematical, Physical and Engineering Sciences, 313(1526), pp.507-535.

Jones, J.E., Davies, A.M., 2007. Influence of non-linear effects upon surge elevations along the west coast of Britain. Ocean Dynamics, 57(4), pp.401-416.

Joseph, A., 2011. Tsunamis: Detection, monitoring, and early-warning technologies. Academic Press, Boston, USA, pp.436.

Kalnay, E., Kanamitsu, M., Kistler, R., Collins, W., Deaven, D., Gandin, L., Iredell, M., Saha, S., White, G., Woollen, J., Zhu, Y., Leetmaa, A., Reynolds, R., Chelliah, M., Ebisuzaki, W., Higgins, W., Janowiak, J., Mo, K.C., Ropelewski, C., Wang, J., Jenne, R., Joseph, D., 1996. The NCEP/NCAR 40-year reanalysis project. Bulletin of the American Meteorological Society, 77 (3), pp.437-471.

Kantha, L., 2006. Time to replace the Saffir-Simpson hurricane scale?. Eos, Transactions, American Geophysical Union, 87(1), pp.3-6.

Kay, S., Caesar, J., Wolf, J., Bricheno, L., Nicholls, R.J., Islam, A.S., Lowe, J.A., 2015. Modelling the increased frequency of extreme sea levels in the Ganges–Brahmaputra–Meghna delta due to sea level rise and other effects of climate change. Environmental Science: Processes & Impacts, 17 (7), pp.1311-1322.

Keers, J. F., 1968. An empirical investigation of interaction between storm surge and astronomical tide on the east coast of Great Britain. Ocean Dynamics, 21(3), pp.118-125.

Kim, K.O., Yamashita, T., Choi, B.H., 2008. Coupled process-based cyclone surge simulation for the Bay of Bengal. Ocean Modelling, 25(3), pp.132-143.

Knaff, J.A., Zehr, R.M., 2007. Reexamination of tropical cyclone wind–pressure relationships. Weather and forecasting, 22(1), pp.71-88.

Krien, Y., Mayet, C., Testut, L., Durand, F., Tazkia, A.R., Islam, A.K.M.S., Gopalakrishna, V.V., Becker, M., Calmant, S., Shum, C.K., Khan, Z.H., 2016. Improved bathymetric dataset and tidal model for the northern Bay of Bengal. Marine Geodesy, 39(6), pp.422-438.

Krien, Y., Testut, L., Islam, A.K.M.S., Bertin, X., Durand, F., Mayet, C., Tazkia, A.R., Becker, M., Calmant, S., Papa, F., Ballu, V., 2017. Towards improved storm surge models in the northern Bay of Bengal. Continental Shelf Research, 135, pp.58-73.

Kurian, N.P., Nirupama, N., Baba, M., Thomas, K.V., 2009. Coastal flooding due to synoptic scale, meso-scale and remote forcings. Natural hazards, 48(2), pp.259-273.

Lay, T., Kanamori, H., Ammon, C.J., Nettles, M., Ward, S.N., Aster, R.C., Beck, S.L., Bilek, S.L., Brudzinski, M.R., Butler, R., DeShon, H.R., 2005. The great Sumatra-Andaman earthquake of 26 december 2004. Science, 308(5725), pp.1127-1133.

Le Cozannet, G., Modaressi, H., Pedreros, R., Garcin, M., Krien, Y., Desramaut, N., 2013. Storm Surges. Encyclopedia of Natural Hazards, Springer Netherlands, pp.940-941.

Lee, H.S., 2013. Estimation of extreme sea levels along the Bangladesh coast due to storm surge and sea level rise using EEMD and EVA. Journal of Geophysical Research: Oceans, 118 (9), pp.4273-4285.

Letetrel, C., Marcos, M., Míguez, B.M., Woppelmann, G., 2010. Sea level extremes in Marseille (NW Mediterranean) during 1885–2008. Continental shelf research, 30(12), pp.1267-1274.

Levin, B.W., Nosov, M.A., 2009. Physics of tsunamis. Springer, Dordrecht.

Lewis, M., Bates, P., Horsburgh, K., Neal, J., Schumann, G., 2013. A storm surge inundation model of the northern Bay of Bengal using publicly available data. Quarterly Journal of the Royal Meteorological Society, 139(671), pp.358-369.

Li, Z., Yu, W., Li, T., Murty, V.S.N., Tangang, F., 2013. Bimodal character of cyclone climatology in the Bay of Bengal modulated by monsoon seasonal cycle. Journal of Climate, 26 (3), pp.1033-1046.

Lillibridge, J., Lin, M., Shum, C.K., 2013. Hurricane Sandy storm surge measured by satellite altimetry. Oceanography, 26 (2), pp.8-9.

Liu, W.C., Huang, W.C., Chen, W.B., 2016. Modeling the interaction between tides and storm surges for the Taiwan coast. Environmental Fluid Mechanics, 4(16), pp.721-745.

Liu, Y., Weisberg, R.H., Vignudelli, S., Roblou, L., Merz, C.R., 2012. Comparison of the X-TRACK altimetry estimated currents with moored ADCP and HF radar observations on the West Florida Shelf. Advances in Space Research, 50 (8), pp.1085-1098.

Lopeman, M., Deodatis, G., Franco, G., 2015. Extreme storm surge hazard estimation in lower Manhattan. Natural Hazards, 78(1), pp.1-37.

Lowe, J.A., Woodworth, P.L., Knutson, T., McDonald, R.E., McInnes, K.L., Woth, K., von Storch, H., Wolf, J., Swail, V., Bernier, N.B., Gulev, S., Horsburgh, K.J., Unnikrishnan, A.S., Hunter, J.R., Weisse, R., 2010. Past and future changes in extreme sea levels and waves. Chapter 11. In: Church, J.A., Woodworth, P.L., Aarup, T., Wilson, W.S. (Eds.), Understanding Sea-Level Rise and Variability. Wiley-Blackwell, London, pp.326-375.

Luettich Jr, R.A., Westerink, J.J., Scheffner, N.W., 1992. ADCIRC: An Advanced Three-Dimensional Circulation Model for Shelves, Coasts, and Estuaries. Report 1. Theory and Methodology of ADCIRC-2DDI and ADCIRC-3DL (No. CERC-TR-DRP-92-6). COASTAL ENGINEERING RESEARCH CENTER VICKSBURG MS.

Lyard, F., Lefevre, F., Letellier, T., Francis, O., 2006. Modelling the global ocean tides: modern insights from FES2004. Ocean dynamics, 56(5), pp.394-415.

Madsen, H., Jakobsen, F., 2004. Cyclone induced storm surge and flood forecasting in the northern Bay of Bengal. Coastal Engineering, 51(4), pp.277-296.

Madsen, K.S., Høyer, J.,L., Tscherning, C.C., 2007. Near-coastal satellite altimetry: sea surface height variability in the North Sea-Baltic sea area. Geophysical Research Letters. 34, L14601.

Mangor, K., 2008. Definitions of Coastal terms. Available from http://www.coastalwiki.org/wiki/Definitions_of_coastal_terms [accessed on 24-06-2017].

Marcos, M., Tsimplis, M.N., Shaw, A.G.P., 2009. Sea level extremes in southern Europe. Journal of Geophysical Research; Oceans, 114 (C1).

Marcos, M., Calafat, F.M., Berihuete, Á., Dangendorf, S., 2015. Long-term variations in global sea level extremes. Journal of Geophysical Research: Oceans, 120(12), pp.8115-8134.

McGranahan, G., Balk, D., Anderson, B., 2007. The rising tide: assessing the risks of climate change and human settlements in low elevation coastal zones. Environment and urbanization, 19(1), pp.17-37.

Mehra, P., Soumya, M., Vethamony, P., Vijaykumar, K., Nair, T.M.B., Agarvadekar, Y., Jyoti, K., Sudheesh, K., Luis, R., Lobo, S., Harmalkar, B., 2015. Coastal sea level response to the tropical cyclonic forcing in the northern Indian Ocean. Ocean Science, 11 (1), pp.159-173.

Melet, A., Gourdeau, L., Verron, J., 2010. Variability in Solomon Sea circulation derived from altimeter sea level data. Ocean Dynamics, 60(4), pp.883-900.

Menéndez, M., Woodworth, P.L., 2010. Changes in extreme high water levels based on a quasi-global tide-gauge data set. Journal of Geophysical Research: Oceans, 115 (C10).

Mercier, F., Rosmorduc, V., Carrère, L., Thibaut, P., 2010. Coastal and Hydrology Altimetry Product (PISTACH) Handbook. Centre National d'Études Spatiales (CNES), Paris, France. CLS-DOS-NT-10-246, SALP-MUP-OP- 16031-CN, 01/00, Version 1.0, October 4th.

Merrifield, M.A., Genz, A.S., Kontoes, C.P., Marra, J.J., 2013. Annual maximum water levels from tide gauges: contributing factors and geographic patterns. Journal of Geophysical Research: Oceans, 118 (5), pp.2535-2546.

Moftakhari, H.R., AghaKouchak, A., Sanders, B.F., Feldman, D.L., Sweet, W., Matthew, R.A., Luke, A., 2015. Increased nuisance flooding along the coasts of the United States due to sea level rise: past and future. Geophysical Research Letters, 42 (22), 9846-9852.

Mohapatra, M., Bandyopadhyay, B.K., Tyagi, A., 2012. Best track parameters of tropical cyclones over the North Indian Ocean: a review. Natural Hazards, 63(3), pp.1285-1317.

Monbaliu, J., Toffoli, A., 2003. Regional distribution of extreme waves. Proceedings of Maxwave final meeting, Geneva, Switzerland.

Monserrat, S., Vilibić, I., Rabinovich, A. B., 2006. Meteotsunamis: atmospherically induced destructive ocean waves in the tsunami frequency band. Natural Hazards and Earth System Sciences, 6(6), pp.1035-1051.

Mori, N., 2009. Freak waves. In: Kim, Y. C. (Eds.), Handbook of coastal and ocean engineering. World Scientific Publishing, New Jersey, USA, pp.1-11.

Mudersbach, C., Wahl, T., Haigh, I.D., Jensen, J., 2013. Trends in high sea levels of German North Sea gauges compared to regional mean sea level changes. Continental Shelf Research, 65, pp.111-120.

Murty, P.L.N., Sandhya, K.G., Bhaskaran, P.K., Jose, F., Gayathri, R., Nair, T.B., Kumar, T.S., Shenoi, S.S.C., 2014. A coupled hydrodynamic modeling system for PHAILIN cyclone in the Bay of Bengal. Coastal Engineering, 93, pp.71-81.

Murty, P.L.N., Bhaskaran, P.K., Gayathri, R., Sahoo, B., Kumar, T.S., SubbaReddy, B., 2016. Numerical study of coastal hydrodynamics using a coupled model for Hudhud cyclone in the Bay of Bengal. Estuarine, Coastal and Shelf Science, 183, pp.13-27.

Murty, T.S., Henry, R.F., 1983. Tides in the Bay of Bengal. Journal of Geophysical Research, 88(C10), pp.6069-6076.

Murty, T.S., Flather, R.A., Henry, R.F., 1986. The storm surge problem in the Bay of Bengal. Progress in Oceanography, 16(4), pp.195-233.

Murty, T.S., Flather, R. A., 1994. Impact of storm surges in the Bay of Bengal. Journal of Coastal Research, Special Issue No. 12, pp.149-161.

Nagarajan, B., Suresh, I., Sundar, D., Sharma, R., Lal, A. K., Neetu, S., Shenoi, S.S.C., Shetye, S. R., Shankar, D., 2006. The Great Tsunami of 26 December 2004: A description based on tide-gauge data from the Indian subcontinent and surrounding areas. Earth, Planets and Space, 58(2), pp.211-215.

Needham, H., Keim, B. D., 2011. Storm Surge: Physical Processes and an Impact Scale, Recent Hurricane Research - Climate, Dynamics, and Societal Impacts, Prof. Anthony Lupo (Eds.), ISBN: 978-953-307- 238-8, InTech, Available from: http://www.intechopen.com/books/recent-hurricane-research-climate-dynamicsand-societal-impacts/storm-surge-physical-processes-and-an-impact-scale.

Needham, H., Keim, B.D., Sathiaraj, D., 2015. A Review of Tropical Cyclone-Generated Storm Surges: Global Data Sources, Observations and Impacts. Reviews of Geophysics, 53(2), pp.545-591.

Neumann, B., Vafeidis, A.T., Zimmermann, J., Nicholls, R.J., 2015. Future coastal population growth and exposure to sea-level rise and coastal flooding-a global assessment. PloS One, 10(3), e0118571.

Neumann, C. J., 1992. The Joint Typhoon Warning Center (JTWC92) model. SAIC, Final Report, Contract No. N00014-90-C-6042, pp.85.

Nikolkina, I., Didenkulova, I., 2011. Rogue waves in 2006–2010. Natural hazards and Earth system sciences, 11(11), pp.2913-2924.

Niyas, N.T., Srivastava, A.K., Hatwar, H.R., 2009. Variability and Trend in the Cyclonic Storms over the North Indian Ocean, Meteorological Monograph No. Cyclone Warning 3.

Park, Y.H., Suh, K.D., 2012. Variations of storm surge caused by shallow water depths and extreme tidal ranges. Ocean Engineering, 55, pp.44-51.

Paul, G.C., Ismail, A.I.M., Rahman, A., Karim, M.F., Hoque, A., 2016. Development of Tide–Surge Interaction Model for the Coastal Region of Bangladesh. Estuaries and coasts, 6(39), pp.1582-1599.

Pethick, J., Orford, J.D., 2013. Rapid rise in effective sea-level in southwest Bangladesh: its causes and contemporary rates. Global and Planetary Change, 111, pp.237-245.

Pidwirny, M. 2006. Ocean Tides. Fundamentals of Physical Geography, 2nd Edition. http://www.physicalgeography.net/fundamentals/8r.html.

Prandle, D., Wolf, J., 1978. The interaction of surge and tide in the North Sea and River Thames. Geophysical Journal International, 55(1), pp.203-216.

Proudman, J., 1955. The propagation of tide and surge in an estuary. In Proceedings of the Royal Society of London A: Mathematical, Physical and Engineering Sciences, 231 (1184), pp.8-24.

Pugh, D.T., 1996. Tides, surges and mean sea-level (reprinted with corrections). John Wiley and Sons, Chichester, pp.472.

Pugh, D., Woodworth, P., 2014. Sea-level science: understanding tides, surges, tsunamis and mean sea-level changes. Cambridge University Press, Cambridge, UK.

Queensland Government, 2001. Queensland climate change and community vulnerability to tropical cyclones: ocean hazards assessment – stage 1. J0004-PR0001C, The State of Queensland (Australia), Department of Natural Resources and Mines, Brisbane, Qld., pp.383.

Rabinovich, A.B., 2009. Seiches and harbor oscillations. In: Kim, Y.C. (Eds.), Handbook of Coastal and Ocean Engineering. World Scientific Publishing, Singapore, pp. 193–236 (Chapter 9).

Rady, M.A., El-Sabh, M.I., Murty, T.S., Backhaus, J.O., 1994. Tide-surge interaction in the Gulf of Suez, Egypt. Marine Geodesy, 17, pp.45-62.

Rao, A.D., Murty, P.L.N., Jain, I., Kankara, R.S., Dube, S.K., Murty, T.S., 2013. Simulation of water levels and extent of coastal inundation due to a cyclonic storm along the east coast of India. Natural hazards, 66(3), pp.1431-1441.

Ray, R.D., 1999. A Global Ocean Tide Model from TOPEX/POSEIDON Altimetry: GOT99.2. National Aeronautics and Space Administration Technical Memorandum, p. 58. NASA/TM-1999-209478.

Ray, R.D., Foster, G., 2016. Future nuisance flooding at Boston caused by astronomical tides alone. Earth's Future, 4(12), pp.578-587.

Rego, J.L., Li, C., 2010. Nonlinear terms in storm surge predictions: Effect of tide and shelf geometry with case study from Hurricane Rita. Journal of Geophysical Research: Oceans, 115(C6).

Remya, P.G., Vishnu, S., Praveen Kumar, B., Nair, B., Rohith, B., 2016. Teleconnection between the North Indian Ocean high swell events and meteorological conditions over the Southern Indian Ocean. Journal of Geophysical Research: Oceans, 121(10), pp.7476-7494.

Resio, D.T., Westerink, J.J., 2008. Modeling the physics of storm surges. Physics Today, No. 9, pp.33-38.

Rhein, M., Rintoul, S.R., Aoki, S., Campos, E., Chambers, D., Feely, R.A., Gulev, S., Johnson, G.C., Josey, S.A., Kostianoy, A., Mauritzen, C., Roemmich, D., D., Talley L., Wang, F., 2013. In: Stocker, T.F., Qin, D., Plattner, G.-K., Tignor, M., Allen, S.K., Boschung, J., Nauels, A., Xia, Y., V., Bex, Midgley, P.M. (Eds.), Observations: Ocean. In: Climate Change 2013: The Physical Science Basis. Contribution of Working Group I to the Fifth Assessment Report of the Intergovernmental Panel on Climate Change. Cambridge University Press, Cambridge, United Kingdom and New York, NY, USA, pp.255-315.

Ribeiro, A., Barbosa, S.M., Scotto, M.G., Donner, R.V., 2014. Changes in extreme sea-levels in the Baltic Sea. Tellus A: Dynamic Meteorology and Oceanography. 66 (1), 20921.

Rickards, L., Matthwes, A., Gordon, K., Tamisea, M., Jevrejeva, S., Woodworth, P., Bradshaw, E., 2015. Celebrating 80 years of the Permanent Service for Mean Sea Level (PSMSL). Proceedings of the International Association of Hydrological Sciences, 365, pp.1.

Roblou, L., Lyard, F., Le Henaff, M., Maraldi, C., 2007. X-track, a new processing tool for altimetry in coastal oceans. In: ESA ENVISAT Symposium, Montreux, Switzerland, April 23-27, 2007, ESA SP-636.

Roblou, L., Lamouroux, J., Bouffard, J., Lyard, F., Le Henaff, M., Lombard, A., Marsalaix, P., De Mey, P., Birol, F., 2011. Post-processing altimeter data towards coastal applications and integration into coastal models. In: Vignudelli, S., Kostianoy, A.G., Cipollini, P., Benveniste, J. (Eds.), Coastal Altimetry. Springer, Berlin, Heidelberg, pp.217-246.

Rossiter, J.R., 1961. Interaction between tide and surge in the Thames. Geophysical Journal International, 6(1), pp.29-53.

Roy, K., Kumar, U., Mehedi, H., Sultana, T., Ershad, D.M., 2009. Initial damage assessment report of cyclone Aila with focus on Khulna District. Unnayan Onneshan-Humanitywatch-Nijera Kori, Khulna Bangladesh, P-6.

Saji, N.H., Goswami, B.N., Vinayachandran, P.N., Yamagata, T., 1999. A dipole mode in the tropical Indian Ocean. Nature, 401 (6751), pp.360-363.

Saji, N.H., Yamagata, T., 2003. Possible impacts of Indian Ocean dipole mode events on global climate. Climate Research, 25 (2), pp.151-169.

Scharroo, R., Smith, W.H.F., Lillibridge, J.L., 2005. Satellite altimetry and the intensification of Hurricane Katrina. Eos, Transactions, American Geophysical Union, 86(40), pp.366-366.

Scharroo, R., Fenoglio, L., Annunziato, A., 2014. Cyclone Xaver seen by SARAL/ AltiKa. EGU General Assembly Conference Abstracts, 16, pp.2923-2924.

Shankar, D., 1998. Low-Frequency Variability of Sea Level along the Coast of India. Doctoral Dissertation, Goa University, Goa, India.

Shankar, D., 2000. Seasonal cycle of sea level and currents along the coast of India. Current Science, 78 (3), pp.279-288.

Sindhu, B., Suresh, I., Unnikrishnan, A.S., Bhatkar, N.V., Neetu, S., Michael, G.S., 2007. Improved bathymetric datasets for the shallow water regions in the Indian Ocean. Journal of Earth System Science, 116 (3), pp.261-274.

Sindhu, B., Unnikrishnan, A.S., 2012. Return period estimates of extreme sea level along the east coast of India from numerical simulations. Natural Hazards, 61(3), pp.1007-1028.

Sindhu, B., Unnikrishnan, A.S., 2013. Characteristics of tides in the Bay of Bengal. Marine Geodesy, 36 (4), pp.377-407.

Singh, O.P., Khan, T.M.A., Murty, T.S., Rahman, M.S., 2001. Sea level changes along Bangladesh coast in relation to the southern oscillation phenomenon. Marine Geodesy, 24 (1), pp.65-72.

Singh, O.P., 2006. ENSO and monsoon induced sea level changes and their impacts along the Indian coastline. Indian Journal of Marine Sciences, 35 (2), pp.87-92.

Sinha, P.C., Rao, Y.R., Dube, S.K., Rao, A.D., Chatterjee, A.K., 1996. Numerical investigation of tide-surge interaction in Hooghly estuary, India. Marine Geodesy, 19, pp.235-255.

Sinha, P.C., Jain, I., Bhardwaj, N., Rao, A.D., Dube, S.K., 2008. Numerical modeling of tide-surge interaction along Orissa coast of India. Natural Hazards, 45, pp.413-427.

Sirota, A.M., Lebedev, S.A., 2008. Storm surges in the Gulf of Finland and the Neva River observed on satellite altimetry data. EGU General Assembly Conference Abstracts, 10, pp.11817.

Small, C., Nicholls, R.J., 2003. A global analysis of human settlement in coastal zones. Journal of Coastal Research, 19(3), pp.584-599.

Sreenivas, P., Gnanaseelan, C., Prasad, K.V.S.R., 2012. Influence of El Niño and Indian Ocean Dipole on sea level variability in the Bay of Bengal. Global and Planetary Change, 80, pp.215-225.

Srinivas, K., Dineshkumar, P.K., Revichandran, C., 2005. ENSO signature in the sea level along the coastline of Indian subcontinent. Indian Journal of Marine Sciences, 34 (2), pp.225-236.

Sundar, D., Shankar, D., Shetye, S.R., 1999. Sea level during storm surges as seen in tide-gauge records along the east coast of India. Current Science, 77, pp.1325-1332.

Talke, S.A., Orton, P., Jay, D.A., 2014. Increasing storm tides in New York Harbor, 1844–2013. Geophysical Research Letters, 41 (9), pp.3149-3155.

Tang, Y.M., Grimshaw, R., Sanderson, B., Holland, G., 1996. A numerical study of storm surges and tides, with application to the north Queensland coast. Journal of Physical Oceanography, 26(12), pp.2700-2711.

Torres, R.R., Tsimplis, M.N., 2014. Sea level extremes in the Caribbean Sea. Journal of Geophysical Research: Oceans, 119 (8), pp.4714-4731.

Trenberth, K.E., 1984. Signal versus noise in the Southern Oscillation. Monthly Weather Review, 112 (2), pp.326-332.

Tsimplis, M.N., Woodworth, P.L., 1994. The global distribution of the seasonal sea level cycle calculated from coastal tide gauge data. Journal of Geophysical Research: Oceans, 99 (C8), pp.16031-16039.

Tsimplis, M.N., Shaw, A.G.P., 2010. Seasonal sea level extremes in the Mediterranean Sea and at the Atlantic European coasts. Natural Hazards Earth System Sciences, 10 (7), pp.1457-1475.

Ullmann, A., Pirazzoli, P. A., Tomasin, A., 2007. Sea surges in Camargue: Trends over the 20th century. Continental Shelf Research, 27(7), pp.922-934.

UN-Habitat, 2016. Urbanization and Development; Emerging Futures. World Cities Report 2016. United Nations Human Settlements Programme (UN-Habitat), Nairobi, Kenya, 2016.

Unnikrishnan, A.S., Sundar, D., Blackman, D., 2004. Analysis of extreme sea level along the east coast of India. Journal of Geophysical Research, 109, C06023.

Unnikrishnan, A.S., Shankar, D., 2007. Are sea-level-rise trends along the coasts of the north Indian Ocean consistent with global estimates?. Global and Planetary Change, 57 (3), pp.301-307.

Unnikrishnan, A.S., RameshKumar, M.R., Sindhu, B., 2011. Tropical cyclones in the Bay of Bengal and extreme sea-level projections along the east coast of India in a future climate scenario. Current Science 101 (3), pp.327-331.

Unnikrishnan, A.S., Nidheesh, A.G., Lengaigne, M., 2015. Sea-level-rise trends off the Indian coasts during the last two decades. Current Science, 108 (5), pp.966-970.

Van Veen, J., 1954. Tide-gauges, subsidence-gauges and flood-stones in The Netherlands. Geologie en Mijnbouw, 16, pp.214-219.

Vignudelli, S., Kostianoy, A.G., Cipollini, P., Benveniste, J. (Eds.), 2011. Coastal Altimetry. Springer, Berlin, Heidelberg, pp.578.

Vilibić, I., Šepić, J., 2010. Long-term variability and trends of sea level storminess and extremes in European Seas. Global and Planetary Change, 71(1), pp.1-12.

Vilibić, I., Monserrat, S., Rabinovich, A.B., 2014. Meteorological tsunamis on the US East Coast and in other regions of the World Ocean. In Meteorological Tsunamis: The US East Coast and Other Coastal Regions. Springer International Publishing, pp.1-9.

Vilibić, I., Šepić, J., Rabinovich, A.B., Monserrat, S., 2016. Modern approaches in meteotsunami research and early warning. Frontiers in Marine Science, 3, pp.57.

von Storch, H., Woth, K., 2008. Storm surges: perspectives and options. Sustainability Science, 3(1), pp.33-43.

Wahl, T., Calafat, F.M., Luther, M.E., 2014. Rapid changes in the seasonal sea level cycle along the US Gulf coast from the late 20th century. Geophysical Research Letters. 41 (2), pp.491-498.

Wahl, T., Chambers, D.P., 2015. Evidence for multidecadal variability in US extreme sea level records. Journal of Geophysical Research: Oceans, 120 (3), pp.1527-1544.

Walden, A.T., Prescott, P., Webber, N.B., 1982. The examination of surge-tide interaction at two ports on the central south coast of England. Coastal Engineering, 6(1), pp.59-70.

Wijeratne, E.M.S., Woodworth, P.L., Stepanov, V.N., 2008. The seasonal cycle of sea level in Sri Lanka and Southern India. Western Indian Ocean Journal of Marine Science, 7 (1), pp.29-43.

Wolf, J., 1978. Interaction of tide and surge in a semi-infinite uniform channel, with application to surge propagation down the east coast of Britain. Applied Mathematical Modelling, 2(4), pp.245-253.

Woodworth, P.L., Blackman, D.L., 2002. Changes in extreme high waters at Liverpool since 1768. International Journal of Climatology, 22(6), pp.697-714.

Woodworth, P.L., Blackman, D.L., 2004. Evidence for systematic changes in extreme high waters since the mid-1970s. Journal of Climate, 17 (6), pp.1190-1197.

Woodworth, P.L., 2006. Some important issues to do with long-term sea level change. Philosophical Transactions of the Royal Society of London A: Mathematical, Physical and Engineering Sciences, 364(1841), pp.787-803.

Woodworth, P.L., Menéndez, M., Gehrels, W.R., 2011. Evidence for century-timescale acceleration in mean sea levels and for recent changes in extreme sea levels. Surveys in Geophysics, 32 (4-5), pp.603-618.

Xu, J., Zhang, Y., Cao, A., Liu, Q., Lv, X., 2016. Effects of tide-surge interactions on storm surges along the coast of the Bohai Sea, Yellow Sea, and East China Sea. Science China Earth Sciences, 59(6), pp.1308-1316.

Zhang, H., Cheng, W., Qiu, X., Feng, X. and Gong, W., 2017. Tide-surge interaction along the east coast of the Leizhou Peninsula, South China Sea. Continental Shelf Research, 142, pp.32-49.

Zhang, W.-Z., Shi, F., Hong, H.-S., Shang, S.-P., Kirby, J.T., 2010. Tide-surge interaction intensified by the Taiwan Strait. Journal of Geophysical Research: Oceans, 115, C06012.

List of Publications

Antony, C., Unnikrishnan, A. S., 2013. Observed characteristics of tide-surge interaction along the east coast of India and the head of Bay of Bengal. Estuarine, Coastal and Shelf Science, 131, pp.6-11.

Antony, C., Testut, L., Unnikrishnan, A. S., 2014. Observing storm surges in the Bay of Bengal from satellite altimetry. Estuarine, Coastal and Shelf Science, 151, pp.131-140.

Antony, C., Unnikrishnan, A.S., Woodworth, P.L., 2016. Evolution of extreme high waters along the east coast of India and at the head of the Bay of Bengal. Global and Planetary Change, 140, pp.59-67.